Back-analysis study of selected Norwegian debris flow and debris avalanche events

A comparison of DAN3D and GeoClaw runout models

Graeme Robert Carey

Master's Thesis in Geoscience
Discipline: Geohazards
Department of Geoscience

Faculty of Mathematics and Natural Sciences

UNIVERSITY OF OSLO
June 2018

Back-analysis study of selected Norwegian debris flow and debris avalanche events

A comparison of DAN3D and GeoClaw runout models

Graeme Robert Carey

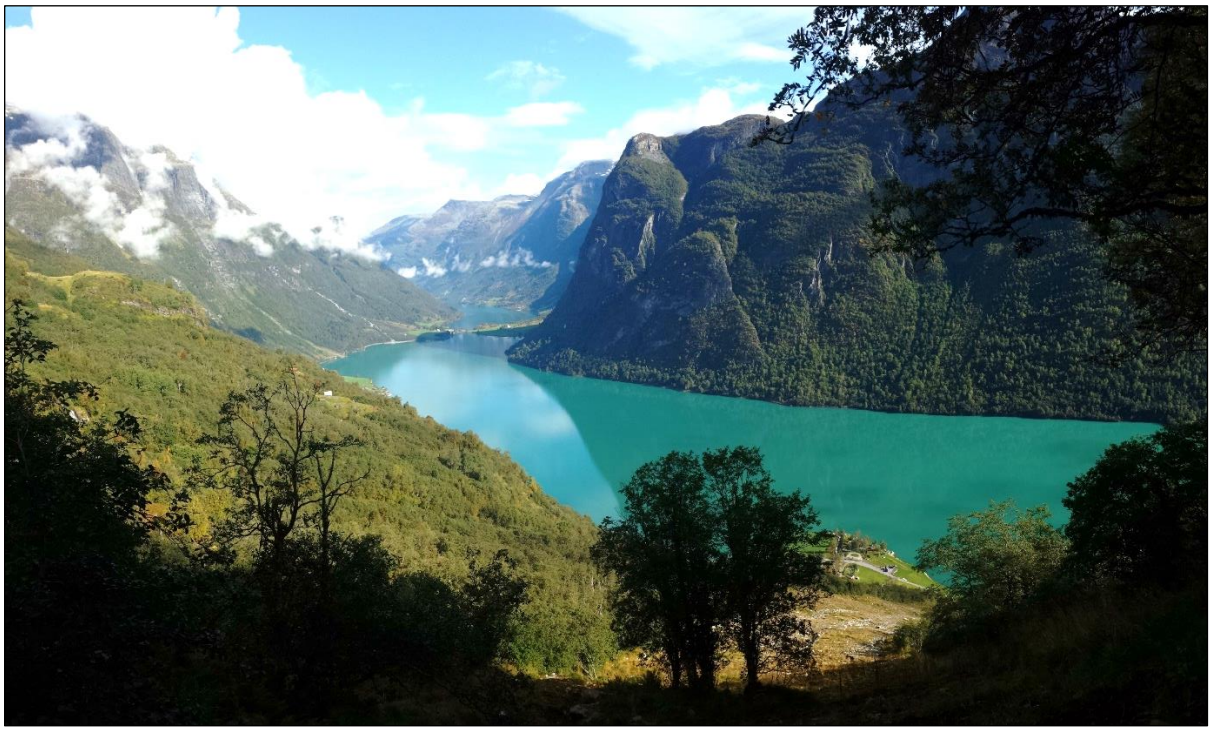

Master's Thesis in Geoscience
Discipline: Geohazards
Department of Geoscience

Det Matematisk-naturvitenskapelige Fakultet

Universitetet i Oslo

June 2018

Supervisors: José Mauricio Cepeda (NGI), Anders Solheim (NGI/UIO)

Back-analysis study of selected Norwegian Debris Flow and Avalanche Events: a comparison of DAN3D and GeoClaw runout models

http://www.duo.uio.no/

Print: Reprosentralen, Universitetet i Oslo

Cover photo: Southern Oldedalen, seen from the initiation zone of Oldedalen 1. Graeme Carey, 2017.

Abstract

Debris flows and debris avalanches represent a large threat to society in Norway. The intensity and frequency of these events is expected to increase over the course of the next 50 years due to changing precipitation patterns related to global climate change. Models are continually being developed and tested to better understand and characterise these events. An important part of creating regional and local-scale hazard maps is understanding the potential runout distance and velocity that can be achieved by these events. This thesis provides a detailed study of four landslide events in western Norway (two debris flows and two debris avalanches) additionally, it compares two software packages used for landslide back-analysis. The work presented is part of the Klima2050 research initiative.

Field visits were conducted at each site in order to develop a better understanding of the event geometry and take soil samples to construct grain size distribution curves for each event. These grain size distributions were used to estimate the static friction of each soil sample. Landslide back-analysis was conducted using DAN3D to determine rheological parameters for each event. Simulations were also conducted in GeoClaw, to compare it with DAN3D and determine its suitability for the runout modelling of debris flow events. Dynamic friction angles calibrated in the models were compared to the static friction angles obtained from the grain size distributions.

Simulation results agree with field observations of the debris flow and debris avalanche events. DAN3D was found to underestimate the runout of the landslide events, but simulations were a good fit with the path geometries. GeoClaw overestimated the material mobility and did not include material entrainment. Therefore, DAN3D is currently the more viable of the two programs for accurately modelling and characterising debris flow and debris avalanche events.

Acknowledgments

I owe thanks to a number of people for giving me advice and aid throughout the course of this thesis.

First, thank you to my supervisors Anders Solheim and José Cepeda for their help and support. Your advice and experience has been invaluable in helping me to complete this project, and I have learned so much from both of you over the last few years.

I would like to thank Mufak Said Naoroz from the University of Oslo Department of Geosciences for his help in setting up the laboratory experiments and completing the grain size analysis curves, and Zhongqiang Liu from NGI for his technical assistance and help working with GeoClaw and the NGI servers. Without your help I would have spent many frustrating hours trying to trouble shoot simulations in GeoClaw, and likely would never have gotten them running. I would also like to thank Krister Kristensen (NGI) for the assistance and advice during the field work in Stryn, as well as helping me to procure the helicopter images of both Oldedalen events. I cannot stress enough how helpful having high quality images from multiple angles taken immediately after the events occurred was in modelling and characterising the sites.

Thanks to Kasper Skjeggestad, Simon Anfinnsen, Daniel Lupp, and Craig Christensen for their help writing Matlab codes, proofreading, and giving me writing tips throughout the last two semesters.

Finally, thank you to all my friends in Norway who helped me settle into life in a new country, and helped me as I tried to learn a new language; even if some of you took a perverse pleasure in confusing me with dialects and writing in nynorsk. Additionally, a special thankyou to everyone in room 214 for the table tennis matches and Friday cakes.

Graeme R. Carey

31.05.2018

Table of Contents

List of Figures

List of Tables

1 Introduction

Flooding and slope instabilities including snow avalanches, rock falls, debris flows, debris avalanches, and quick clay slides, represent the main geohazards present in Norway and the largest threats to the population and infrastructure (Jaedicke, et al., 2008). In Norway, over 150,000 people live in areas threatened by flooding and landslides (Det Kongelige Olje- og Energidepartement, 2012). Globally, more than 3.3 million fatalities were attributed to natural hazards between 1970 and 2010 (The World Bank, 2010). In Norway specifically, these natural hazards have been the direct cause of 2000 deaths in the last 150 years, with snow avalanches having the greatest impact (Jaedicke, et al., 2008). The consequences of landslides can be hard to predict; however, it has been estimated that in an "average" year, 5-7 people in Norway, 18 people in Italy, 25-50 in the USA, 140-150 in China, 170 in Japan, and 180 people in Nepal will lose their lives as a result of landslides (Sidel & Ochai, 2006). In addition, the changing global climate is expected to increase the number of days with (, and intensity of), precipitation events leading to an increase in the number of precipitation-related landslides (Jaedicke, et al., 2008). Due to their high velocities and the large amounts of kinetic energy involved, debris flows and debris avalanches represent a serious risk to people and infrastructure in mountainous and hilly regions. Moreover, their high velocities and energy make them difficult to parameterise and model. This thesis focuses on the back-analysis and site characterisation of a number of debris flows and avalanches that occurred in Southern Norway, using DAN3D (*Dynamic ANalysis of landslides in Three Dimensions*) (McDougall, 2006). In addition, the open sourced modelling software GeoClaw (Berger, et al., 2011) was compared to DAN3D to determine its suitability for future back-analysis work.

This thesis is a part of the Center for Research-based Innovation (SFI) Klima 2050 initiative (http://www.klima2050.no). The stated aim of Klima 2050 is to *"reduce the societal risks associated with climate changes and enhanced precipitation and flood water exposure within the built environment"* (SFI, 2018). The planned eight year research project involves partners from the public and private sector across Norway, as well as many research and education institutions.

This thesis has three main goals:

1. To calibrate runout model parameters of 4 landslide events in Norway using DAN3D in order to assist in the prediction of similar events. Included in this is a physical description and characterisation of the landslide sites themselves.

2. To assess the suitability of GeoClaw for simulations of landslide runout by comparisons with the more widely tested DAN3D software (more than 380 citations in literature, compared with 41 citations for GeoClaw).

3. To develop a user manual to facilitate landslide modelling in GeoClaw.

The user manual created as part of goal number 3 is included as appendix A.

This thesis focuses on four new landslide events (two debris flows and two debris avalanches) in south-western and eastern Norway (Figure 1); one each near both Ringebu and Nesbyen, and two events in Oldedalen.

The thesis is divided into eight chapters including background information and scientific theory (2), a description of the methods used (3), detailed descriptions of the studied sites (4), results (5), a discussion of the presented results (6), and recommendations for improvements and future work (7). Appendices containing information on the detailed DAN3D output files and the aforementioned GeoClaw manual are also included.

Figure 1: Map of southern Norway showing the locations of the landslide events studied in this thesis. Four events were studied for, with two of them located approximately 800 m apart in Oldedalen. Background image from Norgeskart, edited by the author (Kartverket, 2018a)

2 Theory

The following chapter introduces background information for the topics covered in this thesis, beginning with defining landslides, debris flows and debris avalanches. Information on the societal importance of runout modelling, the geological and climatological setting of the study in Norway, and the two modelling software packages used for this thesis is also presented.

2.1 Mass Movement

A landslide, or mass movement, has been defined as the "downslope movement of soil, rocks, and organic matter under the influence of gravity" (Highland, et al., 2008). Despite the relatively simple definition, the types of motion and material involved, and how to best describe them, have been discussed and debated by engineers and geoscientists for decades. This thesis follows the nomenclature and naming conventions proposed by Varnes (1974), and expanded upon by Hungr et al., (2013). The term landslide is used, as mass movement also encompasses snow avalanches and can be misleading.

Classification schemes exist that attempt to describe landslides based on a number of characteristics, such as the type of material involved, volume of material, type of movement, velocity of movement, geometry of the failure area, and an associated deposit's geometry, age, and state of activity (Varnes, 1974). Using primarily type of movement and type of material as distinguishing factors, Varnes proposed a classification of mass movement processes including topple, fall, slide, lateral spread, and flow (Table 1).

For this thesis, the term runout is used to define the maximum length traveled by material as part of a landslide event. The travel angle is the angle between furthest runout point and the initial release point of the landslide.

Table 1: Update to the Varnes landslide classification scheme proposed by Hungr et al (2013). a denotes movement types that may reach extremely rapid velocities. (Hungr et al., 2013)

Type of movement	Rock	Soil
Fall	1. *Rock/ice* fall[a]	2. *Boulder/debris/silt* fall[a]
Topple	3. Rock block topple[a]	5. *Gravel/sand/silt* topple[a]
	4. Rock flexural topple	
Slide	6. Rock rotational slide	11. *Clay/silt* rotational slide
	7. Rock planar slide[a]	12. *Clay/silt* planar slide
	8. Rock wedge slide[a]	13. *Gravel/sand/debris* slide[a]
	9. Rock compound slide	14. *Clay/silt* compound slide
	10. Rock irregular slide[a]	
Spread	15. Rock slope spread	16. *Sand/silt* liquefaction spread[a]
		17. Sensitive clay spread[a]
Flow	18. *Rock/ice* avalanche[a]	19. *Sand/silt/debris* dry flow
		20. *Sand/silt/debris* flowslide[a]
		21. Sensitive clay flowslide[a]
		22. Debris flow[a]
		23. Mud flow[a]
		24. Debris flood
		25. Debris avalanche[a]
		26. Earthflow
		27. Peat flow
Slope deformation	28. Mountain slope deformation	30. Soil slope deformation
	29. Rock slope deformation	31. Soil creep
		32. Solifluction

2.2 Debris flows and avalanches

Debris flows are defined as a *"very rapid to extremely rapid flow of saturated non-plastic debris in a steep channel"* (Hungr, et al., 2001). "Debris" in this context refers to loose, unsorted material of low plasticity, containing more than 20% by volume gravel or coarser clasts, and less than 30% silt and finer particles, and may contain high concentrations of organic material (Hungr, et al., 2001). Debris flows can in this way be differentiated from mud or earth flows, which have a higher percentage of fine material and therefore some plasticity.

Debris flows are a global phenomenon and occur in regions with steep topographic relief and at least some precipitation. They play an important role in erosion processes, carrying sediment down from highland areas to river systems (Hungr, 2005). Josef Stini, an Austrian engineer, is the first author credited with a discussion of debris flows in his 1910 monograph *"Die Muren"*. He described how increased water flow through alpine channels leads to erosion and entrainment of material from the channel sides, eventually resulting in a viscous flow containing silt, sand, gravel, large boulders, and organic material (Stini, 1910; Hungr, 2005). Debris "flows" and "avalanches" were separated by Sharpe (1938), when he differentiated between a rapid flow of saturated unsorted debris in a channel (similar to the definition proposed by Stini (1910)), and a rapid shallow slide on a steep slope, with similar morphology to a snow

avalanche (Hungr, 2005). The absence of a pre-existing channel or flooding flow is the most important differentiation distinction between debris flows and debris avalanches.

From the updated Varnes landslide classification scheme, a debris flow is defined as a *"very rapid to extremely rapid surging flow of saturated debris in a steep channel"* with *"strong entrainment of material and water from the flow path"* (Hungr, et al., 2013). The same paper defines a debris avalanche as a *"very rapid to extremely rapid shallow flow of partially or fully saturated debris on a steep slope, without confinement in an established channel"* that can occur on all scales. Measured velocities for debris flows and avalanches can range from 0.5 m/s to 20 m/s (Costa, 1984). These definitions of debris flow and avalanche are the ones used for this thesis.

Entrainment plays an important role in the development of both debris flows and avalanches, as the initial release volume is often quite small compared to the final volume. This was noted by Stini (1910), and has been a constant factor in the various definitions of "debris flow" that have originated since. For debris flows, periodic damming can occur because of the confining nature of a steep channel and the turbulent nature of a debris saturated flow. Failure of these dams can lead to episodic surging in the debris flow (compared to a steady state flow), increasing entrainment and damage.

In the case of debris avalanches, a relatively small release volume entrains material as it moves downslope. The final shape and volume of the event are therefore controlled by the possible width of the landslide zone, and the thickness of the erodible layer (Hungr, et al., 2013). This often results in landslide scars with a distinct triangular shape (Figure 2), similar to that of a point release snow avalanche.

Figure 2: Example of a debris avalanche, showing the distinct triangular shape and downslope widening of the path. Skredestranda, Eid, Sogn og Fjordane. Photo: Anders Solheim 2017.

2.2.1 Behaviour

Debris flows exhibit characteristics intermediate between sediment charged water floods, and dry rock avalanches while belonging strictly to neither category (Iverson, 2005). While debris flows require saturated sediments by definition, unlike sediment water floods, material is also held in suspension by grain-grain interactions, not just fluid mechanical actions. However, unlike in dry rock avalanches where grains interact almost exclusively through physical contact with one another (collision/adhesion), debris flows are characterised by the additional presence of solid-liquid interactions (Iverson, 2005).

A typical debris flow can be broken down into an initiation zone or source area, a transport zone or path, and a depositional zone (Hungr, 2005). Typically, the initiation of a debris flow is a small slide in the headwall or steep bank of a gully or channel. The initial failure can be a slide, slump, topple, or fall on a slope between 20° - 45° (Costa, 1984). Slopes lower than 20° typically do not have enough gravitational potential energy to trigger sliding, whereas slopes steeper than 45° usually have too little soil cover for a debris flow or avalanche to initiate (Hungr, 2005). The transport zone of a debris flow extends from below the source area to the point where the rate of deposition exceeds that of erosion. Below this point is considered the deposition zone (Norem & Sandersen, 2012). Multiple debris flow or debris avalanche events (or multiple surges within a single event) can form a colluvial fan at the base of a slope, or where channel confinement ends.

The total length (L), or runout, of an event can be measured as the horizontal distance from the release area to the end of the deposition area. The ratio of the total elevation difference between these points (H), over the total runout length can be calculated to give a rough estimate of the angle the material traveled downslope (usually referred to as the travel angle, but also known as the reach angle, α) (Figure 3).

As mentioned above, debris flows often exhibit surging behaviour when the channel is temporarily blocked by large debris. These surges of coarser material can be separated by intersurge periods of watery, fine-grained material that makes it through the blockage (Hungr, 2005). Alternatively, surges can be caused by the non-simultaneous failure of multiple initiation zones, each feeding in to a single transport channel. Debris avalanches have also been known to exhibit surging behaviour, although this is usually due to retrogressive failure increasing the size of the initiation zone (Hungr, 2005). Surges are often characterised by a raised head, or front, composed of large grains followed by a dilute tail of muddy or silty material (Iverson, 2005; Costa, 1984).

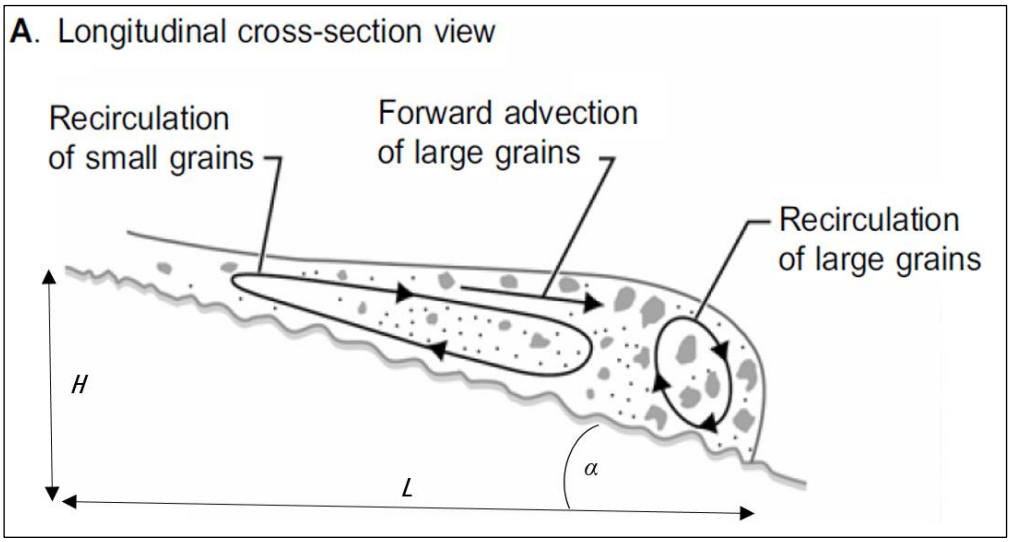

Figure 3: Cross-section of a debris flow surge depicting particle movement paths. Modified from Iverson (2005).

Levees form along the lateral boundaries of a debris flow and are especially prominent along any bends in the channel, where differences in flow velocity will often cause increased deposition on the outside bend (Costa, 1984). This results in levees of differing heights, and field observations are commonly used to estimate the speed of the debris flow (De Blasio, 2011) (Figure 4).

Figure 4: Channel levees beside a debris flow channel in the Rocky Mountains, Canada. The lines indicate the differences in elevation between inner- and outer bends. From Hungr, 2005.

While slope topography and channel geometry are important factors that control the final size, velocity, and runout of a debris flow, other factors such as particle size, erosion, and pore water pressure should also be considered. Erosion of debris flow channels, and entrainment of the material into the debris flow are thought to be driven by two major processes. Firstly, erosion caused by basal drag along the channel bottom, or undrained loading of channel material may create higher pore water pressures in the channel deposits, helping to incorporate those deposits into the debris flow (Hungr, et al., 2005; Sassa & hui Wang, 2005). Secondly, entrainment of material within a debris flow may also occur by the undercutting and destabilisation of channel banks along the flow path. Material that fails from these banks is incorporated into the main mass of the debris flow (Hungr, et al., 2005).

2.2.2 Causes and Triggers

Debris flows occur when saturated, unsorted rock and debris is mobilized by gravity on steep hill slopes. To trigger a debris flow, it is therefore required to have: *1*. a source of fine grained rock and soil debris, *2*. steep slopes in excess of 20°, *3*. a source of water or moisture (Costa, 1984). Sediment saturation is most commonly provided by precipitation events, snow melt, jökulhlaups (glacial lake outburst floods, GLOF), or the failure of volcanic crater lakes (Costa, 1984; Glade, 2004). Debris flows are triggered by either flowing water mobilizing loose soil or rocks on a steep slope or channel, or by another slope movement process (fall, topple, or slide) over loading saturated sediments on a steep gradient (Highland, et al., 2008).

The initial slope instability that develops into a debris flow can be caused by natural factors, anthropogenic factors, or a combination of both. Excavation at the toe of a slope can cause over-steepening of the natural slope angle, leading to failure. Modification of slopes and natural drainage patterns, e.g. by forestry, is the most common cause of slope instabilities in Norway (Schanche, 2014). Removal of vegetation on steep slopes, either by logging or wildfire processes, is a recognized factor leading to increased debris flow susceptibility (Highland, et al., 2008). Debris flows often occur simultaneously with flooding events and extreme precipitation, as well as earthquakes (Hungr, et al., 2013).

The most common debris flow initiation mechanisms in Norway are precipitation or runoff, where shallow flows in saturated or nearly saturated sediments develop into larger debris flows (Meyer, et al., 2012). Precipitation and the presence of moisture can trigger debris flows in four ways (Cepeda, 2009):

1. Increasing pore water pressures, leading to the failure of a slope along a rupture surface.
2. Increasing the slope weight due to wetting and saturation of sediments. The increased weight results in increased loading on the slope, creating instability.
3. Decreasing the slope confinement by eroding material at the base of the slope, resulting in a decrease in overall slope stability.
4. Progressive bulking of sediments entrained by runoff. Flows eventually reach a high enough concentration of solids that they exhibit non-Newtonian characteristics, and have greatly increased erosive capacity.

Precipitation thresholds have been developed to help predict debris flow occurrences. Common practice assigns an “intensity duration” (ID), and makes the assumption that for a given rain duration, there exists an intensity at which a debris flow is almost always triggered (the maximum ID threshold). The minimum ID threshold is the precipitation intensity duration under which a debris flow is very unlikely to be triggered (Meyer, et al., 2012). It has also been noted that the regional climate and soil cover have an impact on landslide initiation thresholds. Areas that receive more precipitation on an annual basis typically have higher thresholds required to trigger debris flow events (Meyer, et al., 2012). To account for these regional variances, Meyer et al. (2012) used a “precipitation day normal” (PDN) term defined as the average precipitation that falls on a typical rainy day (Figure 5).

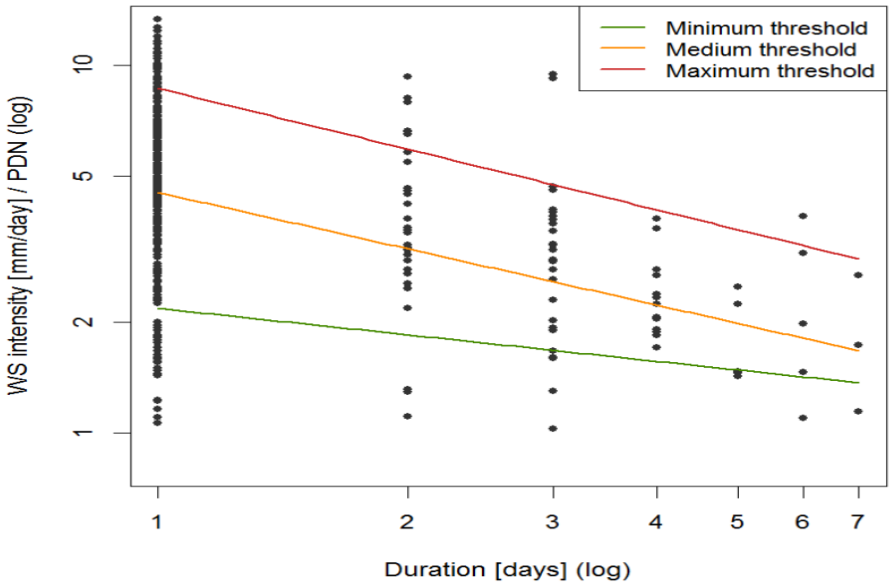

Figure 5: Normalized ID threshold curves for debris flow initiation in Norway, built from an analysis of 502 events. WS stands for water supply. From Meyer, et al. (2012).

2.2.3 Impacts

All slope movement processes greatly affect the built environment and human societies, whether it is directly by damaging houses and infrastructure, or more indirectly by blocking communication and transport routes. In most areas with steep terrain, the greatest threat to human structures and engineering works is from debris flows and avalanches, often recognized as the most destructive types of landslides (Highland, et al., 2008; Davies, 1986). Previous societies dealt with debris flows by experience, knowing about and avoiding high-risk areas due to folklore and local traditions. As the global population increases, such approaches are no longer feasible as humans further develop steep and mountainous regions (Jakob & Hungr, 2005).

In Norway, slope processes and floods are recognized as the main geohazards affecting the population (Jaedicke, et al., 2008), and approximately 72,000 Norwegians live in areas that are at risk from landslides (Det Kongelige Olje- og Energidepartement, 2012). Between 1980 and 2010, landslides in Norway resulted in damage claims for over 1.4 billion Norwegian kroner (adjusted to 2010 value) from national natural hazard funds (Det Kongelige Olje- og Energidepartement, 2012). This number only reflects insurance claims to national funds, and does not include claims to other sources, or the cost of damage to public infrastructure. The Norwegian Public Roads Administration (*Statens Vegvesen*) reports that one third of all registered landslide events (including snow avalanches) result in either partial or total road closures, and 25% of all pavement damages are caused by debris flows, making them the single most damaging type of event to infrastructure (Meyer, et al., 2012). Over 3000 fatalities have occurred in Norway in the last 200 years related to landslides and snow avalanches (Slettan & Smits, 2013). While most of these deaths are attributed to snow avalanches and a few large rock

avalanche events, more than 100 people were killed by landslides in soil between 1900 and 2000 (Figure 6).

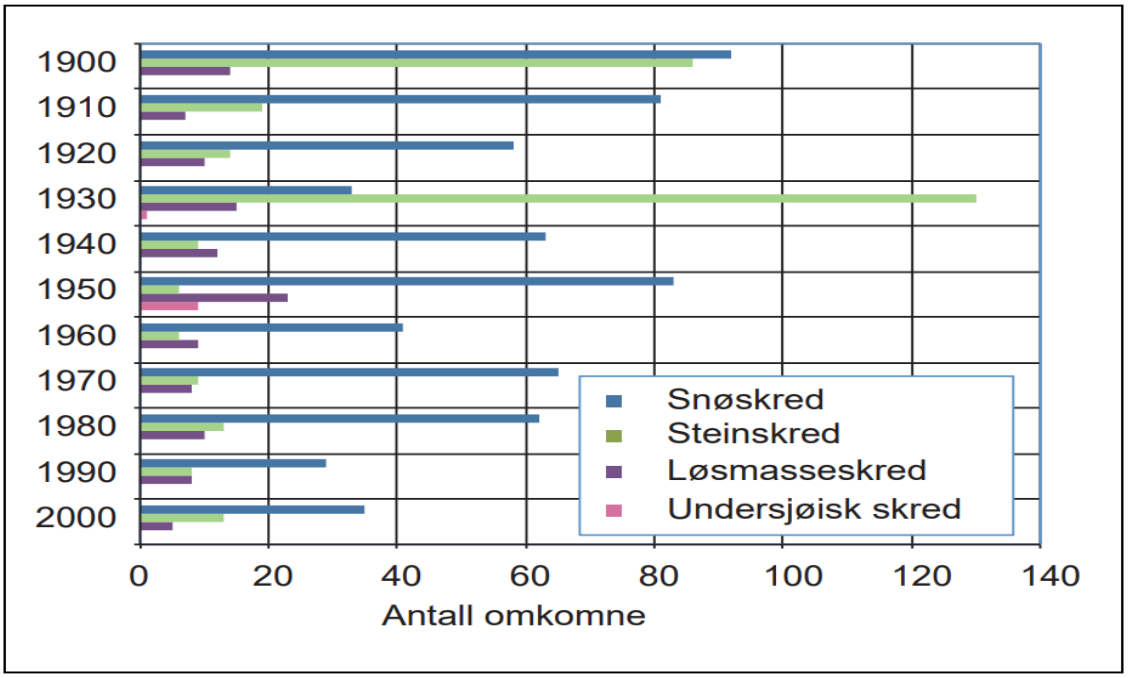

Figure 6: Deaths in Norway between 1900 and 2000 related to snow avalanches (blue), rock avalanches (green), landslides in soil (purple), and submarine slides (pink) (Det Kongelige Olje- og Energidepartement, 2012).

2.3 Selected Runout Models

This thesis uses two runout modelling programs, DAN3D (McDougall, 2006) and GeoClaw (Berger, et al., 2011). DAN3D was selected as it is free for academic use, and relatively easy to set up and run. GeoClaw is based on an open source software, and a variant has already been developed by NGI (BingClaw, Kim & Løvholt, 2017), so the software was available and easy to install on internal servers. Other runout programs that are commonly used in similar studies, such as RAMMS (*RApid Mass MovementS*) (SLF, 2010) and FLO-2D (FLO-2D Software Inc., 2018), require the purchase of costly licenses to use and were therefore not selected. The following sections give a brief overview of the theory behind each program, and the approaches they use when calculating runout.

2.3.1 DAN3D

DAN3D (*Dynamic ANalysis of landslides in 3 Dimensions*) is a program developed for the numerical modelling and dynamic analysis of rapid flow slides (debris flows and avalanches) (McDougall, 2006), based on the earlier program DAN (*Dynamic ANalysis of landslides*) (Hungr, 1995). DAN3D improves upon DAN by no longer requiring the user to input information on the landslide profile and path (allowing forward modelling of landslides, and

modelling of events that occur in more complex terrain), and by better simulating the energy losses within the sliding mass due to complex topographic effects (McDougall, 2006).

DAN3D works on an "equivalent fluid" approach, where user input is required to select a fluid rheology[1] (or rheologies) that the landslide is then modelled on. The internal rheology of the flow material is always assumed to be frictional (and controlled by the internal friction angle, φ), while the basal rheology and associated parameters are selected and calibrated through back-analysis or prior knowledge (McDougall & Hungr, 2009). It is a calibration model, so rheological parameters must be constrained by trial-and-error back-analysis of previous landslide events.

Material entrainment is a key component of debris flows and avalanches. It is accounted for by allowing volume flux across the basal boundary (simulation boundary between the "flow" on top of the "basement/slope"). It is assumed that material only enters the landslide due to basal erosion and scour, and the effects of bank collapse erosion are considered negligible and not accounted for. Further, the bulk density of entrained basal material is assumed to be the same as the bulk density of the initial landslide material. This is valid specifically for debris flows and debris avalanches, where the slide propagates in the same material layer it initiated in (McDougall, 2006).

DAN3D allows the user to select from a number of basal rheologies when modelling a landslide event. Multiple rheologies can also be defined along the path of an individual event (McDougall, 2006). For this thesis, the Voellmy rheology was selected to model landslide behaviour, as it has previously been determined to be a good simulation for rapid debris flows and avalanches (Anfinnsen, 2017; Dahl, et al., 2013; McKinnon, 2010; Cepeda, 2009; Bertolo & Wieczorek, 2005).

The Voellmy rheology combines the frictional and turbulent rheology models, where resistance and drag increase with velocity. This is expressed as (from Dahl et al 2013):

$$\tau = \gamma H \left(cos\alpha + \frac{a_c}{g}\right)(1 - r_u)tan\varphi + \gamma \frac{v^2}{\xi} \qquad \text{[Eq. 1]}$$

where γ is the unit weight of the material, H is the flow depth, α the channel slope angle, a_c the centrifugal acceleration, g acceleration due to gravity, r_u the ratio of the bulk unit weight of water (γ_w) over the bulk unit weight, φ the dynamic basal friction angle, v the velocity, and ξ a turbulence coefficient. A friction coefficient (μ) is used to simplify the friction term, where

$$\mu = (1 - r_u)tan\varphi \qquad \text{[Eq. 2]}$$

One mathematical artifact of the model is unrealistic extended motion within the landslide flow after the main event has come to rest; this must be accounted for by user judgement to control

[1]*Rheology* is defined as the study of deformation and flow of matter (Barnes, et al., 1989). In the context of this thesis, the terms rheology and rheologies are used to describe the mathematical expressions used by various models to simulate the flow and deformation of earth material.

when the simulation is complete (McKinnon, 2010). Further investigation of the solving of the Voellmy equations is outside the scope of this thesis. Back-analysis of the landslide events was conducted by modifying the turbulence and friction coefficients. It should be noted that per equation Eq. 1, increasing the friction coefficient should result in an increase in basal resistance, and increasing the turbulence coefficient should decrease it.

2.3.2 GeoClaw

GeoClaw is an open source software variant of Clawpack (*Conservation LAW PACKage*) designed for modelling of geophysical flows. It is a quasi-3 dimensional (depth-averaged in two horizontal dimensions) model for hyperbolic conservation laws (Kim & Løvholt, 2017; Clawpack Development Team, 2017).

GeoClaw consists of an open source Fortran computational core with interface and visualization programs written in Python (Berger, et al., 2011). Due to its open source framework, the program is easily adaptable and well suited for a number of research purposes (Clawpack Development Team, 2017). GeoClaw currently comes with Coulomb-Voellmy frictional rheological equations installed, and other works have adapted the code to include the Herschel-Bulkley rheology, suitable for mudslides and slides in sensitive clays (Kim & Løvholt, 2017). The Coulomb-Voellmy model has the form:

$$f = \mu_c hg\cos\theta + \frac{gv^2}{\xi} \qquad \text{[Eq. 3]}$$

where f are the frictional forces (resistance), μ_c is the Coulomb friction parameter $\tan\varphi$ (φ is the friction angle), h is the flow thickness, g the acceleration due to gravity, θ is the slope angle, v the flow velocity, and ξ the turbulence coefficient (Kim & Løvholt, 2017). This equation has a very similar form to [Eq. 1], with the notable difference that the friction coefficient is absent, and friction is instead calculated directly from the dynamic friction angle.

While DAN3D is built using a Lagrangian reference frame that moves with the local velocity (McDougall, 2006), GeoClaw formulates the equations of motion using an Eulerian reference frame that is fixed in space (Kim & Løvholt, 2017). An Eulerian reference frame is the conventional approach in fluid mechanics, however models calculated using one require more computational power, as many elements that require computation may be located in "void zones" outside the landslide motion (McDougall, 2006). However, the Lagrangian method is not without downsides; given that the mesh computational elements are connected to each other, distortion problems can arise in models with long runouts.

This thesis does not go into great detail upon the uses and customizability of GeoClaw. Instead, seeks only to compare the results of landslide back-analyses those of DAN3D and hence to determine GeoClaw's current suitability for use as a runout modelling tool for Norwegian debris flows and avalanches.

2.3.3 Rheology/Parameters

Large landslides and debris flows are complex phenomena and often exhibit behaviour intermediary between sliding and flowing (Crosta, et al., 2002). The most common rheological models used in dynamic debris flow analyses to simulate this behaviour are the Coulomb model, Voellmy model, Bingham generalized (or Herschel Bulkley) model, and the quadratic model (Pellegrino, et al., 2015).

Before the development of more sophisticated dynamic methods, a number of empirical formulae were developed from the study of global debris flow events to determine relationships between event volume, runout distance, elevation loss, and travel angle (Rickenmann, 1999). Previous empirical methods to determine landslide or avalanche runout and final volume typically centered around the calculation of a *fahrböschung* (also known as a reach angle, α) (Hürlimann, et al., 2008). The maximum runout of an event (L_{max}) has been related to the volume (V) and elevation drop (H) by the empirical formula:

$$L_{max} = 1.9V^{1.6} * H^{0.83} \quad \text{[Eq. 4]}$$

The reach angle is then related as (Hürlimann, et al., 2008):

$$\tan \alpha = \frac{H}{L_{max}} = 0.97V^{0.105} \quad \text{[Eq. 5]}$$

The laws of energy and mass conservation apply to landslide events, and the runout length is in part determined by the conversion of potential (gravitational) energy to kinetic energy (during sliding or falling) (Cepeda, 2009). Energy losses due to friction along the base and margins of the landslide due to friction are therefore important factors in limiting the runout length.

Corominas (1996) found in an empirical study of multiple landslide events (which included debris flows) that the elevation fall has little to no control on the angle of reach. The angle of reach is more likely controlled by the inherent properties of the material involved, such as inherent friction angle, volume of the sliding mass, and the mechanism of motion (Corominas, 1996). Elevation loss still strongly influences the horizontal travel distance of a landslide event, and a high elevation loss typically results in a landslide with a longer horizontal runout.

Previous studies (Bertolo & Wieczorek, 2005; Cepeda, 2009; Hürlimann, et al., 2008) have established the impacts of the main parameters in the two-parameter Voellmy model on landslide model behaviour. The friction coefficient included in the model largely controls the runout of the landslide simulation, though the initial volume of the slide and the path topography also play important roles (similar to the findings of Corominas (1996), where the inherent friction angle of a material strongly influenced the angle of reach and runout). The turbulence coefficient term influences the velocity attained by the flow.

2.4 Geological and Climatological Setting

This section provides a general overview of the geological and climate setting of Norway, with a focus on Southern Norway and the study area of interest.

2.4.1 Geological Setting

The underlying basement bedrock throughout most of Norway is dominated by metamorphic structures associated with the Caledonian orogeny, 500–400 million years ago (Nordgulen & Andresen, 2008). In parts of southern and western Norway, Proterozoic rocks (1700–900 million years old), and rocks from the Trans-Scandinavian Intrusive Belt (1850–1650 million years old) can be found (Figure 7). The Proterozoic basement rocks consist of granite intrusions, in some places transformed to gneiss by metamorphism related to the Caledonian orogeny. (Nordgulen & Andresen, 2008).

The Caledonian orogeny occurred as the ancient Iapetus ocean closed, leading to the collision of the Laurentian and Baltic continental plates, creating the continent Laurussia (Fossen, et al., 2008). The resulting mountain range resembled the modern-day Himalayas, and was composed of many different thrust sheets detached from Precambrian and late Ordovician basement deposits (Fossen, et al., 2008). The later breakup of Laurussia along the former Laurentian – Baltic border (resulting in the opening of the modern Atlantic ocean) lead to major faulting within Norwegian basement formations.

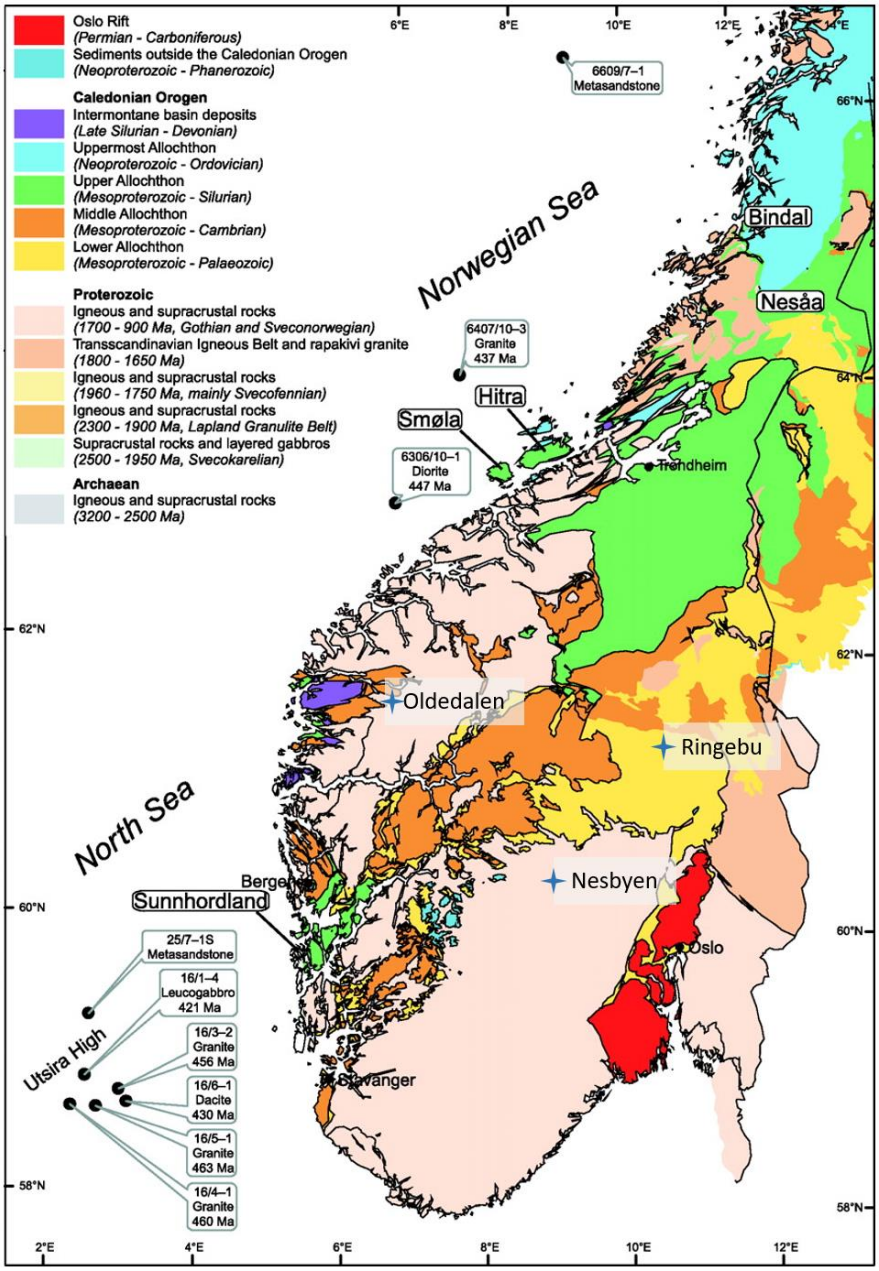

Figure 7: The crystalline composition and ages of basement rocks on the Norwegian continental shelf, with the locations studied in this thesis marked. Modified from Slagstad et al., (2011). The basement bedrock in Oldedalen is granitic intrusions, locally transformed to granitic or dioritic gneiss in some places by metamorphism related to the Caledonian orogeny. Nesbyen and Ringebu are both underlain by quartzite, phyllite, and metasandstone layers from the edges of Baltica basement formations (Nordgulen & Andresen, 2008).

Much of Norway's present landscape was sculpted by glacial processes between 2.6 million and 11,500 years ago. In this time frame, almost 50 distinct climate fluctuations can be observed, indicating a large number of distinct glaciation events (the exact number differs depending on the geologist's definition of a "climatic fluctuation") (Vorren & Mangerud, 2008). Most landforms in Norway, and many of the subsequent geohazard related issues, are related to these quaternary glaciation events (Fredin, et al., 2013). The most obvious example of this is the dramatic fjord landscape in Western and Northern Norway, where high mountain plateaus and peaks fall sharply into deep U-shaped valleys, often ending at sea level, with

elevation changes of up to 2000 m (Fredin, et al., 2013; Vorren & Mangerud, 2008). The erosion rates of Quaternary glaciers have been estimated to range from 10^{-4} mm/year to 10^{-1} mm/year (Delmas, et al., 2009), indicating an uneven distribution of the erosive forces.

Where groundcover in Norway is not simply exposed bedrock, the predominant subaerial soil is till deposited during the last glaciation (Olsen, et al., 2013). This till layer is typically no more than 5 or 6 m thick, although in some large river valleys the mixture of till and fluvial deposits can average closer to 10 m thick, and has been measured at up to 100 m thick in some parts of Gudbrandsdalen (Olsen, et al., 2013).

2.4.2 Climatological Setting

Currently, the Norwegian climate benefits from the warming effects of the North Atlantic Current, making average temperatures more temperate than may be expected given the high latitude (Rossby, 1996). Norway is divided in to two major climatic regions:

1. Marine west-coast climate

2. Continental sub-arctic climate

Coastal, western Norway receives more precipitation than the interior, due to a combination of moist coastal air masses and orographic uplift (Hanssen-Bauer, et al., 2015). Studies have found that south-west oriented slopes in Norway are more susceptible to debris flows, due to enhanced melt runoff driven by more intense solar radiation and wind on these aspects (Meyer, et al., 2012).

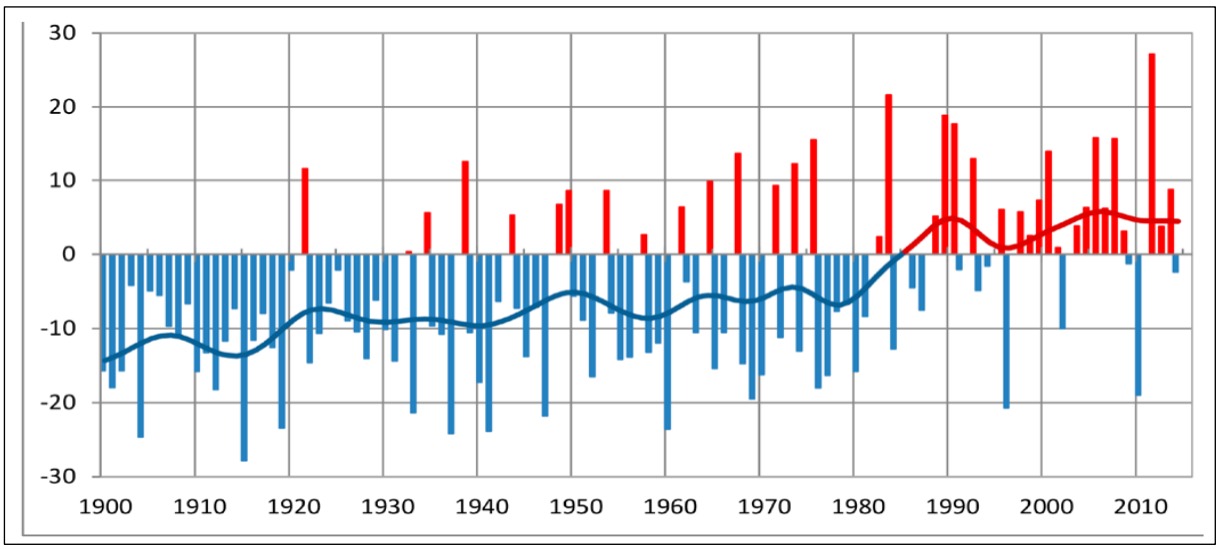

Figure 8: Mean annual precipitation in Norway, presented as deviation (%) from mean annual precipitation during the period 1971-2000. (Hanssen-Bauer, et al., 2015)

In the next 100 years, changes to the global climate are expected to have a large impact on the Norwegian climate. Recent trends have shown an increase in mean annual temperature and

precipitation (Figure 8), with 2016 being 1.5°C above average (Miljødirektoratet, 2017). The mean annual temperature is expected to increase by between 2.3°C–4.6°C by 2100, with the temperature increase being most obvious in winter. Precipitation is expected to increase throughout the country, especially in winter, however summer precipitation may decrease in parts of eastern and southern Norway (Miljødirektoratet, 2017; Sorteberg & Kvamstø, 2008). The number of days with "heavy rainfall" (defined as the 99.5th percentile for daily precipitation between 1971-2000) is expected to double by 2100, with the rainfall intensity for these days also increasing (Hanssen-Bauer, et al., 2015).

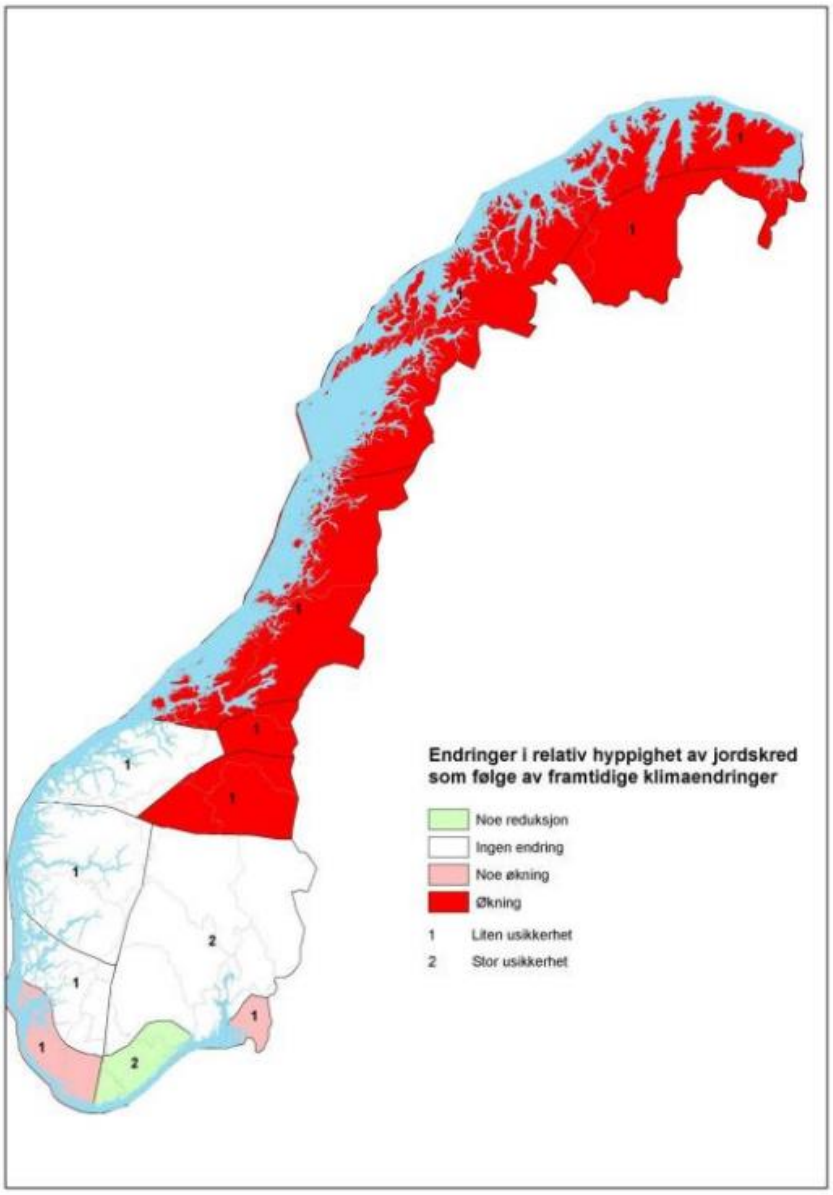

Figure 9: Regional changes in frequency of landslides in soil due to climate change in Norway. Green: some decrease. White: no change from current conditions. Light red: some increase. Dark red: increase. From (Aaheim, et al., 2009).

Figure 9 shows the results of an earlier study of changes in landslide frequency with climate change over the next 50 years, indicating an increase in the expected number of landslide across most of Norway.

2.5 Risk and Hazard Assessment

Interest and awareness in landslide hazard assessment has been steadily increasing globally since the late 1980's and early 1990's (Aleotti & Chowdhury, 1999), likely due to two main reasons: *1.* Increasing awareness of the socio-economic importance of landslides, and *2.* the increased pressure development and urbanization exerts on the environment.

The precise terminology used to define "risk" and "hazard" sometimes changes between disciplines, and a consensus on terms and definitions does not yet exist. This thesis is based on the terminology proposed by Fell et al. in 2005, and modified by McDougall (2006) and Dahl (2011) (Dahl, 2011; McDougall, 2006; Fell, et al., 2005). Here, risk (to either property or human lives) can be defined most simply as the product of hazard and consequence, or mathematically as:

$$R = H\ x\ C \qquad \text{[Eq. 6]}$$

In this context, "hazard" refers to probability of an event occurring at a specific location, while "consequence" encompasses potential damages caused by that event (also called "elements at risk", and takes into account the vulnerability of these elements). More completely, risk can then be expressed as:

$$R = P_L \times P_S \times P_T \times V \times E \qquad \text{[Eq. 7]}$$

Where P_L is the annual frequency of landslide occurrence, P_S is the probability of the landslide runout reaching a certain length (the probability of a certain spatial impact from a landslide), P_T is the temporal probability that the element at risk will be affected by the landslide (in the case of immovable objects such as buildings or infrastructure this is 1, however for humans the value changes depending on the element in question), V is the vulnerability of the element at risk, and E is the value of the element at risk (McDougall, 2006).

Landslide hazard risk assessment and zonation is built upon 4 principle assumptions (Aleotti & Chowdhury, 1999):

1. Landslides will always occur in the same geological, geomorphological, and hydrological conditions as they have in the past
2. The main conditions that lead to or cause slope instability are controlled by identifiable physical factors
3. The degree of hazard can be evaluated
4. All types of slope failures can be identified and classified

To accomplish this, a number of challenges must be overcome, most notably:

1. The discontinuous nature (in time and space) of slope failures
2. The difficulty in identifying the causes and triggering mechanisms of a specific slope failure, and building cause-effect relationships
3. The lack of complete historical information and records regarding these geomorphological processes

While assigning a number to the "risk" or "hazard" related to a given slope failure sounds relatively simple, it quickly becomes difficult due to the number of associated unknowns. Ideally, the perfect landslide hazard map for a give region would contain information on the spatial distribution, temporal distribution (recurrence interval), volume, velocity, travel distance, and retrogression limit of all landslide events within the study area. A flowchart showing the methodology for performing a spatial landslide risk assessment is presented in Figure 10.

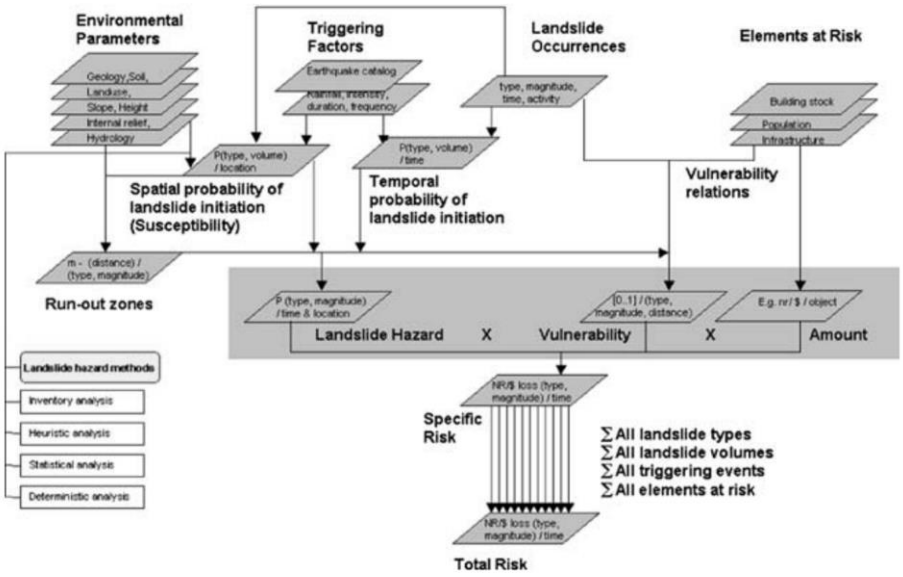

Figure 10: Flow chart detailing the steps required to perform a landslide risk assessment (van Westen, et al., 2006).

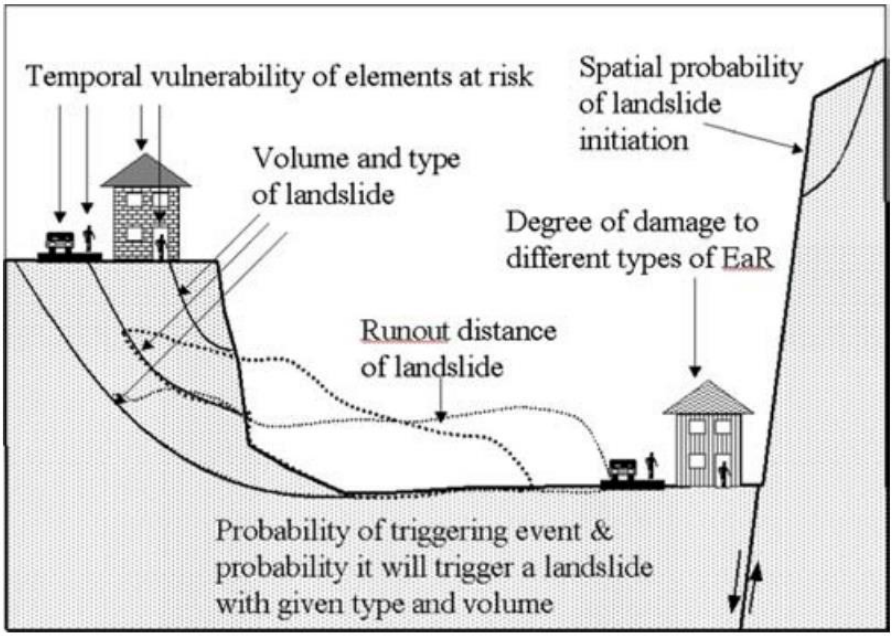

Figure 11: Illustration outlining some of the difficulties in landslide risk assessment. EaR refers to elements at risk. (van Westen, et al., 2006)

Figures 10 and 11 show some of the difficulties and inherent uncertainties that must be accounted for when attempting to perform a landslide risk assessment, and creating hazard zoning maps. In recent years, the emergence of GIS systems and the increasing availability of high quality remote sensing data has made creating and updating landslide inventory maps easier. Improved landslide runout prediction models, and research efforts (including this thesis) focused on better understanding the rheological parameters of flow like landslides will lead to more accurate runout estimations, meaning hazard zoning maps can be more accurately prepared.

In Norway, the development of risk and hazard maps at the national level is the responsibility of the Norwegian Water Resources and Energy Directorate (*NVE*) (Det Kongelige Olje- og Energidepartement, 2012). Geological data from the Norwegian Geological Survey (*NGU*), and topography data from the Norwegian Mapping Authority (*Kartverket*) is combined with an extensive database of over 30,000 historic landslide and snow avalanche events (NVE, 2018) to produce hazard and risk maps for the country. These maps are then used by the national government and municipalities for project and land-use planning. Back-analysis studies such as this thesis are an important part constructing these maps, as the model parameters calibrated from such studies can be used to better predict the runout and spatial probability of future landslide events. Figure 12 is an example of a landslide hazard map from near Loen, Stryn municipality, Norway.

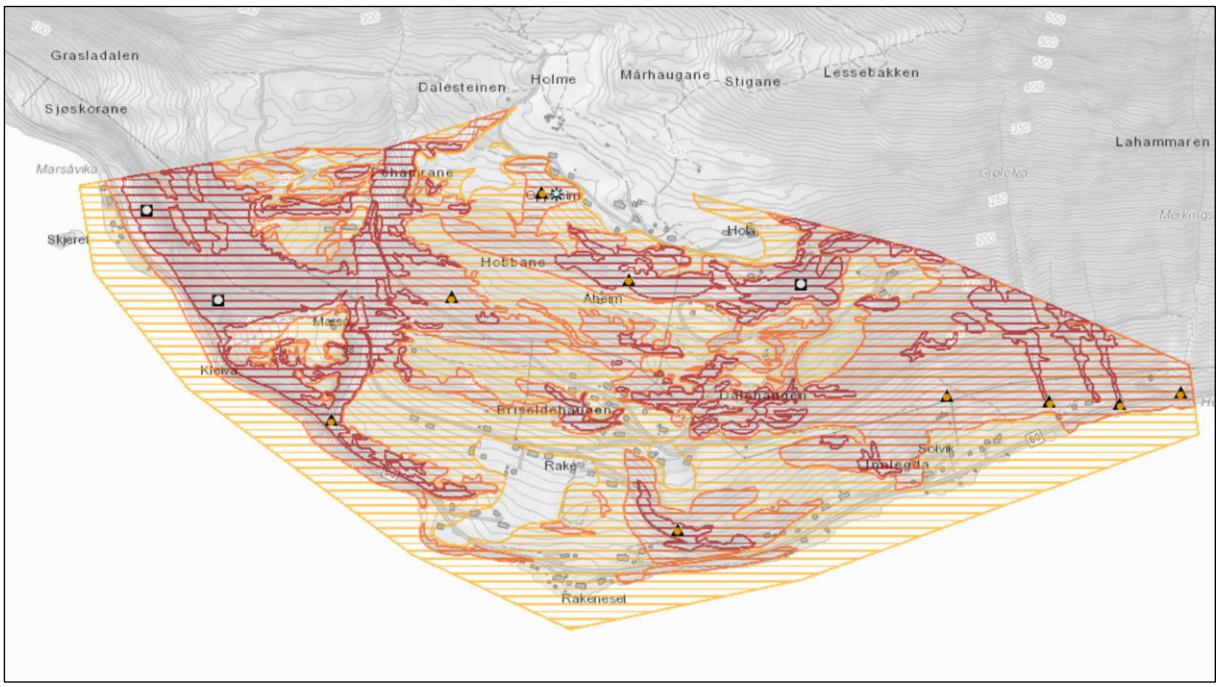

Figure 12: An example of a landslide hazard map for an area of Nordford, near Loen, Norway. Taken from NVE atlas (NVE, 2018). The coloured areas represent areas with an annual probability of an event of 1/100 (red), 1/1000 (orange), and 1/5000 (yellow). Orange circles on black triangles represent debris flow hazards, grey circles on black squares represent rock fall, and a blue circle with radiating black lines represents snow avalanche.

3 Methods

The following section presents the methods used to collect and analyse data for this thesis, ranging from the initial field work and sample collection, the processing of imagery data to create topographic data files, and the process used to determine the back-analysis parameters.

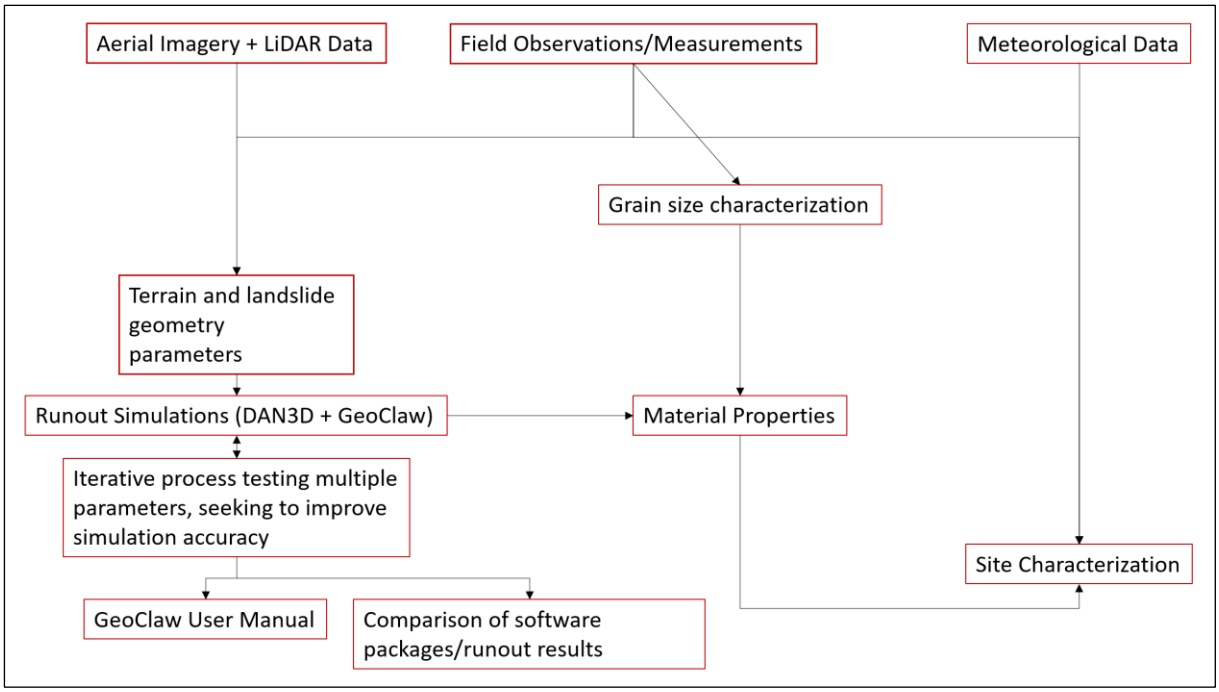

Figure 13: Flow chart showing the processes followed in this thesis.

3.1 Field Work

After selecting locations and case studies for the thesis, site visits were conducted in late spring and early fall 2017. The goals of these site visits were:

1. to obtain a better understanding of the area geometry than could be obtained simply by analyzing aerial photos and satellite imagery;

2. to retrieve soil samples from the events for use in constructing grain size distribution curves; and

3. where possible, to closely investigate the landslide release area, track, and deposit, with the hope of identifying any remaining features such as levees, channel erosion, and markings on trees or structures that could be used to validate model results.

The Nesbyen site was selected in late May 2017 due to the frequency of debris flow events in the area, and the availability of high quality LiDAR and aerial photography data. A visit to the site was conducted on June 14th, with partially overcast skies but otherwise favourable weather

conditions. Three soil samples were taken from the site, one from the initial release area, and two from the channel banks approximately 40m downslope from the release area.

The Ringebu and both Oldedalen sites were selected in August 2017 due to the availability of remote sensing data, and the complexity of the slides themselves (the split channels from Oldedalen 2, and the size and large curve to Oldedalen 1). These sites were visited September 12th - 14th 2017, and soil samples were collected.

From all the field investigations, a total of 10 soil samples were collected. Samples were taken from the track and release area of Oldedalen 1, multiple locations in both tracks of Oldedalen 2, and the release area of Ringebu. These samples contained grains ranging in size from clay to coarse gravel. Larger clasts present in the samples were photographed beside the sample, with a measuring stick serving as a scale, but were not transported back for further testing (due to logistical challenges).

3.2 Grain size analysis

Grain size analysis was performed on 7 of the 10 samples collected during the field work described in the previous section. Three samples were not analyzed, as the total bulk weight of the sample was too small to give a representative depiction of the sample when sieving (following sample size guidelines relating to the largest present grain diameter (Statens vegvesen, 2014)).

Due to the wide range of grain sizes present in till material, three different methods for determining cumulative grain distributions were used in combination with one another to return the final grain size distributions. The coarsest (large gravel and small cobble) sized components were manually measured and appended to the curves. Sieving was used to separate all fractions between 16 mm and 0.5 mm, and a Coulter test was used to determine the grain size distribution of the smallest fraction (0.5–0.002 mm).

Lab analysis was conducted at the Department of Geosciences sedimentology lab at the University of Oslo. Grain sizes were classified based on the Wentworth scale of grain classifications (Table 2).

Table 2: The Wentworth scale for grain classification, reproduced by the author from (Wentworth, 1922).

Millimeters (mm)		Micrometers (μm)	Phi (ϕ)	Wentworth size classes	
	4096		-12.0	*Boulder*	*Gravel*
	256		-8.0	*Cobble*	
	64		-6.0	*Pebble*	
	4		-2.0	*Granule*	
	2.00		-1.0	*Very coarse sand*	*Sand*
	1.00		0.0	*Coarse sand*	
1/2	0.50	500	1.0	*Medium sand*	
1/4	0.25	250	2.0	*Fine sand*	
1/8	0.125	125	3.0	*Very fine sand*	
1/16	0.0625	63	4.0	*Coarse silt*	*Silt*
1/32	0.031	31	5.0	*Medium silt*	
1/64	0.0156	15.6	6.0	*Fine silt*	
1/128	0.0078	7.8	7.0	*Very fine silt*	
1/256	0.0039	3.9	8.0	*Clay*	*Mud*
	0.00006	0.06	14.0		

3.2.1 Sample preparation and sieving

In sieving, the percentage of the total sample weight within each grain size interval (example: 2–1 mm) is measured and cumulatively plotted.

The samples collected in the field (2–4 kg in weight, though all contained some moisture) were spread out on a large tray, and mixed evenly to ensure that any subsample was representative of the grain size distributions present. The sample was then divided into four equal portions, and two diagonal portions were removed. The remaining half sample was then again thoroughly mixed, and divided in half. One of these portions (or ¼ of the total sample collected in the field) was then prepared for further testing. As the samples collected were slightly damp from the field, and most large clasts had a thin film of clay material covering them, wet sieving was used to prepare the samples for analysis. In a large, flat bottomed cylindrical dish, the sample was gently washed through 2000 μm and 500 μm sieves in order to remove clay and silt particles stuck to larger gravel clasts. All water and silt particles that passed through the sieves were collected in the cylindrical dish. The samples and water were then placed in plastic containers, and set to dry for 24 to 48 hours in an oven at 75°C.

After drying, the samples were weighed to determine the total weight of sediment in each. Samples were then passed through standard 16000 μm, 8000 μm, 4000 μm, 2000 μm, 1000 μm, and 500 μm square aperture sieves, being agitated and shaken vigorously for a 5–8 minutes to ensure that all grains of appropriate sizes had filtered through. Each size fraction (>16000 μm, 8000–16000 μm, etc.) was then carefully removed from the sieve onto a sheet of standard A3 paper, and then weighed in a plastic container of known mass. In this way the mass of sample in each grain size category greater than 500 μm was calculated. All grains with size less than

500 μm were also collected and weighed, and were analysed using a Beckman-Coulter machine. For further, detailed information on the sieving process and standards, refer to the handbook by the Norwegian Public Roads Authority (Statens vegvesen, 2014).

3.2.2 Coulter test

To accurately determine the distribution of silt and clay particles within the samples, laser diffraction tests using a Beckman Coulter LS 13 320 laser diffraction particle size analyzer were conducted. The instrument measures the scattering patterns generated as particles of various sizes, suspended in water, are illuminated by laser light. The volume of sample suspended in water is measured, as well as the volume and diameter of each particle. The instrument then plots the cumulative distribution of particles within each sample. To simplify the calculations and reduce computational requirements, all particles within the analysis are treated as perfect spheres, so that only one parameter is necessary to define them (diameter) (Beckman Coulter, 2011).

The portion of each sample remaining after sieving (below 500 μm) was thoroughly mixed, and placed on a scale and zeroed. Approximately 0.2 g – 0.7 g of material representative of the total sample (depending on the grain size of the sample) was removed and placed in a small glass beaker. Five to ten millilitres of 5% calgon (natriumpyrophosphate) solution was added to the beaker, and it was then left for 5 minutes in an ultrasonic bath to ensure grain dispersion. The sample was then added to the Beckman Coulter analyzer, and if necessary more was prepared so that the obscuration in the machine was between 8% and 12%. A minimum of two tests were done per sample. If the results of the two tests were similar, they were averaged and taken as the grain size distribution for that sample. If large irregularities existed, the analyzer was cleaned and recalibrated, and the samples were tested again.

3.2.3 Appending large clasts

The maximum sieve size available during the analysis was 16 mm, and the largest clasts collected in the field were on the order of pebbles and small cobbles (Table 2). These large clasts were manually added to the grain size curves. The clasts were measured and weighed, and then added at the end of the grain size distribution curves in the appropriate size categories. For the largest clasts where the weight could not be determined by scales (the weight was above the maximum measurable by the scales used by the author), the weight was calculated first by measuring the volume (using a ruler, and making assumptions about the clasts shape; either roughly spherical or rectangular), and then by multiplying the volume by an assumed density of 2.7 g/cm^3 (standard value for granites and gneiss).

3.2.4 Grain size distribution curves

As the different methods used to determine the grain size distribution return slightly different parameters, the data must be converted to be plotted together. The Coulter analysis returns the

volume percentage of a sample below a certain grain size threshold, while sieving returns the weight percent. Results from the Coulter analysis were therefore adjusted by multiplying by the weight of the Coulter sample. Grain size curves could then be constructed plotting cumulative weight percent by grain size. The final curves are presented in Chapter 5.

3.3 Runout Simulations

Runout simulations were conducted using both DAN3D and GeoClaw software packages, changing the input parameters for the Voellmy rheology to attempt to best model the observed landslide events.

3.3.1 DAN3D – Numerical Parameters

In addition to the back-analysis of the selected landslide cases, a brief inspection of the impact the numerical parameters have on simulation outputs in DAN3D was conducted, with the aim being to see if non-default parameters significantly improve the model results. To accomplish this goal, the Nesbyen case was selected, as it had the most available data, and therefore the fewest unknowns.

Simulations were set up to individually test the impact of changes to the time-step, number of particles simulated, and smoothing length constant, with all other parameters being held constant. Erosion was not modelled for these simulations. Friction and turbulence coefficient values of 0.12 and 550 m/s^2 were used, as intermediary values within the range of possible parameters for this site.

The final runout achieved by these simulations and the modelled deposit geometry was compared to field observations to determine simulation validity.

3.3.2 DAN3D

Input data in DAN3D is classified into three major subgroups: grid files (topography data), material properties, and control parameters. (O. Hungr Geotechnical Engineering Inc., 2010)

Control parameters represent the numerical properties used to run the back-analysis equations, and are not related to the material properties of the sites themselves. The control parameters in DAN3D are:

- number of materials to be simulated (maximum 4),
- number of particles (maximum 4000),

- erosion rate (which can be either entered based on prior knowledge, or calculated by DAN3D based on the differences between initial and final volume, and the length of the erodible zone), and

- time-step, the time interval between each calculation.

The setup of experiments testing the impact of these control parameters on simulations results is discussed in section 3.3.3 DAN3D – Numerical Parameters. For the back-analysis simulations, the default control parameter values were used (2000 particles, and a time-step of 0.1 seconds).

Grid files in DAN3D consist of the path topography file, source topography file, and erosion map file. The path topography file contains the topography of the surface over which the landslide flows, while the source topography file is defined as the depth of the sliding mass at the initial time. An erosion map file contains information on the materials spatial distribution but is only required if more than one material is being used in the simulation (i.e. the landslide path passes through different materials, and the user wishes to simulate their effects). Erosion files were used for both Oldedalen cases to attempt to simulate the presence of Oldevatnet Lake. Each grid file needs to have identical size dimensions for the program to function properly. The path topography files were created using publicly available LiDAR data from before the landslide occurred, downloaded from hoydedata.no (Kartverket, 2017). One meter resolution digital elevation models (DEMs) were used for each case. For the Nesbyen case, LiDAR data was also available from after the landslide, so the source topography file could be created by subtracting the two DEMs, returning the volume of material that was "missing" from the source area. For all other cases, the source topography file was created in ArcGIS (ESRI, 2011) based on field observations of the release area and aerial photos. A detailed guide into preparing the path and source topography files for DAN3D can be found in a report prepared by the International Center for Geohazards (ICG, 2010).

DAN3D includes 10 different material properties that can be edited based on the user's choice of material rheology (frictional, Newtonian, plastic, Bingham, or Voellmy). Several materials with different rheologies can be used simultaneously, depending on how many materials were selected in the control parameters, and whether or not an erosion map file has been created for the simulation. For this thesis, simulations were conducted using the Voellmy rheology. The internal friction angle (φ_i) was set to 35° (the default value in DAN3D). The friction coefficient (μ) was tested systematically at values of 0.1, 0.15, 0.2 and 0.3 for the different landslide cases, with this range being defined by previous studies (Quan Luna, et al., 2013). The turbulence coefficient (ξ) was varied from 150–1000m/s^2, again with the range being defined by previous studies. The unit weight of each landslide was set to 20 kN/m^3 (the default value in DAN3D), and the maximum erosion depth was determined from field observations. This approach of systematically varying the turbulence and friction coefficients in isolation was time consuming, however it allowed for a good understanding of the sensitivity of the program software and each simulation case to changes in the parameters. An accurate estimation of the back-analyses parameters for each case was obtained by comparing results from the systematic analysis to the

real observed landslide event. Simulations using these estimated variables were run to double-check their validity.

Results for each simulation were extracted from the DAN3D output files, as well as screen captures of the depositional plot taken with the final time-step. As DAN3D does not return a final runout parameter (the program returns the coordinates of each particle at any time-step, and also the final coordinates of the center of mass), the screen captures were overlain on aerial photos and the runout distance measured using ArcGIS. A full list of input parameters and detailed run results for each landslide case is presented in appendix B. These results were compared to field observations and aerial photos of the landslide events to validate the back-analyses.

3.3.3 GeoClaw

Similarly to DAN3D, GeoClaw requires information on path and source topography files to simulate a landslide event. However, GeoClaw cannot simulate material erosion, or the presence of more than one material, so an erosion map file is not necessary.

Two compare the results from the two programs, simulations with identical parameters were run. To do this, simulations with no erosion were run in DAN3D for the following sets of input parameters:

Table 3: Sets of parameters used during simulations to compare DAN3D and GeoClaw.

μ	0.15	0.15	0.15	0.1	0.2
ξ (m/s²)	150	450	750	450	450

For each of these simulations, a maximum run time of 600 seconds was used, with a time-step of 0.1 seconds.

A more detailed guide to setting up landslide simulations using GeoClaw is included in appendix A.

Results in GeoClaw are presented as plots and a text file containing four columns (deposit thickness, velocity in the x direction, velocity in the y direction, and elevation above sea level of each grid node with topography data) generated for each minute of the landslide event. From this data it was possible to determine the extent of the landslide runout and maximum thickness of deposit, and follow how they evolved with time. Unlike in DAN3D, the "maximum velocity" of the landslide is not returned as an output, as only data from each minute is returned in the output files (the maximum velocity of the landslide likely does not fall exactly on second 60 or 120, so is likely not returned). GeoClaw simulation results were analysed using Matlab and ArcGIS software, and compared with the results obtained from DAN3D.

4 Site Descriptions

The following chapter contains information on each of the sites studied in this thesis. Information on the site morphology, geologic setting, and geography is presented.

4.1 Nesbyen Arnegårdslie

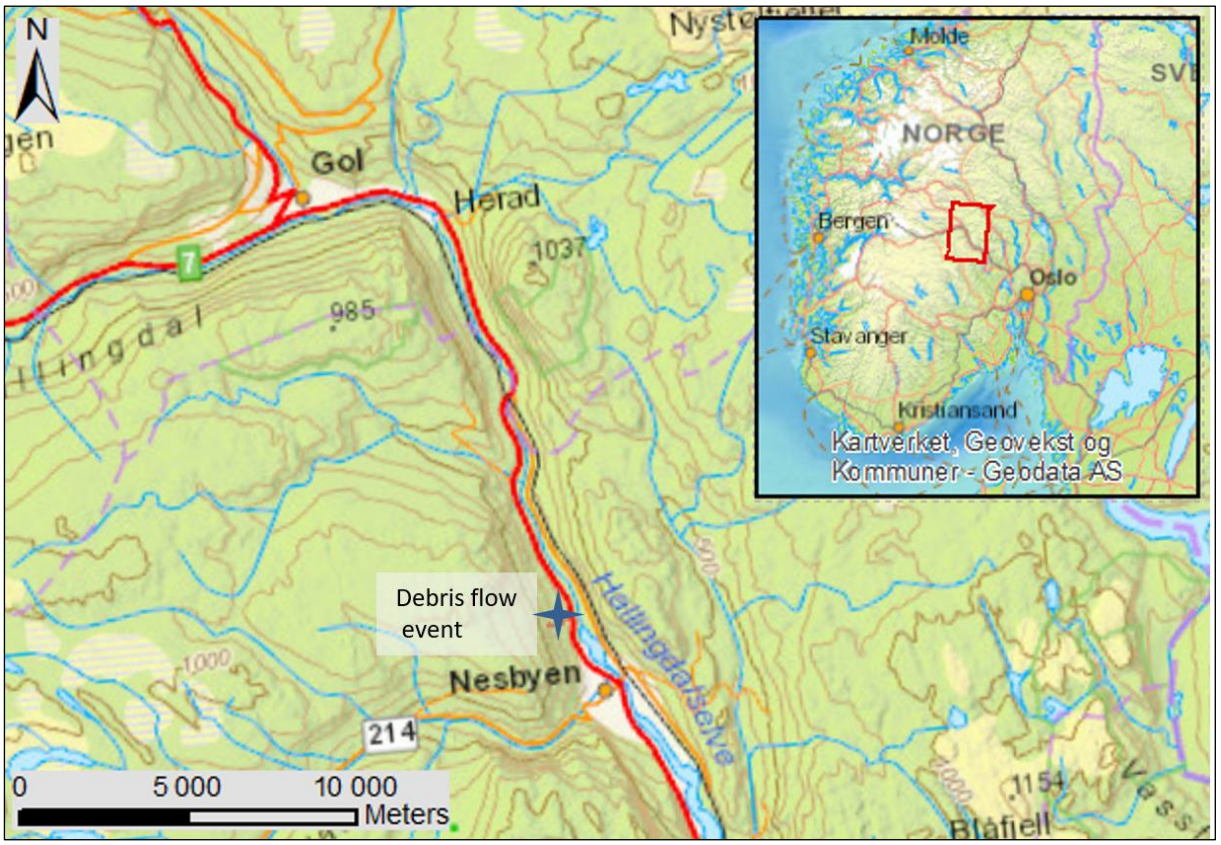

Figure 14: Topographic map of northern Hallingdal, showing the location of the studied debris flow event north of Nesbyen.

The Nesbyen site is located in Arnegårdslie, 2 km north of the town of Nesbyen, administrative center of the Nes Municipality, Buskerud County (Figure 14). The debris flow occurred on 25.05.2013 following sustained heavy precipitation the previous days. The site is located on an east-facing slope of the Hallingdalen valley. The debris flow initiated at two locations 65 m apart along a forestry track, 390 meters above sea level (masl). The two initiation zones merge into one channel 180 m down-slope. A number of previous debris flow events have been recorded in the immediate vicinity (though not in the same channel as this event) in 1982, 1996, 2007, and 2011. One of the 2007 events occurred 150 m north from the main channel of this (2013) debris flow (Figure 15). The debris flow has a runout length of 660 m, and an elevation difference of 216 m, giving a travel angle of 18° and H/L ratio of 0.33. The landslide damaged two houses along Alfarvegen, and resulted in the evacuation of 21 people. After the event, a berm was constructed to protect the community from future events (NGI, 2013a).

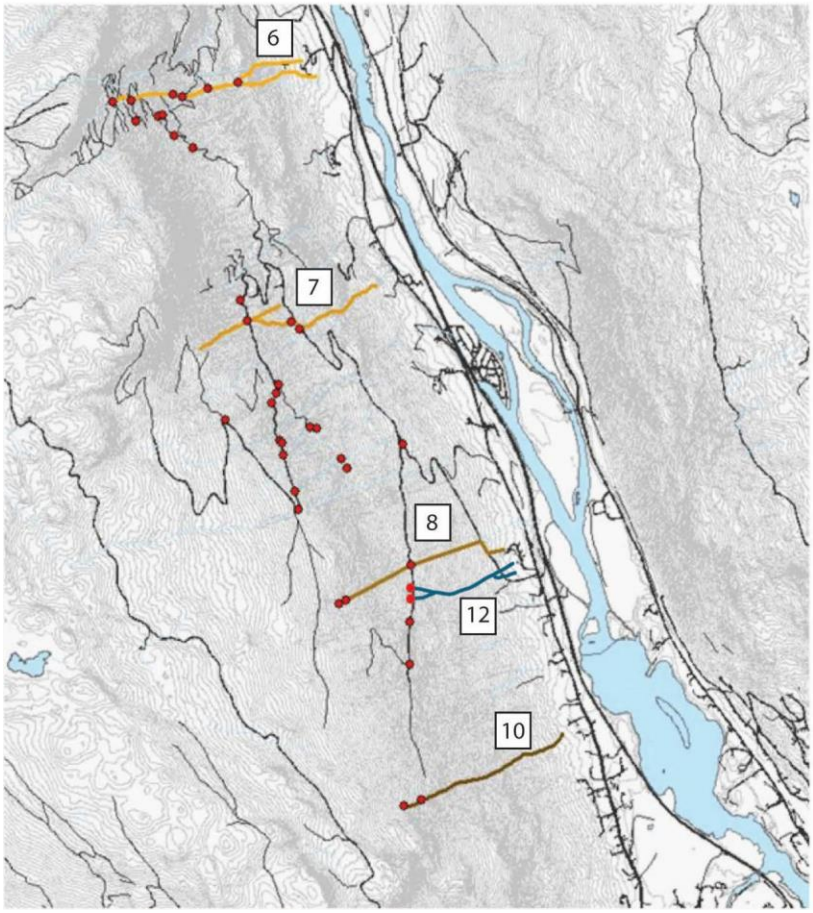

Figure 15: Landslide events along the valley side north of Nesbyen. Events from 2007 (6, 7, 8), 2011 (10), and 2013 (this study, 12) are shown. Red dots indicate other areas of noted slope failures that did not develop into debris flows or avalanches. The authors of the report drew attention to the apparent clustering of these failures along the forest roads (black lines). (Bargel & Lund, 2016).

4.1.1 Terrain

The debris flow channel is situated on an open slope with an average angle of 20°. With the exception of a few cleared areas, the hillside is thickly covered in vegetation (mixed forest), and a number of forestry roads and tracks make their way up the slope. The top of the valley is situated 850 masl, and there is a river (Hallingdalselva) at the bottom, 160 masl. As shown in Figure 15, a number of debris flow channels exist along the slope, most originating along the forest roads. The landslide event discussed in this thesis crossed this road again toward the end of its runout, before ending in a group of six houses along Alfarvegen.

4.1.2 Bedrock and Soil Characteristics

Basement bedrock in the area is mapped as consisting of Precambrian quartzite and metasandstones with some migmatite and gneiss intrusions (NGU, 2018a). Few outcrops of exposed bedrock exist in the study area, as it is covered by a thick layer of surficial material.

These surficial deposits are mostly glacial till on the western side of the valley, with fluvial and glacial fluvial deposits on the Hallingdalselva flood plain (Figure 16).

Figure 16: Quaternary sediments map of part of Hallingdalen, with the extent of the Nesbyen debris flow shown as the red polygon, center (NGU, 2018b).

4.1.3 Release Area

As stated above, the debris flow event had two separate release areas, 65 m apart, which merge in to a single channel downslope. The debris flow occurred along an unpaved forest track, where failure of two 10m x 10m areas initiated the debris flow (Figure 17). The initial volume of the event was calculated to be 460 m^3, which is consistent with rough volume estimates from shortly after the landslide occurred sizing the two release areas at 200 m^3 and 300 m^3, respectively (total initiation volume of approximately 500 m^3) (NGI, 2013a).

Figure 17: The larger of the two initiation zones, as seen from the forestry road. (Bargel & Lund, 2016)

4.1.4 Transport Zone and Deposition

The smaller of the two initiation zones eroded a channel 8–10 m wide, before merging with the channel eroded by the larger initiation zone after 180 m. This larger channel is 20–25 m wide, and has a slope angle of 25°. The channel banks are undercut and appear stratified, with a top layer of till mixed with organic matter (30–50 cm) above a sandy till layer. Soil samples were collected from both layers, 45 m below the initiation point of the main channel (Figure 18). After the two channels merge, the debris flow path continues 400 m downslope with an angle of 22° before the channel again splits before crossing the forest road, diverted by a small change in topography and group of trees. This section of the path gradually narrows downslope (from 20 m where the channels merge to 15 m before they split again). The channel is eroded to bedrock in the center, with some large boulders deposited along the center. Aerial imagery from shortly after the landslide shows large organic debris and large boulders deposited along the channel margins, with a concentration of boulder debris where the channel splits (180 m west of the houses).

Figure 18: Aerial image of Nesbyen debris flow, dated 26.05.2013 (day after the event). Base image from Norge i bilder, edited by the author (Kartverket, 2018b).

There are two depositional areas associated with the debris flow event (Figure 18) due to the split in the channel. This split occurs just before the transition from transport to deposition. One deposition area along the road west (behind) the houses and in trees there, and the other around two of the houses and properties (Figure 19). The majority of the material took the more northerly path, and was deposited around the houses, impacting two of them and damaging the driveways and yards. There is no available data on the depositional lobe within the trees. The deposition along Alfarvegen is mostly fine-grained material, with the inclusion of some small boulders and pieces or large organic debris (branches, maximum 2 m in length) on the top of the finer grains. The debris is no more than 1 m thick.

Figure 19: Depositional lobe beside Alfarvegen 289. (Bargel & Lund, 2016)

Since the event, extensive land works have been completed to reshape the road behind the houses, and to construct a berm to protect the community from future events. Due to these changes, no record of the debris flow deposits currently exists, and the extent and depth of the deposits must be inferred from imagery dating from shortly after the event and external reports (Kartverket, 2018b; NGI, 2013a).

4.2 Oldedalen 1

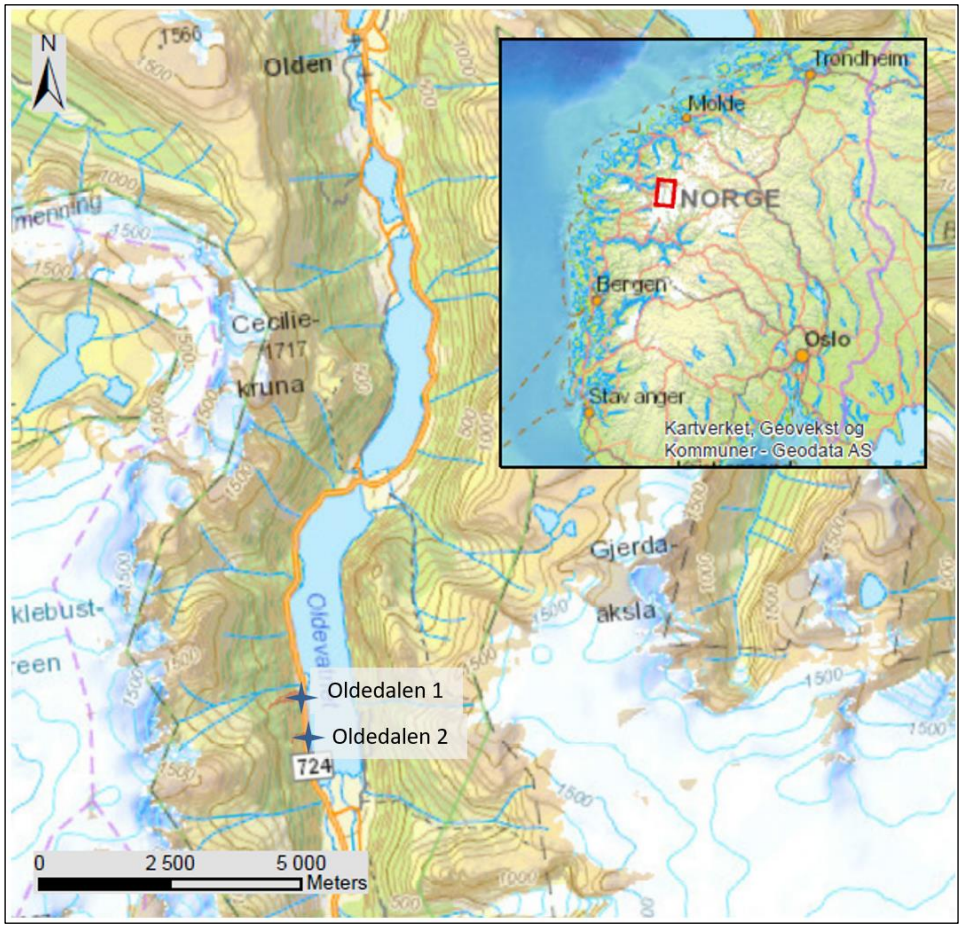

Figure 20: Topographic map of Oldedalen, with the two landslide events studied in this thesis marked at the south end of Oldevatnet Lake.

Both Oldedalen sites are located on an east facing slope on the west side of the south end of Oldevatnet Lake, 13 km south of Olden, Stryn Municipality, Sogn og Fjordane County (Figure 20). The events are 800 m apart, with Oldedalen 1 being the more northerly event. Both occurred south of the hamlet of Yri, which itself is built upon a debris fan created by the Yrielva River. While a number of snow and debris avalanche scars as well as debris flow channels can be observed along the slope on Oldevatnet's west shore, most have not been active in recent times (NVE, 2018). The Oldedalen 1 event is a debris avalanche, with a small portion of the flow volume leaving the main channel and moving as a debris flow 80 m north of the main channel before rejoining it 75m from the lake. The debris avalanche initiates at a point 480 masl, then travels 790 m down to the lake (33 masl), giving the event an H/L ratio of 0.57 and

a travel angle of 29°. Both landslides occurred November 15, 2013 after intense precipitation. Numerous other landslide events occurred in the area at the same time as a result of the same weather system (NVE, 2018).

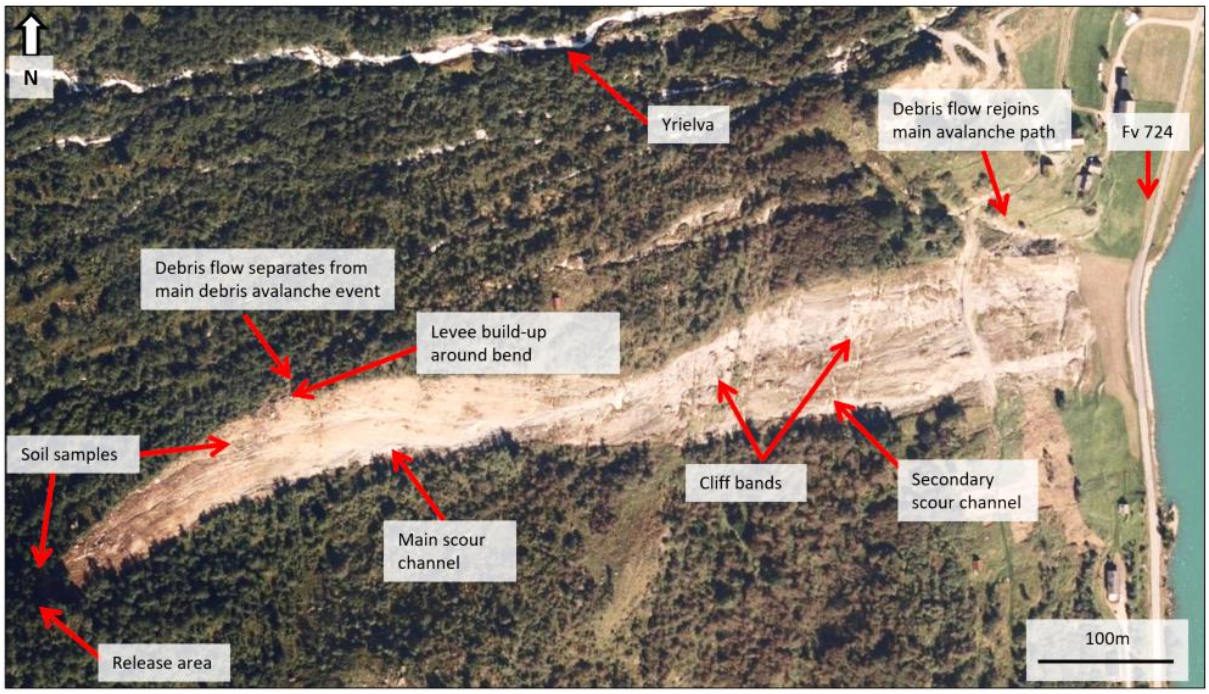

Figure 21: Aerial imagery of Oldedalen 1, dated 21.09.2015. Image from Norge i bilder, edited by the author (Kartverket, 2018b).

4.2.1 Terrain

Oldedalen is long U-shaped glacial valley, approximately 1 km wide at the base. The east side of the valley is quite steep, rising from the lake shore (33 masl) to parts of Jostedalsbreen glacier (1200 masl) in 1 km (slope angle averaging just over 45°). The west side of the valley is slightly gentler with Myklebustbreen glacier (1600 masl) located 3 km from the lake, giving an average slope angle of 27°. The debris avalanche occurred on an open slope, just south of the bowl formed by Yrielva and runoff from Myklebustbreen. A number of runoff channels are sub-parallel to the landslide path, but do not intersect. Regional road 724 (Fv 724) passes along the west shore of the lake (Figure 21 and 22).

The hill side is covered with a mixed deciduous/coniferous forest, with thick undercover of shrubs and long grasses. Tree line is approximately 700 masl.

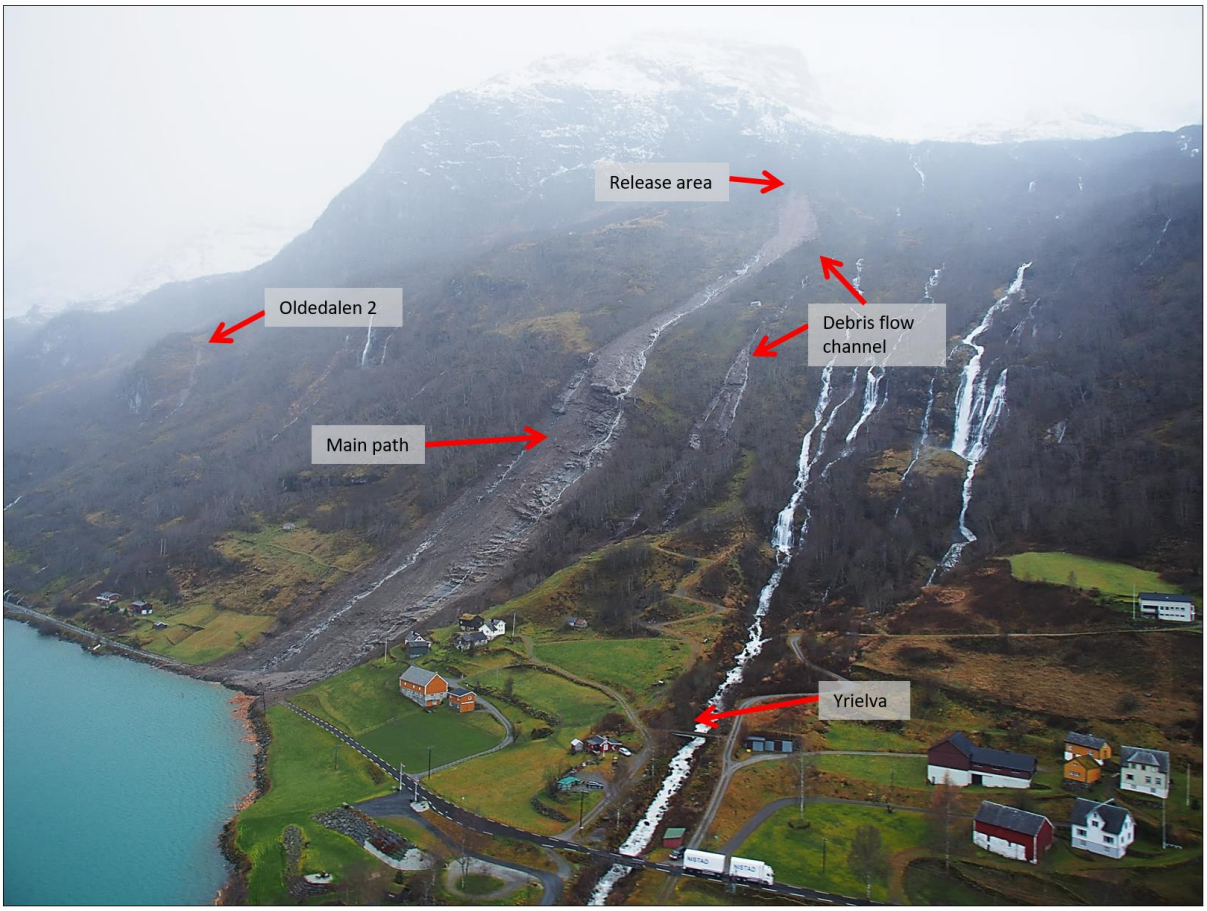

Figure 22: Helicopter photo from Yri, taken the day of the two landslide events, showing Oldedalen 1 in the foreground with the upper part of Oldedalen 2 visible at left. Background image by Jan Helge Aalbu, Statens Vegvesen, edited by the author.

4.2.2 Bedrock and Soil Characteristics

The bedrock in southern Oldedalen is composed of quartz monzonite, dioritic to granitic gneiss, and migmatite (NGU, 2018a). Igneous formations from 950–1000 million years ago have been metamorphosed and in some places transformed to gneiss by the Caledonian orogeny (Fossen, et al., 2008). Surficial deposits in the area are dominated by glacial till layers and deposits from past landslide events (Figure 23). The areas marked as "landslide material" in Figure 23 correspond to rockfall areas with visible talus in air photos.

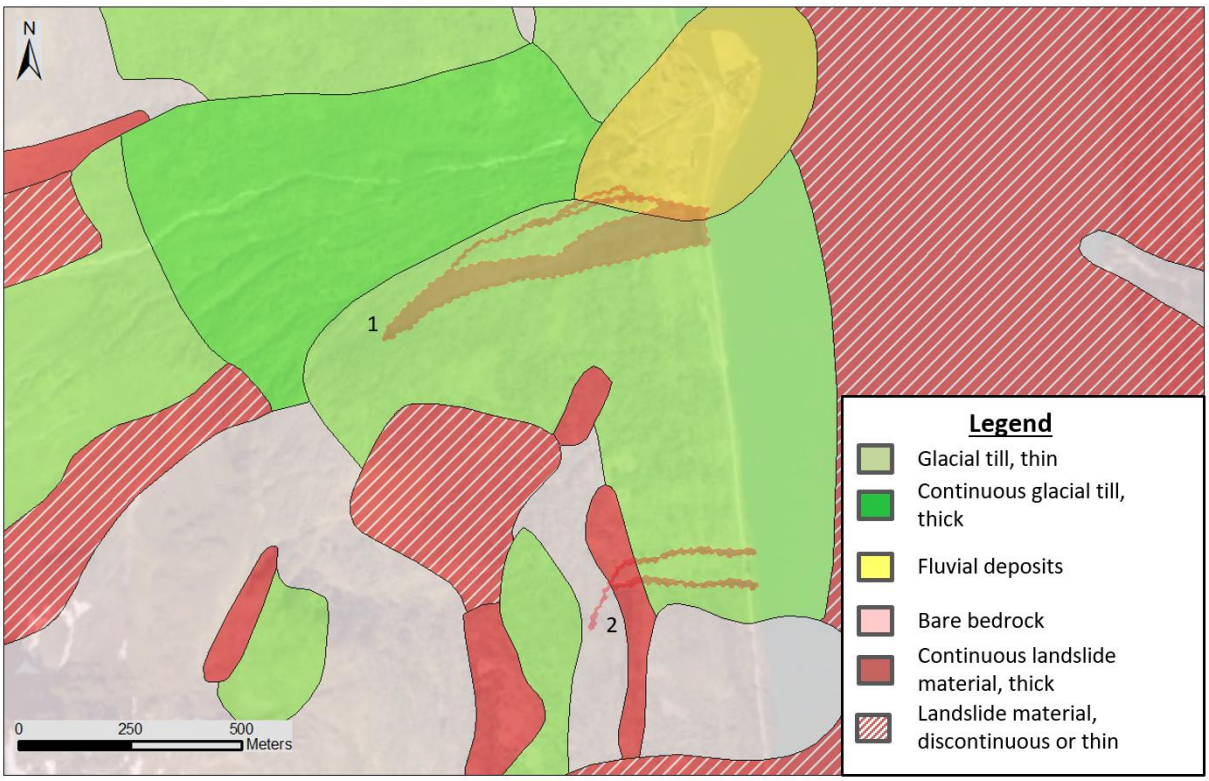

Figure 23: Quaternary sediments map for southern Oldedalen, with polygons representing the extent of both landslide events (labeled 1 and 2) (NGU, 2018b).

4.2.3 Release Area

The release area is a roughly triangular area, 8m wide at the top, 23 m wide at the bottom, and 30 m long. The slope dips to the north east at an angle of 28°. The depth is up to 1.5 m along the margin in some places. Failure did not remove all surficial material from the initiation zone, as the area is still covered with soft, reworked till deposits. At the base of the release area, a stand of 4 trees remains in the middle of the landslide path, showing bark damage and splash marks from the event, but remaining otherwise intact (Figure 24). A number of small drainage channels are present in the soft material, however these have likely been created by erosion processes and rainwater runoff after the landslide, when stabilizing vegetation was removed.

Figure 24: (A) Downslope view from the top of the initiation zone, showing the stand of trees that remained, and the ground cover of reworked till material. (B) Mud and boulders piled against the upslope side of the trees, and visible damage to branches up to 2 m above the ground (red arrows). (C) Bark damage and hanging clumps of mud/vegetation on the upslope side of the trees.

4.2.4 Transport zone and Deposition

From the base of the initiation zone, the channel widens to 55 m as the debris avalanche traveled downslope. This upper portion of the transport zone has a slope angle of 28°, same as the initiation zone. The groundcover is reworked sandy till material, with many cobble size clasts and some boulders (Figure 25). After 200 m, the path angle changes from sub-parallel to the slope to and begins flowing parallel to the slope dip (due east), likely deflected due to gravity. This creates a slight bend in the channel, and some deposition is observed on the outside edge of the bend. A portion of the landslide material did not change direction, and creates a small channelized debris flow north of the main debris avalanche path (Figure 21 and 22).

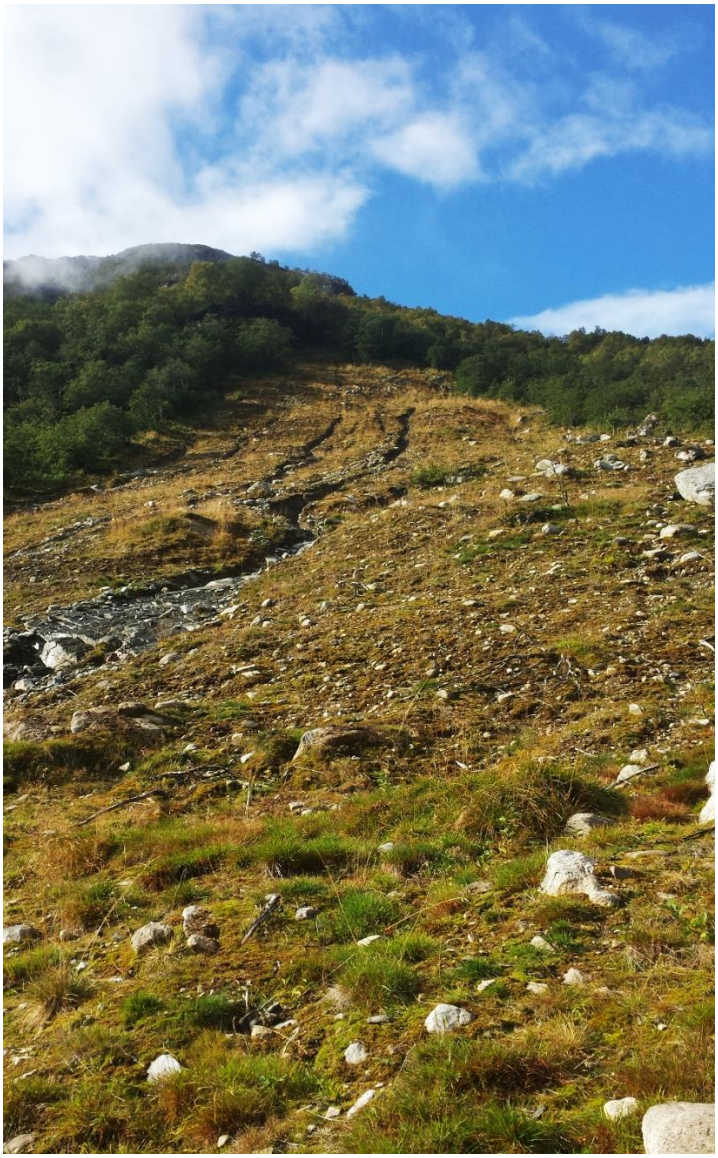

Figure 25: Looking upslope towards the initiation zone from the bend in the path. Large boulders and some organic material have been deposited along the outside of the bend, and a small levee has been built up to the right of the large boulder (right of frame). The three runoff channels visible in the center of the path have been created by the erosion of runoff water from post-landslide precipitation events. Up to 1 m of reworked till remains in the landslide path.

Below the bend, the gradient of the slope increases, and a thick layer of till (up to 1.5 or 2 m in some places) is in spots eroded down to bedrock. The terrain is eroded in small channels, which may have been at least partially created by runoff after the landslide event. For 260 m after the bend, the path remains consistently 50 m wide. Along the south edge of the path, a 12 m wide channel has been eroded to bedrock, indicating where the debris avalanches erosive force was greatest. The channel is up to 1.5 m incised in some places, while the path margins show an additional 1 to 1.5 m erosion.

After this middle segment (now 415 m down path from the initiation zone), the path widens to 80 m and passes over a number of cliff bands (Figure 26 B). The average slope angle is 36°; however it is locally much steeper (up to 65° in some spots). The main eroded channel switches to the north side of the path, and widens to 30 m. Soil cover is very thin, and there are numerous

patches of exposed bedrock. Banks at the edge of the path indicate varying erosion depths of 0.5 m to 1.5 m. Some boulders have been deposited along channel and path, but very little deposition is otherwise evident.

Figure 26: (A) Upslope view from the top of the cliff bands, beside the main scour channel. (B) Downslope view over the cliff bands towards Oldevatnet and Yri.

Below the cliff bands, the slope gradient is shallower (21°), down to Fv 724 beside Oldevatnet Lake. A second sub-channel eroded to bedrock is present along the south side of the main path, originating below the cliff bands. Photos taken the day of the event show some material deposition in this area. The channelized debris flow that left the main debris avalanche at upper portion of the path rejoins the main path here, 120 m from the lake. The landslide runout ended in the lake, and no information on the depositional lobe is available as no bathymetry surveys have been conducted. The landslide path is 100 m wide where it meets the lake.

4.3 Oldedalen 2

The second site in Oldedalen is a debris flow located 780 m south of Oldedalen 1, along Fv 724 and the west shore of Oldevatnet Lake (Figure 20). The debris flow split into two parallel channels 65 m apart when passing over a cliff band 270 m from the road. The release area is 311 masl, and the event has a runout of 458 m, giving an H/L ratio of 0.61 and a travel angle of 31°. The two channels are renamed channel 1 (northern channel) and channel 2 (southern channel) (Figure 27) for ease of differentiation. Channel 1 is marked as a creek on topographic maps of the area and can be identified in aerial photos from 2004 (Kartverket, 2018a).

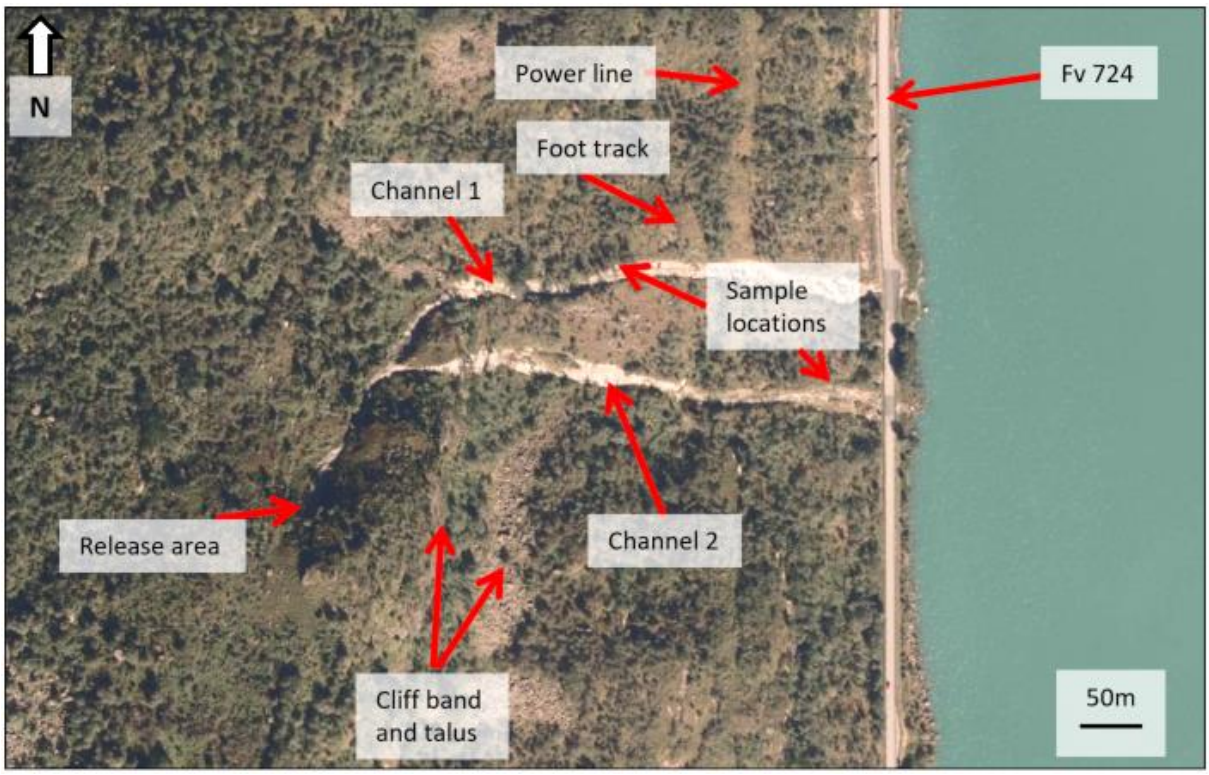

Figure 27: Aerial image of the debris flow, dated 21.09.2015. Background image from Norge I bilder, edited by the author (Kartverket, 2018b).

4.3.1 Terrain

The east-facing slope along this part of Oldevatnet has a number of benches created by large cliff bands, with rock fall zones and talus cones visible at the bases of the cliffs. Both active and inactive drainage channels can be identified on the slope. A power line runs parallel to Fv 724, 60 m west of the road surface. An overgrown footpath crosses the slope and channels parallel to the road and the power line, 90 m west of the road. The vegetation in the area is covered in sparse deciduous forest of thin, short trees with thick undergrowth coverage of long grasses and 1–2 m bushes where no trees are present.

4.3.2 Bedrock and Soil Characteristics

The bedrock underlying both Oldedalen sites is the same on the 1:250000 regional bedrock map available from NGU (NGU, 2018a). A 1:50000 map for southern Oldedalen is not available.

Although the Quaternary sediments map (shown in Figure 23) indicates bare bedrock in the release area of Oldedalen 2, air photos and field observations show otherwise. The release area is covered by a thin layer of glacial till, and should be marked as such. In other areas, the soil map from NGU is consistent with observations from the field and aerial imagery.

4.3.3 Release area

The release area of Oldedalen 2 was not directly accessed during field work, due to difficulties accessing the site without climbing equipment. The release area is located on a north dipping bench above a large cliff band, with a slope angle of 21°. The west (uphill) bank of a creek collapsed along a 40 m length, triggering the debris flow. The channel is thin, but well defined, eroded as deeply as 2.5 m in some places and no more than 10 m wide. The release area is eroded down to bedrock along its length. At the base of the release area a bedrock outcrop narrows the channel to less than 4 m across (Figure 28).

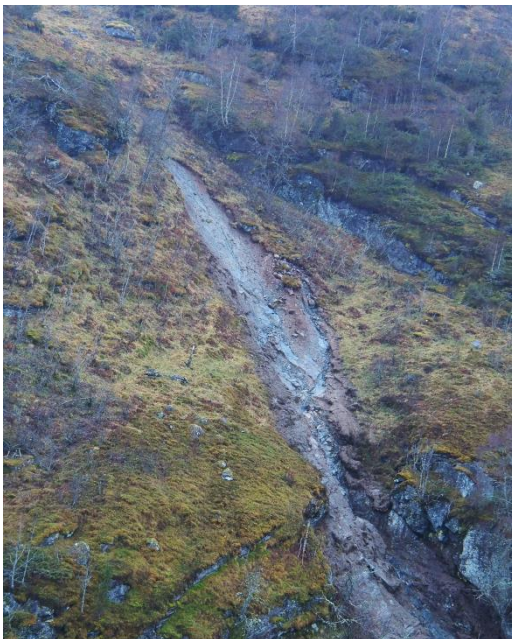

Figure 28: Oblique image of the release area, taken from a helicopter the day of the debris flow. Photo by Jan Helge Aalbu, Statens Vegvesen.

4.3.4 Transport Zone and Deposition

100 m below the initiation zone, channel 2 breaks off from the main channel, and flows over the cliff band. Channel 1 continues a further 50 m north, before also turning east over the cliff band. Both channels then remain parallel for the final 260 m to Oldevatnet (Figure 27).

Channel 1 is 16 m wide at its widest point, and has a slope angle of 29° from the cliff band down to the road surface. The channel is blocky rather than smooth, and has the appearance of a large staircase (Figure 29(A)). The channel is eroded down to bedrock along its length, and varies from 2–3 m deep. The channel is still active as a drainage channel, and any sand- or gravel-sized debris deposited by the debris flow has since been washed away. Some boulder- and cobble-sized material lies loosely on the steps within the channel, though this may have fallen from the banks due to subsequent precipitation events. The banks of the channels are quite steep, and composed of thin layer of organic material over a thick till layer. Large boulders are entrained within the till and visible along the channel banks.

Channel 2 is slightly wider than Channel 1 (averaging 12 m compared to 10 m), and has a much smoother base; the blocky steps are not present. The channel is also eroded to bedrock with similar depths incised in the banks.

Figure 29:(A) Looking upslope at the blocky channel steps and eroded banks of channel 1. Photo Anders Solheim, 2017. (B) Helicopter photo shortly after the event, by Jan Helge Aalbu, Statens Vegvesen.

4.4 Skjeggestad, Ringebu

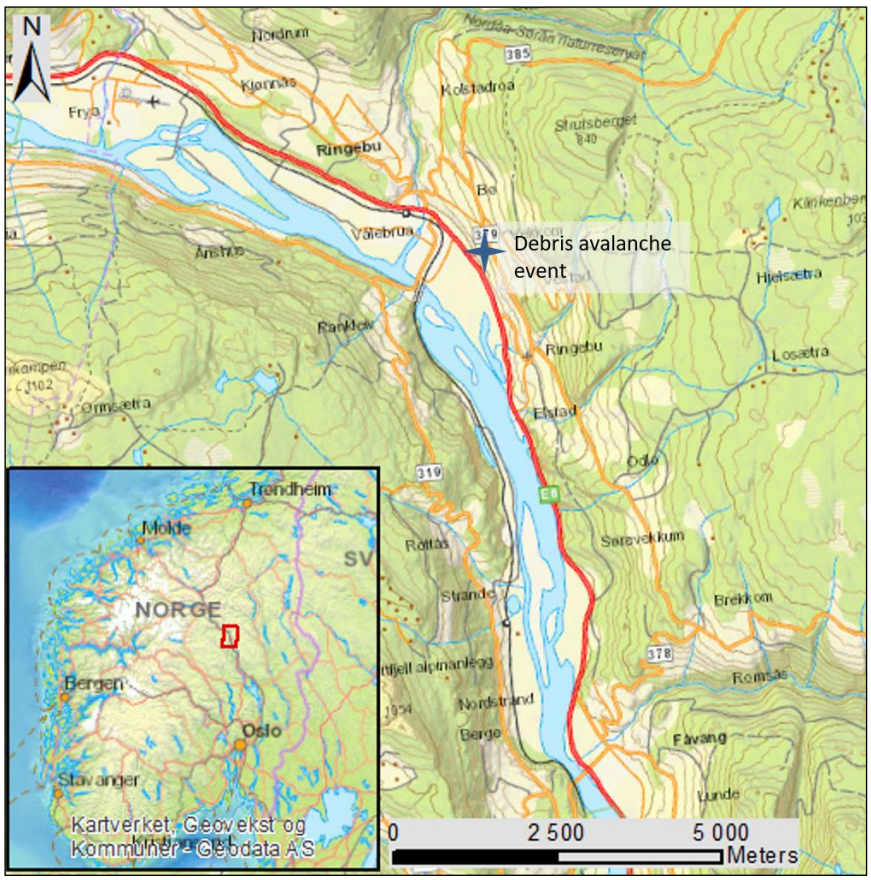

Figure 30: Topographic map of Gudbrandsdalen, showing the debris avalanche event along the E6 southeast of Ringebu.

The debris avalanche occurred 24.05.2013, on a southwest-facing slope behind the community of Skjeggestad, 1 km south of Ringebu along the E6, administrative center of Ringebu Municipality, Oppland County (Figure 30). The initiation zone is 255 masl. The debris avalanche ran out 175 m, ending at 186 masl. Its H/L ratio and travel angle were 0.4 and 22°, respectively.

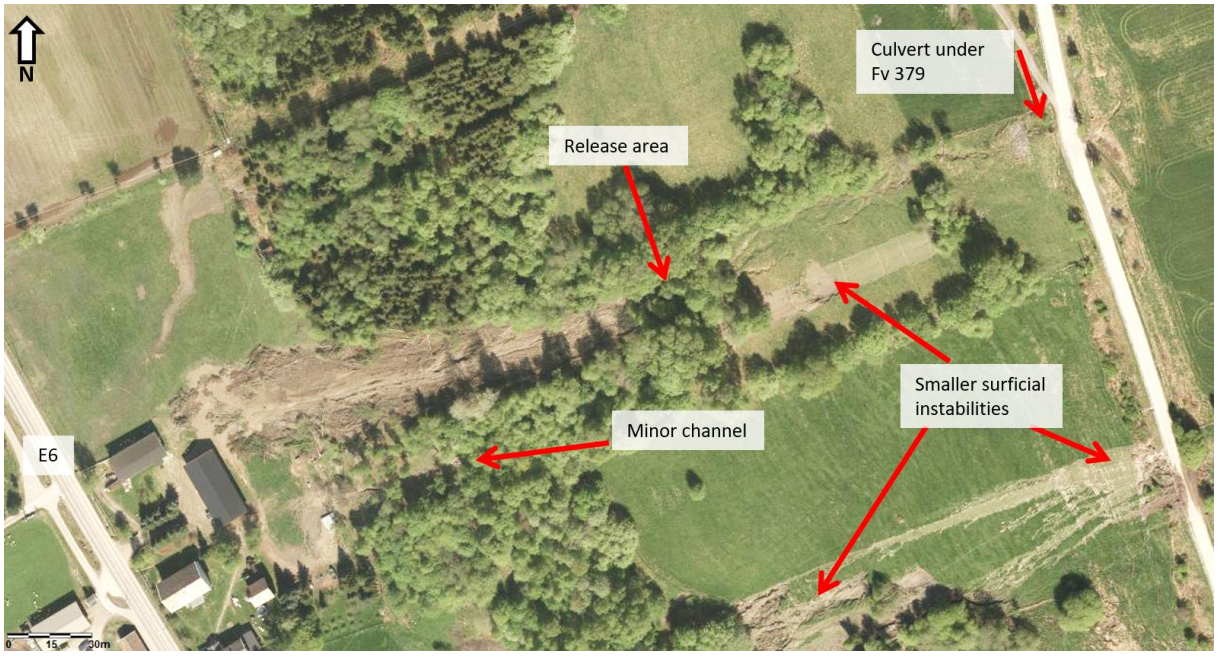

Figure 31: Aerial image dated 25.05.2013, the day after the debris avalanche event occurred. The full extent of the impact area can be seen. Background image from Norge i bilder, edited by the author (Kartverket, 2018b).

A number of slope movement events of varying sizes occurred in the area as part of an extreme precipitation event (the same event triggered the Nesbyen debris flow, 113 km to the south west) (NGI, 2013b). The debris avalanche damaged one house and property, and caused the evacuation of 3 houses.

4.4.1 Terrain

The event occurred on the lower south-west facing slope of Gudbrandsdalen, a major U-shaped glacial valley in southern Norway. Ringebu and the E6 highway are built along the fluvial plain beside Gudbrandsdalslågen. While parts of the slope are covered with mixed deciduous and coniferous forest, large parts of the area are pasture and grazing lands, or used for other agricultural purposes. The debris avalanche occurred in a wooded strip separating two pastures, on a slope of 26° (note that the travel angle mentioned in the previous section is different than the slope angle mentioned here. The travel angle is the angle between where the event initiated and where it stopped, and is almost always lower than the slope angle as landslides can continue for some distance on relatively flat terrain). A flat field of 60 m separates the houses along the E6 from the base of the slope. A powerline passes up the slope 75 m to the north of the landslide path.

4.4.2 Bedrock and Soil Characteristics

Bedrock in the Ringebu region consists of quartzite and metasandstone, remnants of the basement of the Baltica continental plate. The debris avalanche extends from slopes covered with glacial till material onto the fluvial plain of Gudbrandsdalslågen, where thick fluvial deposits exist (Figure 32).

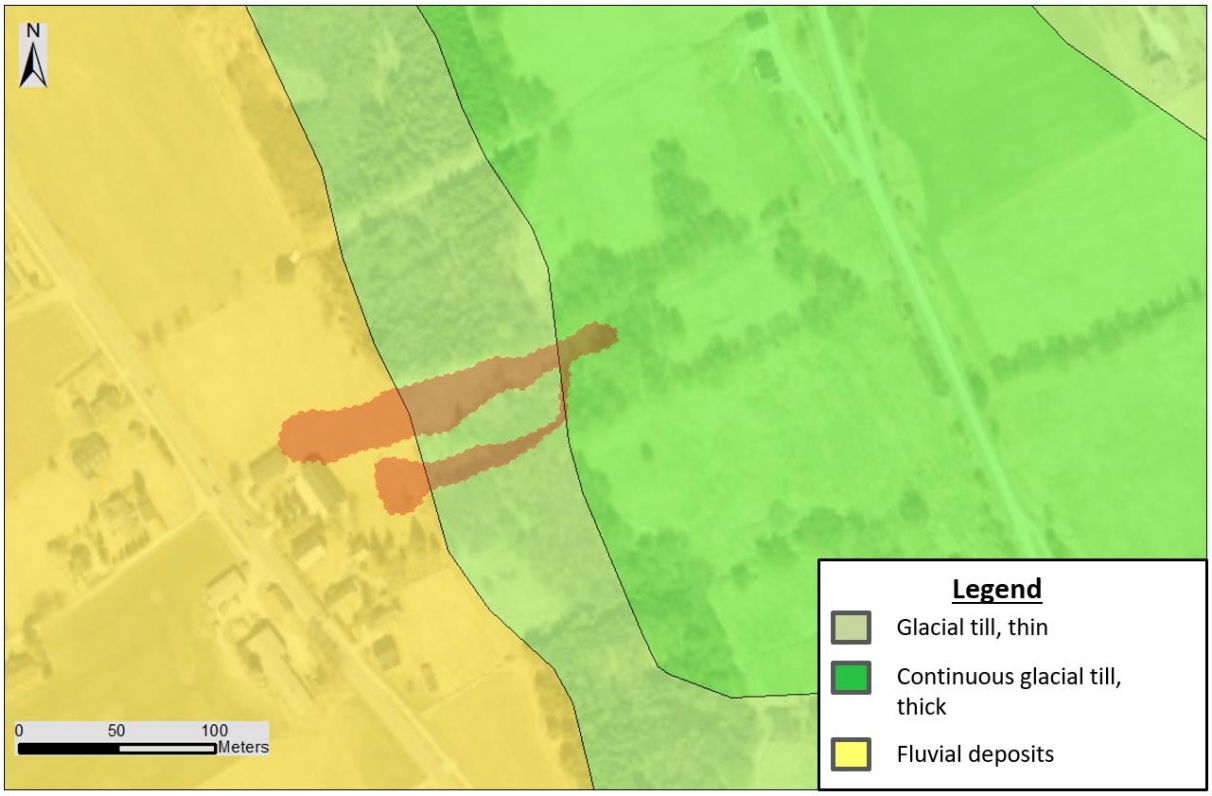

Figure 32: Section of a Quaternary sediments map for Ringebu municipality, with the debris avalanche event marked as a red polygon (NGU, 2018b).

4.4.3 Release Area

A small, unmarked drainage passing through a culvert under Vekkomsvegen (Fv 379) 177 m upslope from the release area may have triggered the debris flow. The release area is roughly triangular, approximately 11 m wide at the base and 18 m long, dipping west south-west at 23°. The depth along the margin is 30–50 cm. The top layer of soil is dominated by grasses and organic material, underlain by fine grained till, with numerous cobble-sized clasts.

4.4.4 Transport zone and Deposition

The debris avalanche path splits into a major and minor channel 30 m below the release area. After the split, both channels are parallel. The minor channel is very narrow at the top (less than 5 m), and widens to 15 m where it leaves the trees at the base of the slope. The channel is mostly obscured by trees, but can be seen in an oblique photograph taken from helicopter the day of the event (NGI, 2013b) (Figure 33). Both channels share a common slope angle of 25°.

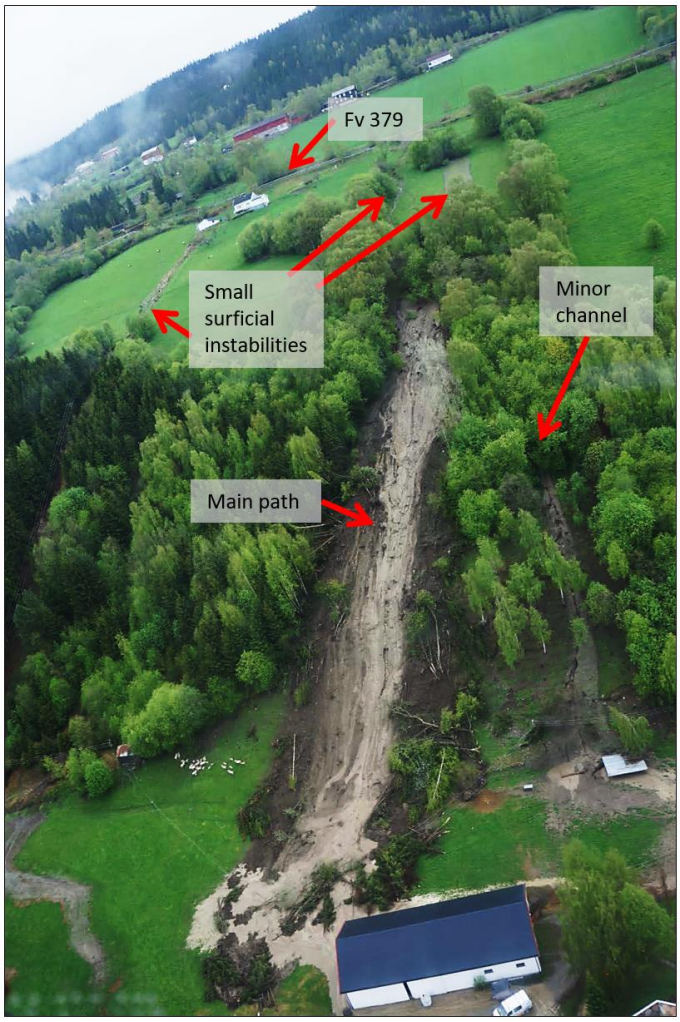

Figure 33: Oblique photo taken from a helicopter the day of the event. From (NGI, 2013b) edited by the author.

The main channel gradually widens from the release area to a maximum of 35 m where it exits the treed slope. The path is not very channelized, and only difference of 30 – 50 cm exists between the path and the margins. Most of the material is below 0.5 mm in diameter, with only a few larger clasts mixed with large organics.

Depositional lobes extended 55 m from the edge of the forested slope for the main channel, and 20 m for the minor. The lobe of the main path is 35 m wide at its widest. The lobe is less than 1 m thick, and composed of fine-grained material, with large organic debris resting on top. The debris impacted a barn at the base of its runout, but did no major damage. A temporary shelter at tree line was destroyed by the lobe of the minor channel. Damage caused by the event was quickly cleaned up and deposited material removed; no deposits or damage caused by the debris avalanche are currently visible.

4.5 Summary of the selected sites

Table 4 summarizes the information presented in this chapter for each of the selected landslide events. The high H/L ratios for the two Oldedalen events are a result of the landslide runouts being truncated by Oldevatnet Lake. The final volume values are estimated from the best calibrated DAN3D simulations, discussed further in chapter 5.

Table 4: Summary of the landslide cases studied.

Site	Runout length (m)	Elevation loss (m)	H/L	Final volume (m^3)
Nesbyen	660	216	0.33	3600
Oldedalen 1	790	447	0.57	15000
Oldedalen 2	458	278	0.61	2300
Ringebu	175	69	0.4	350

5 Results

The following sections present the results from the grain size analysis of soil samples collected at each site, followed by the results of back-analysis simulations in DAN3D and a comparison of results obtained from both DAN3D and GeoClaw software's.

5.1 Grain size analysis

At the Nesbyen site, grain size samples were taken along the channel bank. Two layers were identified in the soil, with a sample being taken from each. Both samples are composed predominantly of sand and gravel material, with a low percentage of silt and finer grains (Figure 34). This is consistent with NGU's classification of the surficial deposits as glacial till (Figure 16).

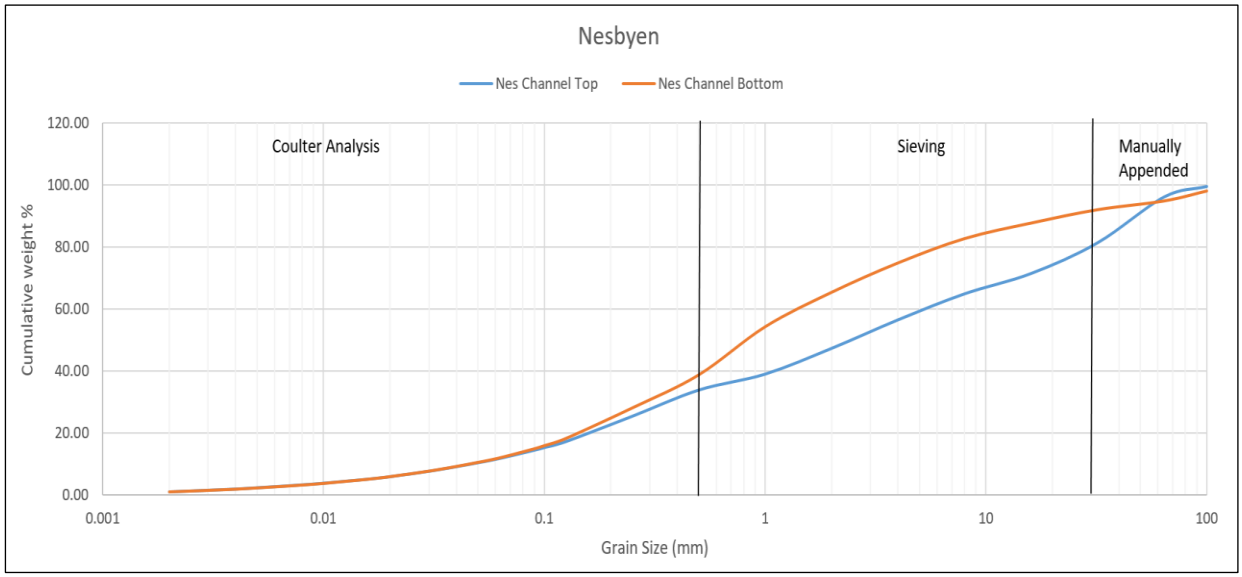

Figure 34: Grain size distribution curve showing the samples taken from Nesbyen. The ranges of the different data analyses are marked.

The samples from Oldedalen 1 contain a higher percentage of silt and sand, and there is no obvious difference between the samples taken from the release or from the path (Figure 35). Neither of the samples labeled "*Oldedalen 1 – initiation*" or "*Oldedalen 2 – ch2*" contained clasts greater than 64 mm, hence the early termination of their distribution curves. This does not mean that larger clasts were not present at those locations, simply that they were not collected when sampling due to lateral variability. The sample from the second channel of Oldedalen 2 ("*Oldedalen 2 – ch2*") contains less sand than the other samples, and contains a higher percentage of coarse gravel and larger clasts.

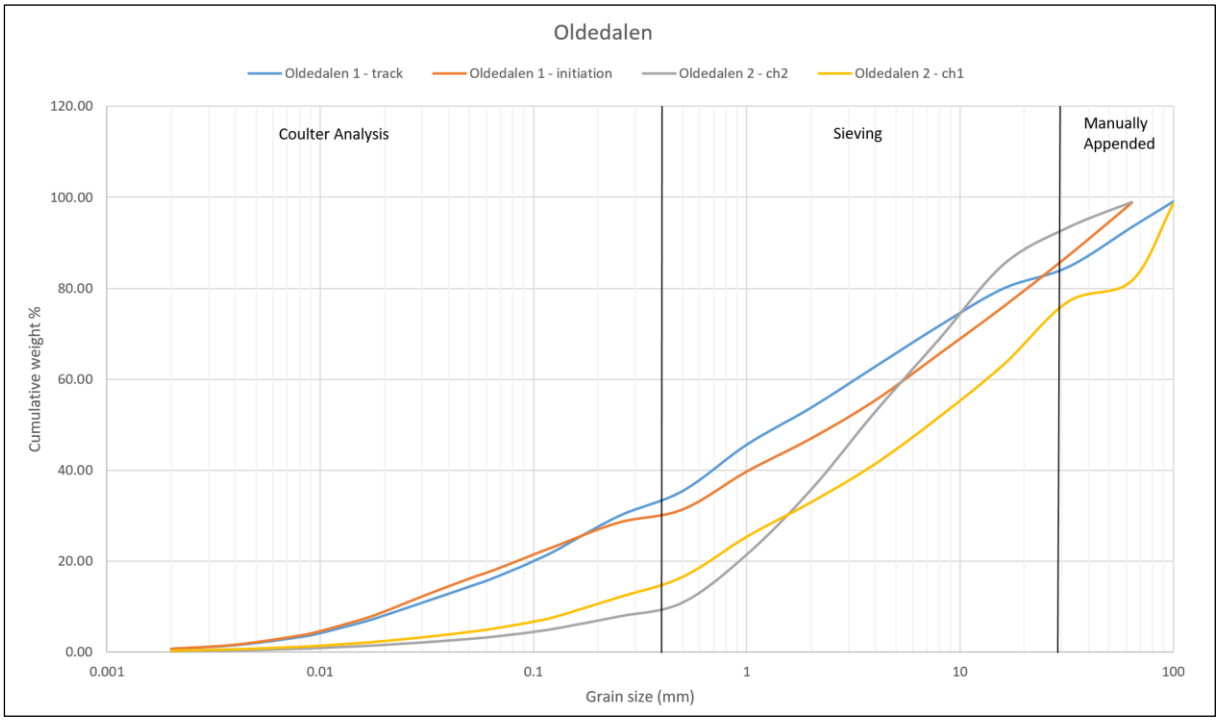

Figure 35: Grain size distribution curves for the samples from Oldedalen.

Only one sample was collected from the release area of the debris avalanche at Ringebu. This sample is notably different from the other cases in that it contains a much higher percentage of silt and fine grained sand (4% clay and 38% silt) (Figure 36).

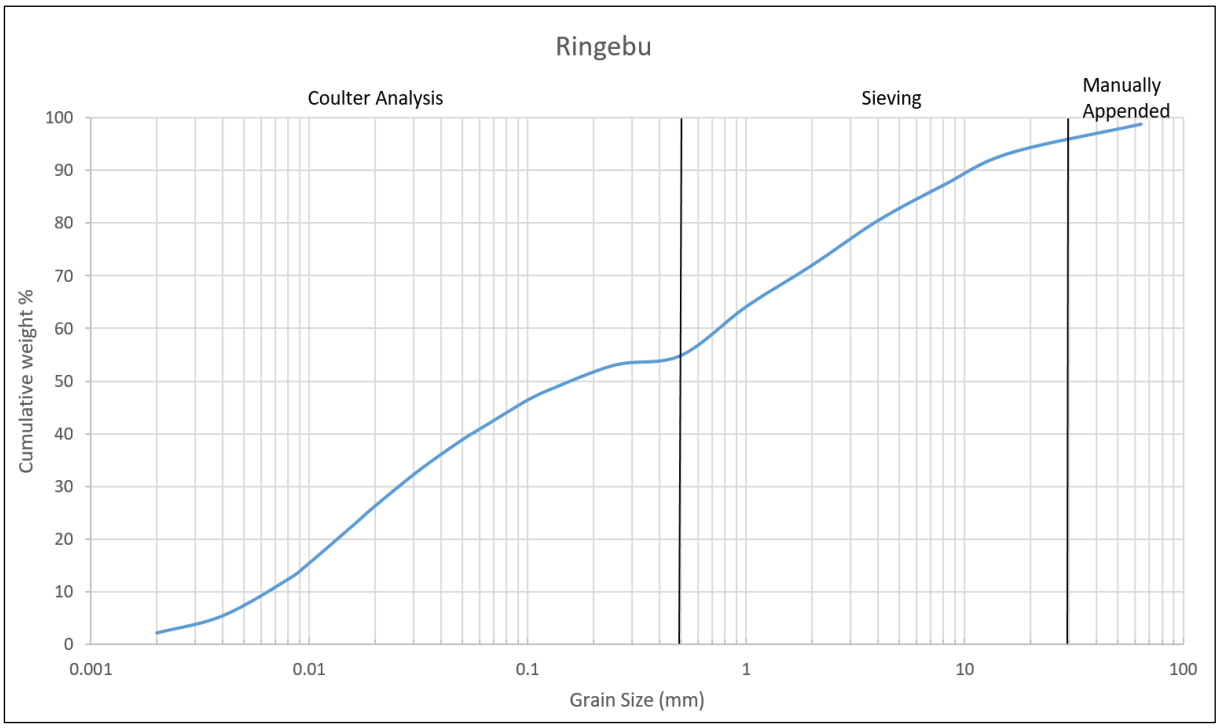

Figure 36: Grain size distribution curve for the sample from Ringebu.

5.2 DAN3D

The results from back-analysis of each landslide event in DAN3D are presented, as well as the results of testing the numerical parameters for the Nesbyen case.

5.2.1 Numerical Parameters

In addition to rheological parameters, numerical parameters used in Dan3D (time step, number of particles, and smoothing length coefficient) were varied while the friction and turbulence coefficients, and erosion rate were held constant to see if the numerical parameters greatly affect the back-analysis results. This was done for the Nesbyen case, as it has the least uncertainty about the initial release volume (topography data was available for both before and after the landslide). Each simulation was run using a friction coefficient of 0.12, turbulence coefficient of 550, and no erosion. The results of varying the simulation time step are presented in Table 5.

Table 5: Impact of changing the simulation time-step.

Run	Time Step (s)	Max Velocity (m/s)	Runout (m)	T. Angle (°)	Diff. Runout (%)
RT1	0.05	12.0	540	19	-14.3
RT2	0.1	12.2	540	19	-14.3
RT3	0.15	12.2	540	20	-14.3
RT4	0.2	11.9	553	20	-12.2
RT5	0.3	12.0	553	20	-12.2
RT6	0.5	13.1	553	21	-12.2

Changing the time-step had very little observable impact on the results.

Table 6: Impact of increasing the number of particles simulated. The maximum number of particles that can be simulated in Dan3D is 4000.

Run	Particles	Max Velocity (m/s)	Runout (m)	T. Angle (°)	Diff. Runout (%)
RP1	1000	12.2	535	20	-15.1
RP2	2000	12.2	540	19	-14.3
RP3	3000	12.8	558	19	-11.4
RP4	4000	12.2	563	19	-10.6

Increasing the number of particles in the simulation lead to runout lengths more closely resembling the observed value (Table 6). However, this requires more computational power and time to run each simulation.

Table 7: Impact of changing the smoothing length constant.

Run	Smoothing Length	Max Velocity (m/s)	Runout (m)	T. Angle (°)	Diff. Runout (%)
SL1	1	43.4	585	19	-7.1
SL2	2	13.0	570	19	-9.5
SL3	3	13.0	570	19	-9.5
SL4	4	12.2	540	19	-14.3
SL5	5	12.0	545	20	-13.5
SL6	6	12.0	530	20	-15.9
SL7	7	11.9	525	20	-16.7

The smoothing length constant is a value used by Dan3D to determine the radius of influence of each simulation particle (width of the Gaussian interpolation kernel). Lowering the constant resulted in a landslide composed of particles that do not interact with each other. While this had a runout length approaching the observed value, the measured velocity and geometry of the deposits was not realistic. Increasing the smoothing length constant shortens the runout length of the observed landslide (Table 7).

For all other simulations, the default numerical parameters in Dan3D were used (time-step = 0.1, number of particles = 2000, and smoothing length constant = 4).

5.2.2 Nesbyen

Figure 38 shows the extent of the runout of the Nesbyen landslide, mapped from aerial imagery and photos taken shortly after the event occurred (red dashed line) overlain on a DAN3D simulation. The estimated runout length and corresponding travel angle of the event are 660 m and 18 degrees, respectively. The final volume was estimated at between 3500 m^3 and 4000 m^3. The results of 28 simulations run in DAN3D systematically varying the turbulence and friction coefficients are presented in Table 8.

Table 8: Results of Dan3D analysis of the Nesbyen event. Only those simulations with the lowest friction coefficient (μ) came close to matching the observed runout length. Increasing the turbulence coefficient (ξ) increased the final volume of the landslide.

Run #	μ	ξ (m/s²)	Length (m)	Max. V (m/s)	Volume (m³)	Diff. Volume (%)	Diff. Length (%)
1	0.1	100	513	7.1	2582	-32.1	-18.6
2	0.1	250	581	9.6	3626	-4.6	-7.8
3	0.1	400	604	11.1	4174	9.9	-4.1
4	0.1	550	609	12.1	4442	16.9	-3.3
5	0.1	700	610	13.0	4533	19.3	-3.2
6	0.1	850	619	13.6	4735	24.6	-1.7
7	0.1	1000	631	14.1	4890	28.7	0.2
8	0.15	100	495	6.5	1944	-48.8	-21.4
9	0.15	250	523	9.0	2876	-24.3	-17.0
10	0.15	400	563	10.5	3263	-14.1	-10.6
11	0.15	550	564	11.5	3546	-6.7	-10.5
12	0.15	700	565	12.2	3727	-1.9	-10.3
13	0.15	850	566	13.1	3946	3.8	-10.2
14	0.15	1000	580	13.2	4026	5.9	-7.9
15	0.2	100	419	6.2	1143	-69.9	-33.5
16	0.2	250	496	8.5	1903	-49.9	-21.3
17	0.2	400	498	9.9	2262	-40.5	-21.0
18	0.2	550	519	10.8	2555	-32.8	-17.6
19	0.2	700	527	11.3	2698	-29.0	-16.3
20	0.2	850	529	11.8	2850	-25.0	-16.0
21	0.2	1000	533	12.4	2883	-24.1	-15.4
22	0.3	100	192	5.6	672	-82.3	-69.5
23	0.3	250	220	7.4	712	-81.3	-65.1
24	0.3	400	227	8.6	751	-80.2	-64.0
25	0.3	550	229	9.4	821	-78.4	-63.7
26	0.3	700	340	9.9	906	-76.2	-46.0
27	0.3	850	374	10.1	996	-73.8	-40.6
28	0.3	1000	376	10.6	1081	-71.5	-40.3

Figure 37 shows nine simulations with different turbulence and friction coefficients. Only those with a friction coefficient of 0.1 come close to reaching the runout of the event, and the two simulations with higher turbulence coefficients have higher final volumes than was estimated by field observations.

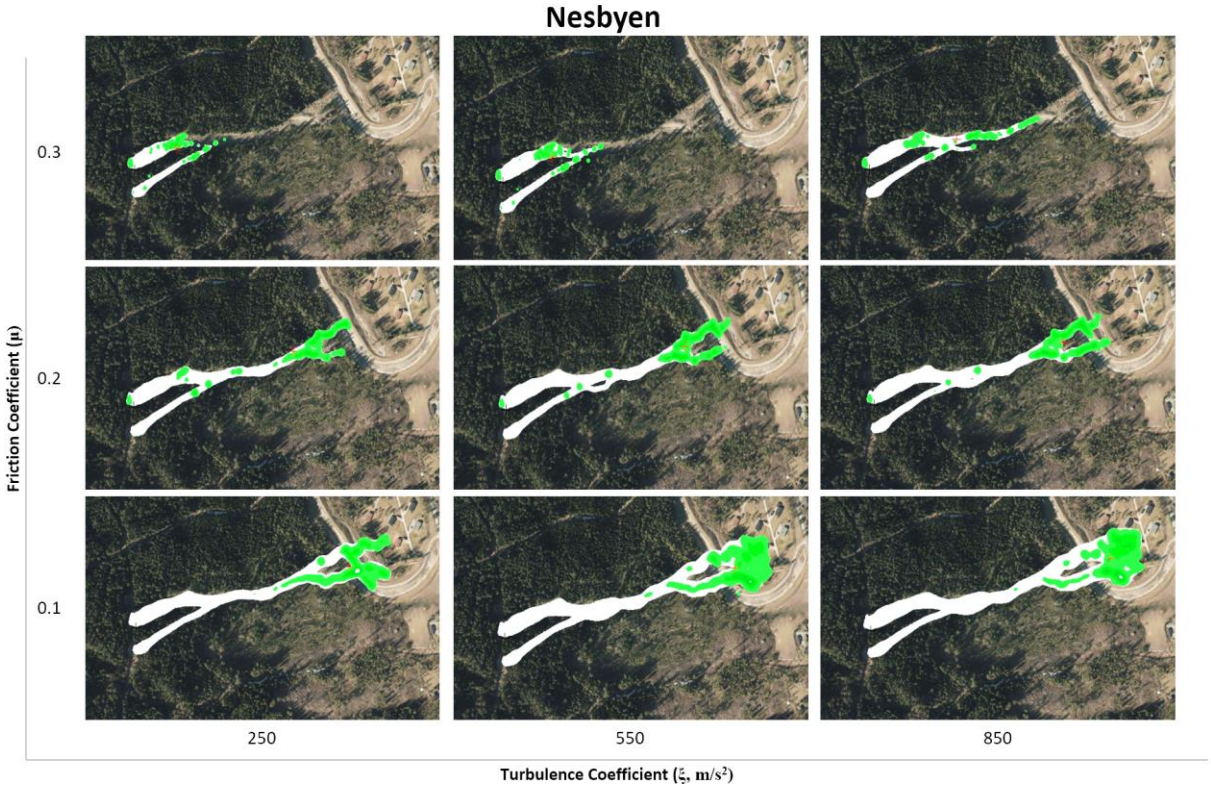

Figure 37: Plots showing simulated deposit thickness. Grey represents landslide impact area, light green 0-0.5m deposits, and darker green 0.5-1.5 m deposits.

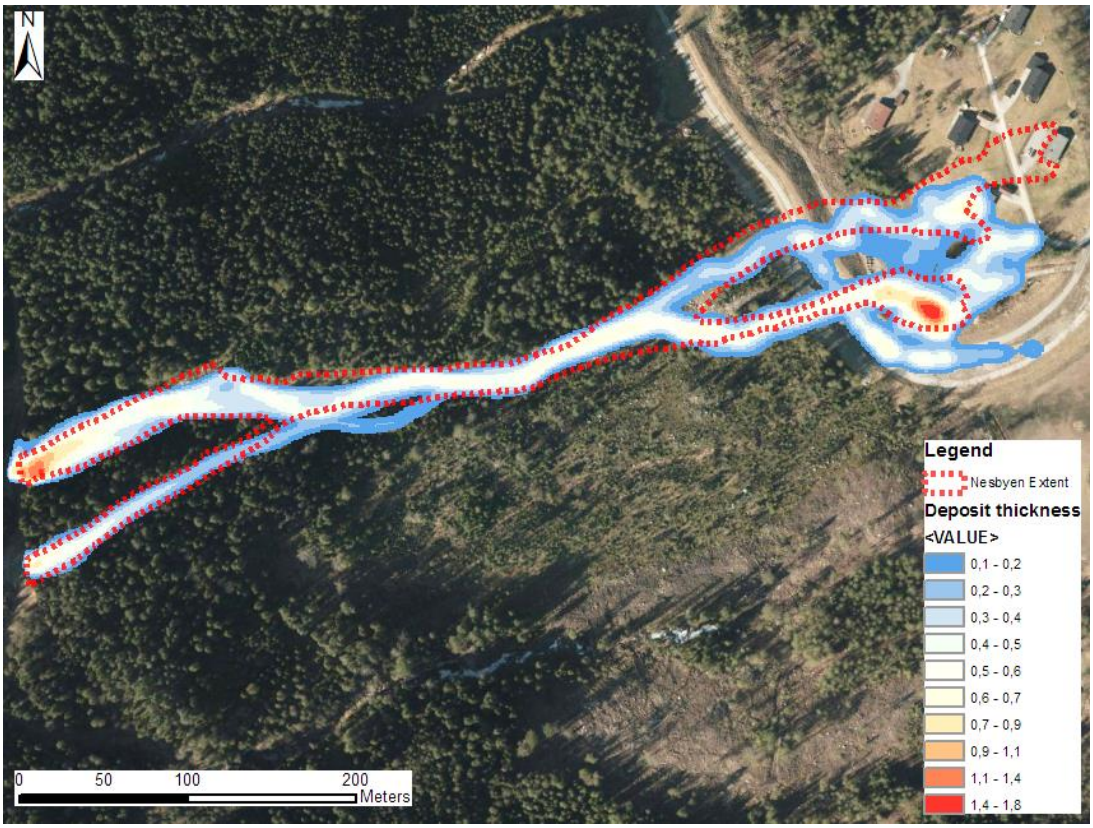

Figure 38: Results from a DAN3D simulation (u = 0.08, ξ = 700) with the actual event polygon (red dotted line), as interpreted from aerial imagery.

As shown in Figure 38, DAN3D consistently slightly overestimates the width of the channel, especially near the initiation zone. Interestingly, while DAN3D correctly modelled the channel splitting towards the bottom, the location of the channel split is only slightly off. As mentioned above, the DAN3D models underestimate the runout of the debris flow event. The calibrated best parameters for the debris flow event in DAN3D are μ between 0.07 – 0.09, and ξ between 600 m/s^2 and 800 m/s^2. The simulation shown in Figure 38 uses parameter values within these ranges.

5.2.3 Oldedalen 1

Figure 39 presents nine Dan3D simulations of Oldedalen 1. The program continuously underestimated the width of the lower part of the main channel, while seeming to overestimate the width in the smaller north channel. As the program cannot model the effects of a lake on the landslide runout and deposition (rapid removal of material) the depth and lateral extent of the deposit at the bottom is greatly overestimated.

The friction coefficient for this site is estimated to be 0.18 to 0.2, with the turbulence coefficient between 350 and 450. The final volume is estimated to be around 15,000 m^3, however this is a very rough estimation. Figure 40 shows a landslide simulation with values within these ranges overlain on a polygon outlining the actual event boundaries. This simulation had a final volume of 15,600 m^3.

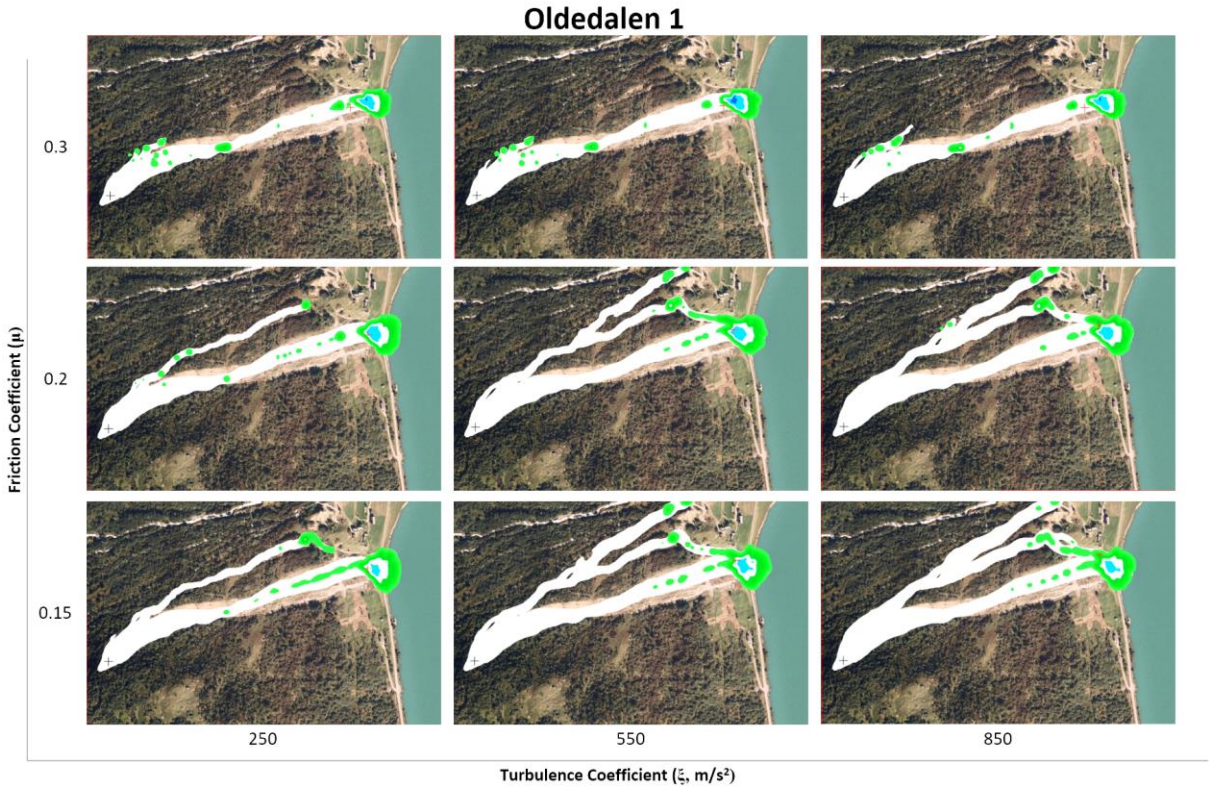

Figure 39: Simulations for Oldedalen 1. Higher turbulence coefficients overflow the side channels. None of the simulations accurately depict the size of the main channel (underestimates). Grey represents landslide impact area, light green 0-1m deposits, darker green 1-2 m deposits, light blue 2-3m, and dark blue 3-5m.

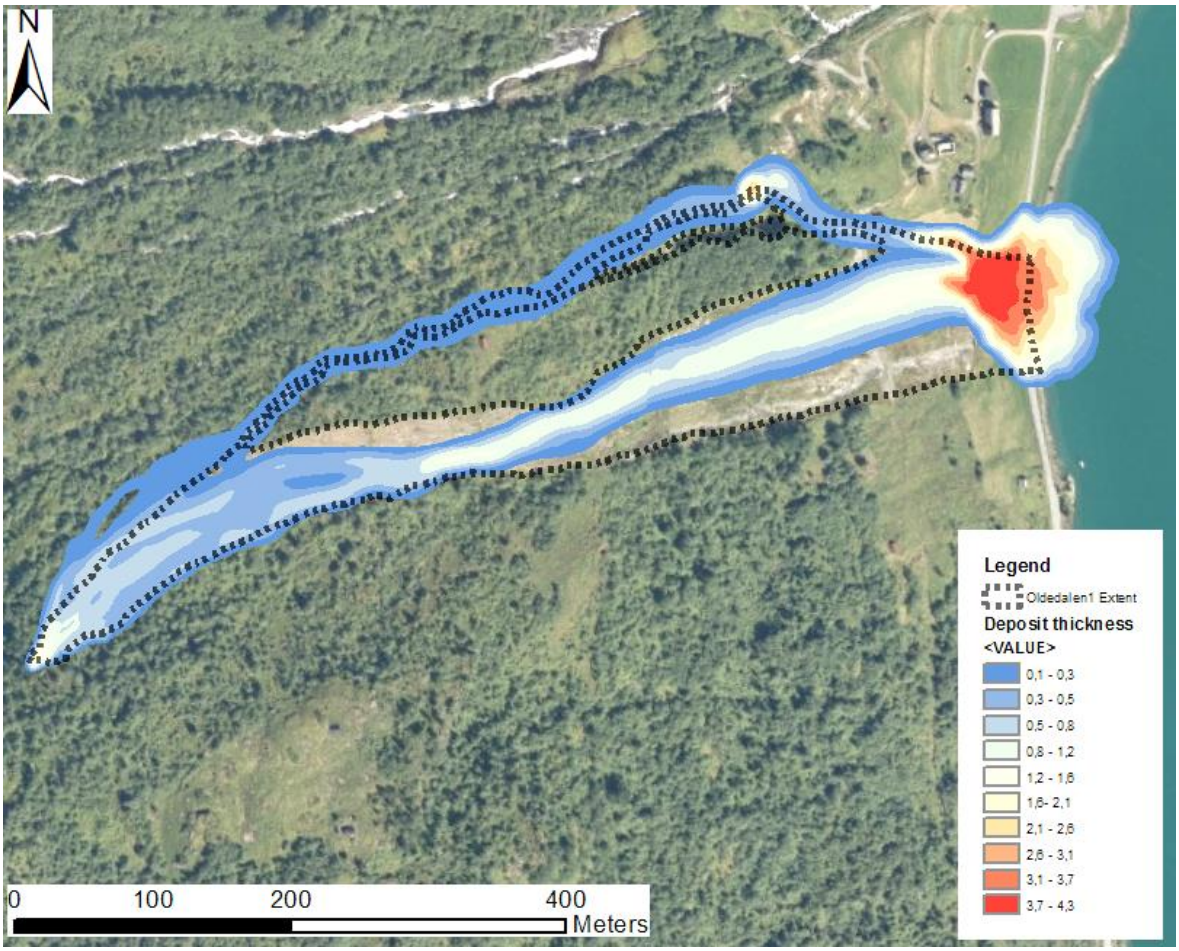

Figure 40: DAN3D result from Oldedalen 1 (u = 0.185, ξ= 400) with the polygon of the event (black dotted line) mapped from aerial imagery.

As mentioned for the Nesbyen case, the DAN3D simulations appear to the debris flow channel width, as it was mapped from aerial photos. The width of the path in the debris avalanche portion of the flow is underestimated.

5.2.4 Oldedalen 2

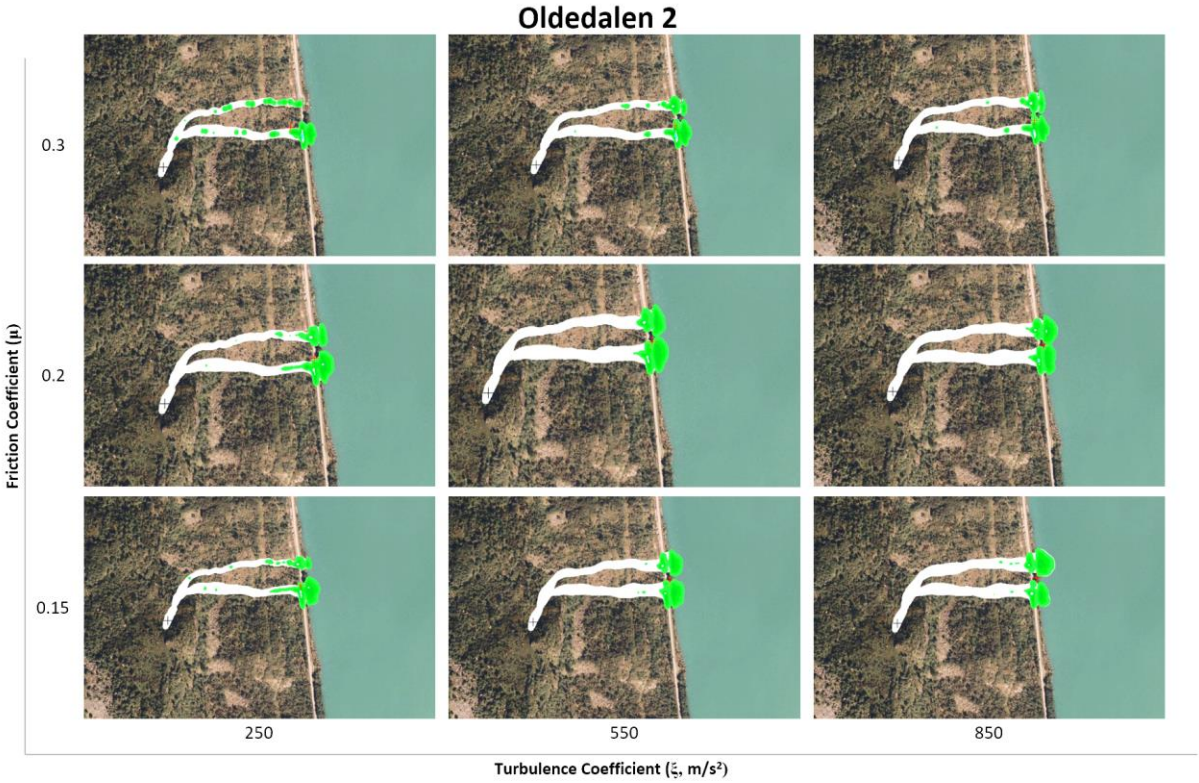

Figure 41: Simulations of Oldedalen 2. Grey represents landslide impact area, light green 0-0.5m deposits, and darker green 0.5-1.5 m deposits.

Simulations for Oldedalen 2 with higher friction coefficients do not reach the full runout length in the northern channel (Figure 41). Increasing the turbulence coefficient increases the lateral impacts of the channels, resulting in overestimates of channel width. The channels are for the most part very well defined, and changing back-analysis parameters does not greatly alter the flow path of the landslide (compared to Oldedalen 1 or Nesbyen cases). The friction and turbulence coefficients can probably be assumed to be very close to Oldedalen 1 due to the sites geographical and geologic similarities. The final volume is estimated to be between 2350 m^3 and 2800 m^3. The site appears less sensitive to changes in the rheological parameters than Oldedalen 1.

Figure 42: DAN3D simulation of Oldedalen 2 using the same back-analysis parameters as Figure 40, with the observed real landslide extent shown by the black dotted lines.

As mentioned for the two previous cases, the channels modelled in DAN3D are slightly wider than those observed in aerial imagery (Figure 42).

5.2.5 Ringebu

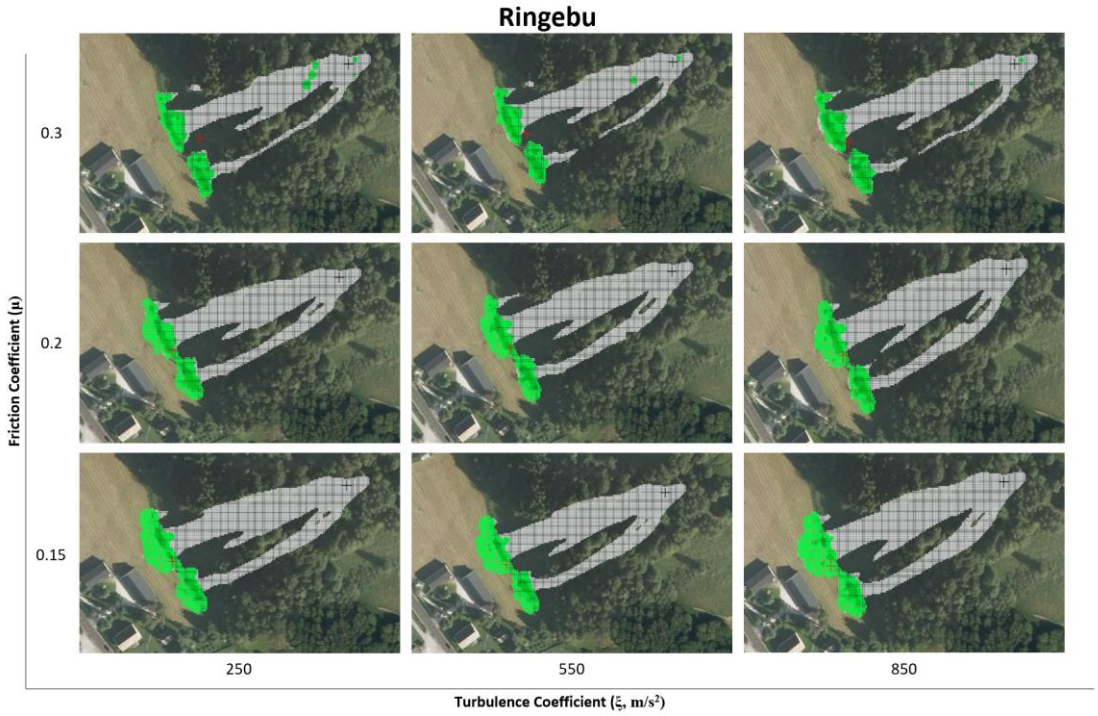

Figure 43: Dan3D simulations of the Ringebu event. Grey represents landslide impact area, light green 0-0.5m deposits, and darker green 0.5-1.5 m deposits.

Dan3D overestimates the size of the southern channel, and the volume that flows down it (the deposit there is larger than it should be). None of the simulations shown in Figure 43 reach the true runout length, as most of the forward progress of the landslide is quickly stopped after the landslide exits the trees onto the field. The friction coefficient is assumed to be between 0.08 and 0.12, and the turbulence coefficient between 350 m/s^2 and 600 m/s^2. The debris avalanche is quite small, with an initial volume estimated from photos and field work to be around 150 m^3 and a final volume around 350 m^3.

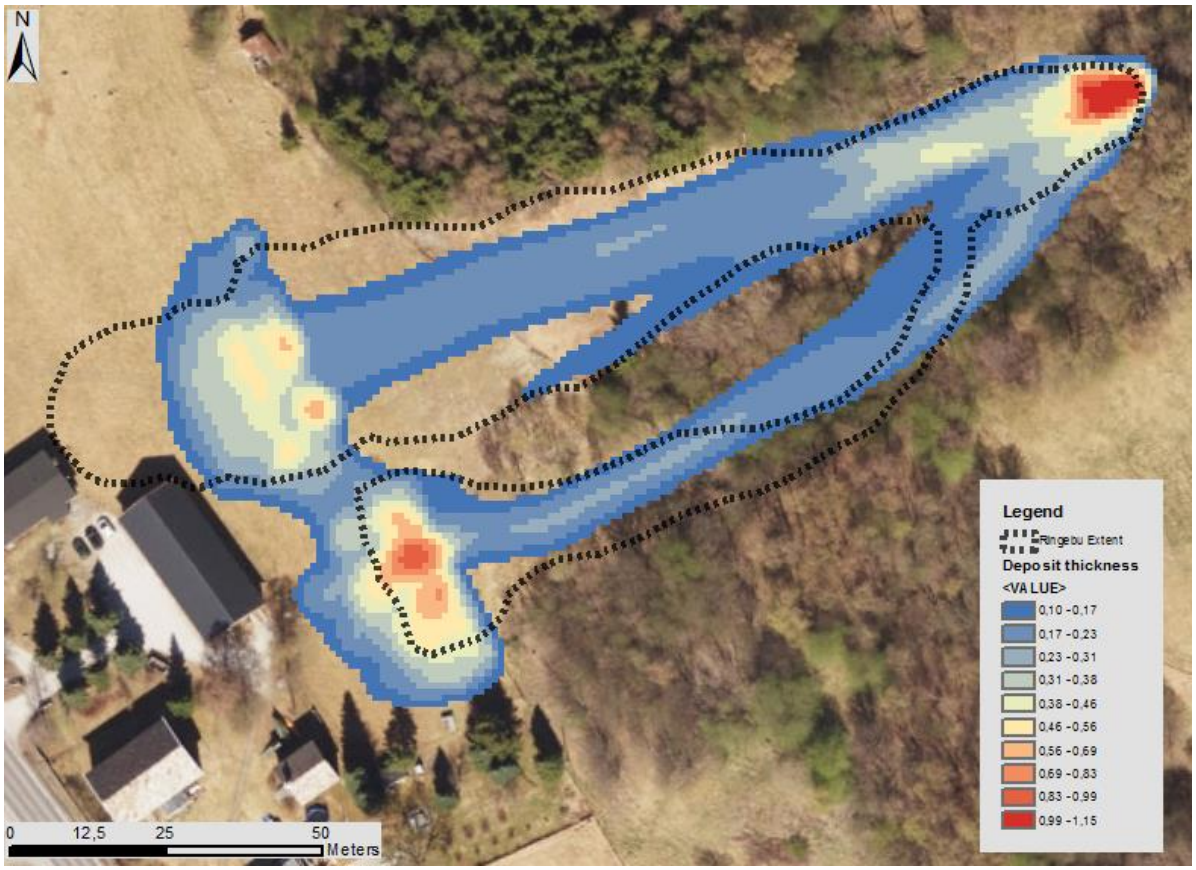

Figure 44: DAN3D simulation with parameters μ = 0.1, ξ = 400 with the mapped landslide extent polygon (black dotted lines). The exact location of the southern channel is hard to determine, as it is obscured by trees in aerial photos and cannot be identified on the DEM.

The model shown in Figure 44 predicts a wider depositional lobe and southern channel, and a shorter runout than observed.

Table 9: Simulation results from Ringebu compared to observed values (runout 166 m, volume 330 m^3).

Run #	μ	ξ (m/s^2)	Length (m)	Max. V (m/s)	Volume (m^3)	Diff. Length (%)
1	0.15	100	162	5.3	406	-11.0
2	0.15	250	162	7.0	409	-11.0
3	0.15	400	163	8.4	408	-10.4
4	0.15	550	163	8.6	408	-10.4
5	0.15	700	164	9.5	410	-9.9
6	0.15	850	166	9.9	411	-8.8
7	0.15	1000	167	10.1	413	-8.2
8	0.2	100	159	4.9	398	-12.6
9	0.2	250	159	6.4	403	-12.6
10	0.2	400	159	7.3	403	-12.6
11	0.2	550	160	8.2	404	-12.1
12	0.2	700	160	8.2	404	-12.1
13	0.2	850	160	8.5	405	-12.1
14	0.2	1000	161	9.0	406	-11.5
15	0.3	100	149	4.1	330	-18.1
16	0.3	250	149	5.0	356	-18.1
17	0.3	400	149	5.7	369	-18.1
18	0.3	550	150	6.3	377	-17.6
19	0.3	700	151	6.5	382	-17.0
20	0.3	850	151	7.0	383	-17.0
21	0.3	1000	152	7.4	386	-16.5

As is shown in Figure 43 and 44, none of the simulations reach the observed runout length, however most are close to the final observed volume. The fractured deposits generated by the simulations with friction coefficient = 0.3 are not realistic or consistent with field observations. Table 9 presents the results of 21 simulations in DAN3D, showing the changes in runout length, volume, and maximum velocity with changing friction and turbulence coefficients.

5.3 GeoClaw

To attempt to compare the results obtained from running landslide simulations in GeoClaw with those from Dan3D, a set of five simulations was run in each program, with identical parameters (Table 10).

Table 10: Simulation numbers and corresponding variable sets used for the GeoClaw and DAN3D comparison simulations.

Simulation	1	2	3	4	5
μ	0,15	0,15	0,15	0,1	0,2
ξ (m/s²)	150	450	750	450	450

While these values may not have been optimal back-analysis parameters for each landslide, the goal of the simulations was the compare the results obtained from each program, not to try to determine the physical parameters. The numerical parameters used for the simulations are shown in Table 11.

Table 11: Numerical simulation parameters used for simulations comparing DAN3D and GeoClaw.

Erosion Rate	0
Time-step	0.1
Maximum run-time*	600s

GeoClaw cannot calculate material erosion, so the erosion rate was set to zero in DAN3D for experiment consistency. Each landslide case was run for a maximum run-time of 600 seconds, with the exception of Oldedalen 2, which ran for 300 seconds.

To better compare the visual outputs of the two programs, images in this section (Figures 45, 46, 47, and 48) show DAN3D results with a margin cut-off thickness (minimum deposit thickness that is plotted) of 0.01 cm, unlike figures in the previous section on DAN3D that use a 0.10 cm cut-off.

5.3.1 Nesbyen

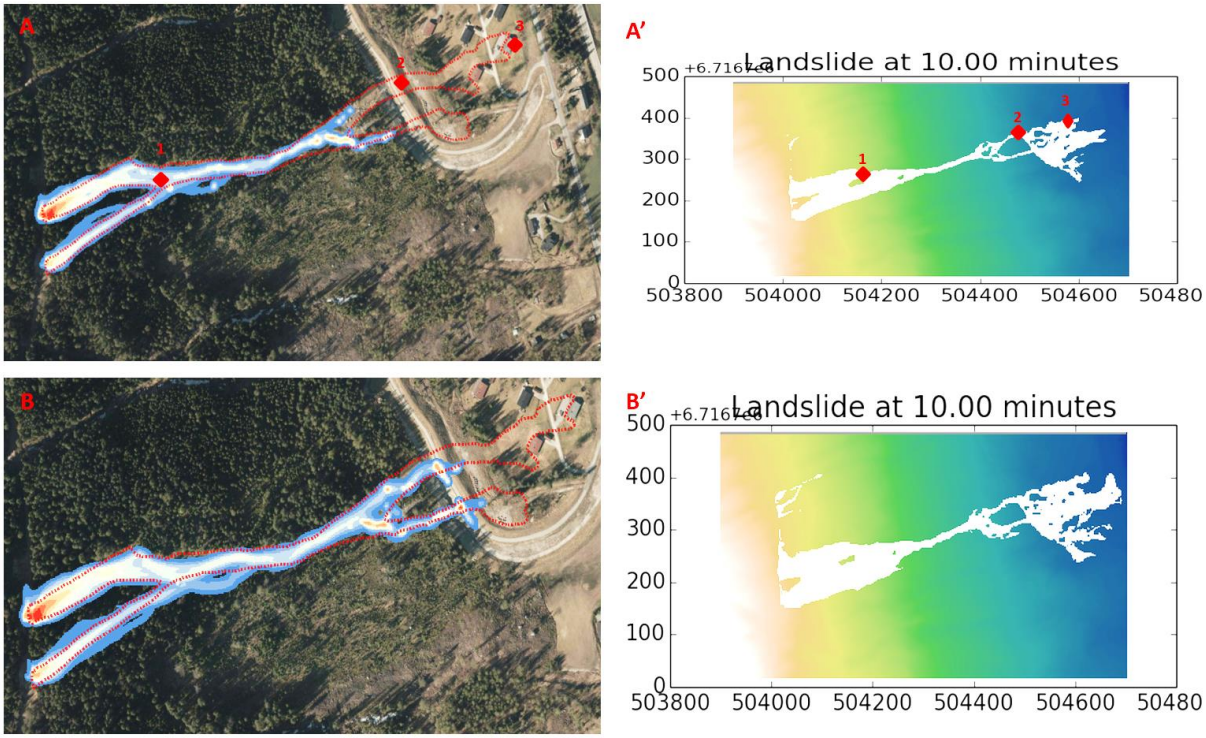

Figure 45: Comparison of simulation results from Nesbyen in DAN3D (A, B) and GeoClaw (A', B'). A and A' show the results from simulation 1, while B and B' present results from simulation 3, at the final time-step (600 seconds). Both simulations show a much higher mobility in GeoClaw than in DAN3D. The numbered locations are included to help reference and compare the two image sets. Thicknesses in figures A and B range from 0.01 cm (blue) to 140 cm (red). Images A and B show the outline of the real debris flow event (dashed red lines). The horizontal and vertical axes in A' and B' represent UTM coordinates.

Figure 45 compares the results from DAN3D and GeoClaw for two of the simulations (1 and 3) from the Nesbyen debris flow.

Recorded deposit depths in GeoClaw are similar to those modelled by DAN3D, however upon flattening out the material in GeoClaw is much more mobile, and the final deposits modelled are thinner, but more laterally extensive.

Some of the initial material in GeoClaw is modelled as moving north, downslope along the forest road from the release area. This is highly unlikely to have actually occurred given the geometry of the source area observed in the field.

Table 12 shows the evolution of runout distance with time for each GeoClaw simulation of the Nesbyen landslide. As the turbulence coefficient is increased, the time required to reach a specific runout length is decreased (i.e. the landslide reaches that runout faster)

Table 12: The maximum runout length of each GeoClaw simulation (Nesbyen) at a given output time. Runout distance was calculated using the UTM coordinates of the topography file and ArcMap. Simulation numbers refer to the simulations with friction and turbulence coefficients explained in Table 10.

Simulation	1	2	3	4	5
Time (min)	Runout (m)				
1	250	390	426	405	385
2	415	520	555	570	490
3	525	580	615	620	525
4	575	620	625	635	580
5	590	630	630	645	600
6	600	645	635	650	610
7	629	650	640	660	615
8	635	655	650	665	620
9	645	660	655	670	625
10	660	665	660	685	630

5.3.2 Oldedalen 1

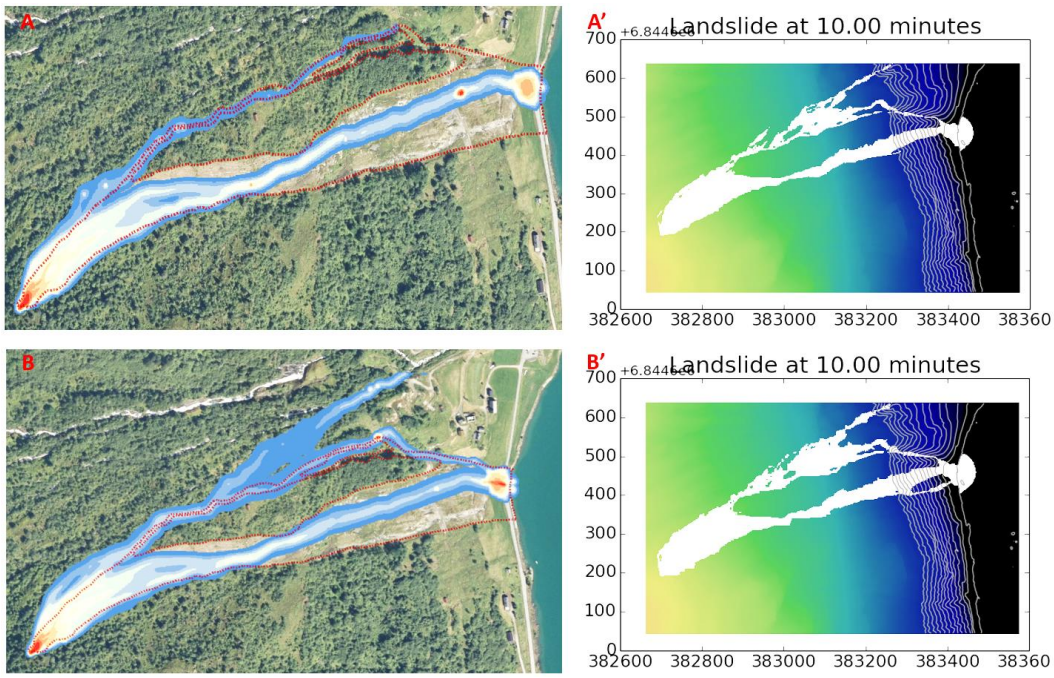

Figure 46: Dan3D (A, B) and GeoClaw (A', B') results for Oldedalen 1 from simulations 1 and 3, respectively. Images A and B show thicknesses from 0.01 cm (blue) to 150 cm (red). The outline of the debris avalanche is also shown (red dashed line) on A and B.

Figure 46 compares results for Oldedalen 1 in both DAN3D (*A*, *B*) and GeoClaw (*A'*, *B'*). Without including any erosion, the final volume of the landslide in Dan3D is greatly underestimated. The higher mobility of the material in GeoClaw leads to more of the landslide being diverted along subsidiary channels north of the main path.

Table 13: GeoClaw simulation output times and related runout lengths from Oldedalen 1. Oldevatnet Lake is located 785 m from the release area, constraining the length of event runout. Simulation numbers refer to the simulations with friction and turbulence coefficients explained in Table 10.

Simulation	1	2	3	4	5
Time (min)	Runout (m)				
1	375	600	740	635	545
2	656	780	785	785	780
3	780	785	785	785	785
4	785	785	785	785	785
5	785	785	785	785	785
6	785	785	785	785	785
7	785	785	785	785	785
8	785	785	785	785	785
9	785	785	785	785	785
10	785	785	785	785	785

Changing the friction or turbulence coefficients does not affect the total runout length of the landslide (constrained by Oldevatnet) however it does impact how quickly the landslide reaches the lake (Table 13). Increasing the turbulence coefficient, or lowering the friction coefficient reduces the time required for the landslide to reach the lake.

5.3.3 Oldedalen 2

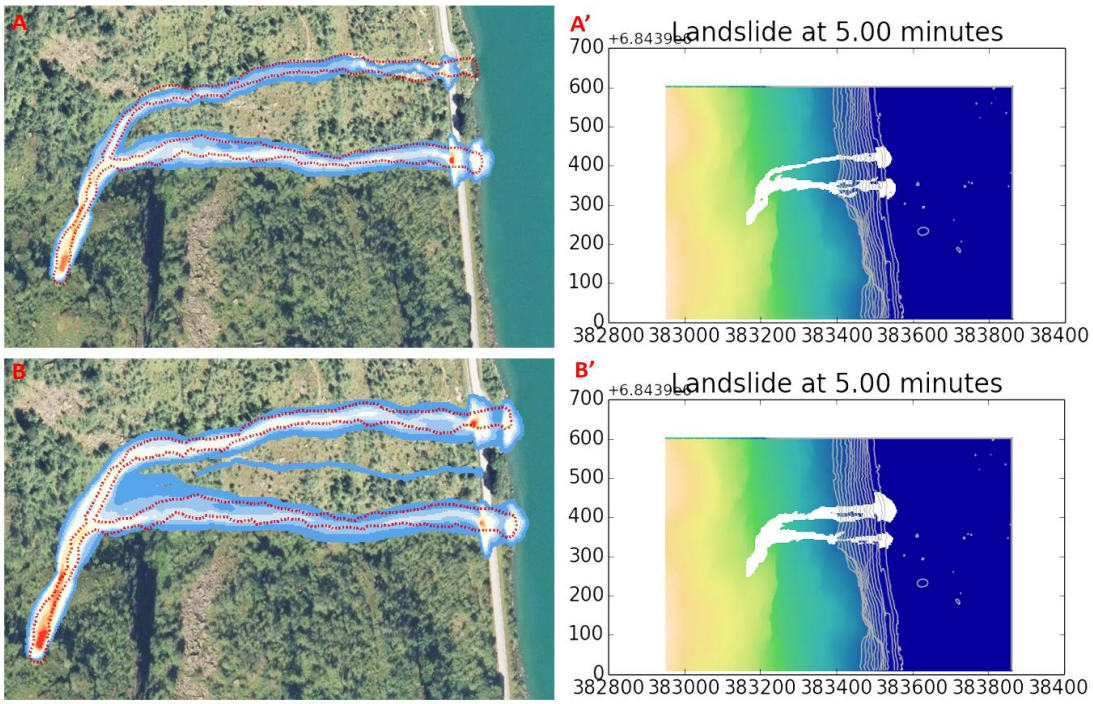

Figure 47: Dan3D (A, B) and GeoClaw (A', B') results for Oldedalen 2 from simulations 1 and 3. For images A and B the thickness ranges from 0.01cm (blue) to 180cm (red). The outline of the debris flow event is included (red dashed line).

Figure 47 presents a comparison of two simulations (1 and 3) for Oldedalen 2 in DAN3D and GeoClaw. In both programs, increasing the turbulence coefficient seems to increase the volume

of material that travels in the northern channel, however the effect is much more noticeable in GeoClaw. DAN3D models the formation of two depositional lobes, along Fv 724 and at the lake level. GeoClaw shows only one depositional lobe, at the lake level. Similarly to Oldedalen 1, the final volume of each simulation is an underestimate as the models do not included erosion and entrainment of material. The modelled landslides occur very rapidly, with GeoClaw simulations reaching the full runout extent within the first 60 seconds for turbulence coefficients higher than 150 m/s^2 (Table 14).

Table 14: GeoClaw simulation output times and related runout lengths from Oldedalen 2. Simulation numbers refer to the simulations with friction and turbulence coefficients explained in Table 10.

Simulation	1	2	3	4	5
Time (min)	Runout (m)				
1	370	465	465	465	460
2	460	465	465	465	465
3	465	465	465	465	465
4	465	465	465	465	465
5	465	465	465	465	465

5.3.4 Ringebu

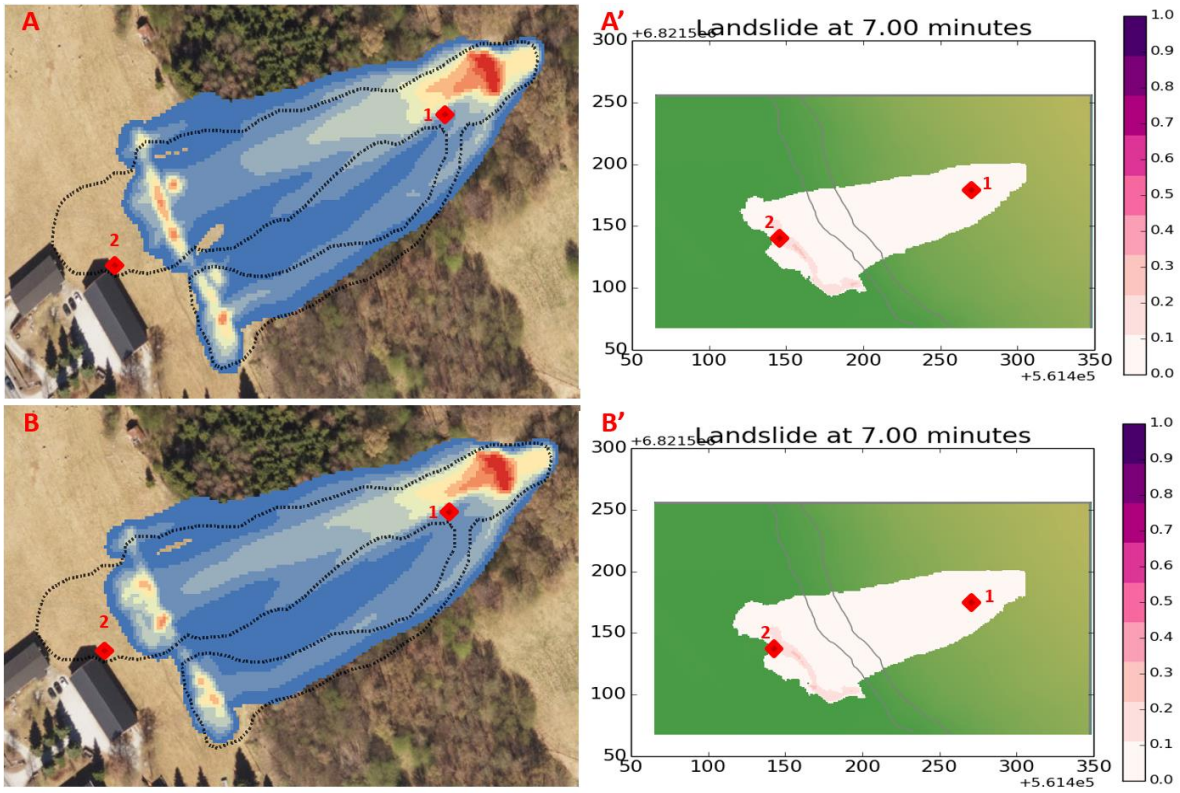

Figure 48: Dan3D (A, B) and GeoClaw (A', B') results for Ringebu simulations 1 and 3. For images A and B the thickness ranges from 0.01 cm (blue) to 110 cm (red). The outline of the debris avalanche event is included (black dashed line).

Figure 48 shows a comparison of simulations 1 and 3 for the Ringebu debris avalanche event. Consistent with simulations run on the other events, DAN3D presents an underestimate of final runout, while GeoClaw overestimates the runout and path width. Table 15 presents the runout achieved by each GeoClaw simulation at different simulation times.

Table 15: GeoClaw simulation output times and related runout lengths from Ringebu. Simulation numbers refer to the simulations with friction and turbulence coefficients explained in Table 10.

Simulation	1	2	3	4	5
Time (min)	**Runout (m)**				
1	146	150	150	152	148
2	155	157	160	160	155
3	158	163	170	165	162
4	162	170	175	173	167
5	167	173	177	176	170
6	169	177	180	177	172
7	171	181	183	180	173

6 Discussion

This chapter contains a discussion on the results presented in Chapter 5, focusing on the capability of the two runout modelling programs used to accurately model the landslide events.

6.1 Grain size analysis

One of the goals of collecting soil samples from the studied sites was to observe differences between the static internal friction angle that can be obtained from the grain size distribution curves, and the dynamic friction angle used as part of the Voellmy rheology (atan μ). From a soil mechanics viewpoint, glacial till is a difficult material to predict as it is characteristically neither clay nor sand, and does not conform to standard depositional models (Bell, 2002). Of the collected samples, those from Oldedalen 2 show the greatest concentration of coarse clasts (less than 15% of the samples by weight consist of grains smaller than medium sand), Nesbyen and Oldedalen 1 are both broadly similar with 35% – 40% of the samples by weight containing grains smaller than medium sand. Ringebu has the highest concentration of finer grains, with 55% of the sample weight consisting of grains finer than medium sand. Given that the geotechnical properties of tills are typically governed by their clay content (Bell, 2002), the samples are loosely grouped into three classes; with Oldedalen 2 in one class, Ringebu in another, and Nesbyen and Oldedalen 1 in the final class (Table 16)

The friction angle of granular soils increases with grain roughness, angularity, density, and grain size. Well-graded soils have higher friction angles than their poorly graded counterparts, and a soil will have a friction angle that is 1°- 2° lower when wet (Ameratunga, et al., 2016).

Holtz et al., (2010) explains how soils can be classified and described based on their grain size distributions (for example, a “silty gravel” specifies a soil where more than 50% of the material is larger than 4.75 mm, and more than 12% is silt particles smaller than 0.075 mm). Previous works have constructed tables correlating soil classification with relative soil density and internal (static) friction angle. These friction angles are static friction angles and differ from the dynamic friction angle used by the runout programs (which was within the range of 4° - 10° after the calibration of the runout simulations). The classifications, static internal friction angles of the soil samples, and the calibrated dynamic friction angles for the studied landslide sites are presented in Table 16.

Table 16: Soil sample classifications and related static internal friction angles.

Sample	Classification	Internal friction angle (°)	Dynamic friction angle (°)
Nes Channel Top	SM - silty sand	26 - 29	4.60
Nes Channel Bottom	SM - silty sand	26 - 29	4.60
Old 1 - Track	SM - silty sand	26 - 29	10.50
Old 1 - Initiation	SM - silty sand	26 - 29	10.50
Old 2 - Channel 1	GM - silty gravel	27 - 31	10.50
Old 2 - Channel 2	SP - poorly graded sand	26.5 - 30	10.50
Ringebu	SC - clayey sand	26 - 29	5.70

Table 16 shows that the soil samples collected from the Oldedalen 1 and 2 sites exhibit slightly different characteristics, and that the assumption made during modelling that material from each site would behave similarly is possibly false. However, the differences in static friction angle are minor, and may have only a negligible impact on the results. This difference in material properties indicates slightly different groundcovers at the two sites, possibly deriving from the slope geometry (Oldedalen 1 being an open slope while Oldedalen 2 is channelized).

6.2 Physical similarities and differences between the events

While all four events studied were caused by precipitation events, the Ringebu and Nesbyen events were the result of a spring storm system in southern Norway, and the two Oldedalen events occurred in November. Snowmelt may have therefore had at least some impact on the initiation of the Oldedalen events, with runoff from snow higher up the mountain side contributing to the water present on the slope. Snow is not thought of have been a factor in either the Nesbyen or Ringebu events, as no snow was still present at those locations in late May 2013.

Nesbyen and Oldedalen 2 both exhibit classic channelized flow characteristics of debris flows, while Ringebu and Oldedalen 1 have wider paths and occur on more open slopes, appearing more as debris avalanches. The presence of running water in small drainage channels at surface may have contributed to the initiation of the Ringebu, Nesbyen, and Oldedalen 2 events.

The Ringebu area is covered by a thick soil layer, containing a noticeably higher percentage of finer grain sizes than the other sites. While soil cover at the Nesbyen site is also quite thick, the hill cover is much rockier, and the soil contains more boulder-sized clasts. Compared to the other two sites, the soil cover in Oldedalen is relatively thin.

The relatively high H/L ratios for the two Oldedalen events are a result of the runout being stopped by Oldevatnet Lake. Given the volume of material involved, Oldedalen 1 at least could be expected to have had a longer runout if the lake was not present. The H/L ratio of the Ringebu

event is also likely anomalously high due to the low volume of the debris avalanche. This event could have been expected to have a slightly longer runout, due to the predominance of fine-grained material. The Nesbyen site was debris flow was highly channelized, possibly explaining its longer runout and lower H/L ratio.

6.3 Runout models

The following sections present a discussion of the results from the runout simulations for each of the studied landslide sites (in both DAN3D and GeoClaw).

6.3.1 Numerical Parameters

When testing the numerical parameters used in DAN3D, it was found that the original default parameters give the best results for the modelling of small to medium-sized debris flows and avalanches. Any improvements in model accuracy as a result of these changes were for the most part quite small and insignificant when compared to the increased computational requirements and costs.

For a case with relatively smooth slope topography such as Nesbyen, changing the simulation time-step did not greatly impact the results. Lowering the time-step greatly increases the time required to run each simulation, without increasing simulation accuracy. Increasing the time-step slightly increased the simulation runout distance, however a time-step that is too large can produce unrealistic or geometrically inaccurate results. Experimenting with larger time-steps (0.5 s – 1.0 s) for the Oldedalen 2 case resulted in large variances in the recorded simulation velocity and created unrealistic path geometries, depending on when the debris flow event interacted with the cliff band.

Increasing the number of particles used in the simulations increased the simulation accuracy, as was expected. However, increasing the number of particles also resulted in much longer simulation times and more instances of the program crashing due to memory loss. 2000 particles is a good intermediary number between low accuracy coarse estimations and obtaining more detailed results in a timely manner. It should also be noted that including erosion in the models will slow down the simulation further. For very small landslides, such as the Ringebu case, further work with increased particle counts could be conducted to attempt to improve accuracy. Running larger landslide cases, such as Oldedalen 1, with 3000 or 4000 particles would require more computing power than was available to the author for this thesis.

Increasing the smoothing length constant lowered the maximum velocity of the simulations, and also reduced the runout length. A smoothing length constant of one results in unrealistically high recorded velocities (43 m/s), as well as unrealistic deposit geometries (Figure 49). Setting the smoothing length constant between 3 and 5 returned simulations that were closest to the observed event.

Figure 49: Simulation in DAN3D (Nesbyen) with the smoothing length constant set to 1. This resulted in unrealistic geometries in the release area, and along the debris flow path and in the deposition area.

6.3.2 Nesbyen

The Nesbyen debris flow was the only site to have available LiDAR data from both before and after the landslide event, so it is assumed to have the most accuracy when estimating the initial release volume and the size of the source area. Additionally, previous reports were available for the site and were used to validate the release volume assumptions. The initial volume of the landslide calculated by subtracting the before and after DEMS over the source area is within the range of values estimated by NGI (NGI, 2013a).

Of the initial 28 simulations run with systematic increases in turbulence and friction coefficients, most were underestimates of the final runout length. Those which did approach the final runout length greatly overestimated the final volume and lateral extent of the debris flow in the depositional zone. DAN3D does not take into account the influence of buildings or wooded areas on the development of the deposition zone, so some difference between the model results and the observed geometry was expected. The simulation with the best fit from DAN3D has a friction coefficient of 0.087, and a turbulence coefficient of 550 m/s^2. The simulation reached a maximum velocity of 13 m/s.

Running simulations without erosion to compare to GeoClaw showed the importance of including erosion for DAN3D simulations. Without erosion, the final volume of the landslide is much too low, and the event does not travel anything even approaching the real runout distance. Increasing erosion or initial volume in DAN3D was found to result in an increase in the runout length, independent from any changes to the friction coefficient.

At low turbulence coefficients, both GeoClaw and DAN3D show similar path morphologies, though the deposits in GeoClaw are thinner but more laterally extensive. The GeoClaw simulations show much higher mobility in the material, resulting in more extensive deposits and a longer runout length. The maximum deposit depth in GeoClaw is less than 30cm, again

indicating a high mobility, and that the used friction angle may be too low. Additionally, material from the source area was seen to flow down the forest road in the high turbulence coefficient simulation in GeoClaw. This is unrealistic and did not happen. Similarly to DAN3D, in GeoClaw the turbulence coefficient controls the velocity of the flowing material, and the friction angle is the main control on the runout distance. This can be seen in Table 12, where the runout distance is longest for simulation 4 (lowest friction angle) and shortest for simulation 5 (highest friction angle). Increasing the turbulence coefficient in simulations 1, 2 and 3 affects the time the material takes to reach a given runout length (i.e. impacting the speed at which the material is moving downslope).

6.3.3 Oldedalen 1

As the runout of the debris avalanche ended in the Oldevatnet Lake, calibrating the friction coefficient based on model runout distance was difficult for this event.

None of the simulations properly modelled the width of the main path; all were underestimates of the actual width. On the other hand, the simulations tended to overestimate the amount of material that went into smaller channels north of the main path. Increasing the turbulence coefficient increased the volume of material diverted here. In those simulations with a turbulence coefficient higher than 550 and a low friction coefficient, material continued north towards Yrielva, something that was not observed in the actual event (none of the houses or farms in Yri were impacted by the debris avalanche event, beyond the damage to Fv 724).

Simulations with no erosion included travel down the main path, but cover less than a third of the true width and are large underestimates of the final volume of the event. Attempting to start the simulation with higher initial volumes, and no erosion, results in more material being diverted north to Yrielva and impacting Yri. While there is no LiDAR data available from after the debris avalanche event, this knowledge of which areas were impacted by the event helps to constrain the size of the initial release, and helps to give at least a rough indication of the final volume of the event.

Using this information, a DAN3D simulation with friction coefficient 0.185 and turbulence coefficient 400 was run. This simulation gave the best fit to the observed landslide event, but still underestimated the width of the main path.

DAN3D and GeoClaw cannot accurately depict the deposit of the landslide because the material entered Oldevatnet Lake. The build-up of material at the base of the slope observed in these simulations is therefore unrealistic. Without this buildup and lateral spreading, the modelled depositional area would actually be thinner than shown.

As erosive forces played a large role in the debris avalanche event, DAN3D performs better than GeoClaw when modelling the event. Similarly to the Nesbyen case, when comparing the two programs, the material in GeoClaw has a higher mobility than in DAN3D. GeoClaw also overestimates the material and impact of the minor north channel. Both programs are consistent

in that the overestimate of the minor channel is greater when using a higher turbulence coefficient.

6.3.4 Oldedalen 2

Oldedalen 2 was the least sensitive of the studied landslide events to changes in the friction or turbulence coefficients in DAN3D. As runout is constrained by Oldevatnet Lake it is again difficult to assess the impact of changing the friction coefficient (similar Oldedalen 1). At low turbulence coefficients, the high friction coefficient (0.3) simulations did not reach the full runout in the northern channel. This provides at least some information on a possible upper bound.

The northern channel is well established and marked as a drainage on topography maps, and deposits consistent with previous debris flow events were observed along the channel banks. There is no evidence of the southern channel being active before neither in aerial photos of the site nor in the soil record. Despite this, both programs accurately predict the location of the second channel.

The mechanism causing the debris flow to split into two channels is unknown as the area could not be accessed during field work. It is possible a boulder partially blocked one of the paths during the event, causing material to back up and flow over the side, but this is conjecture. When running simulations in DAN3D, the two channels would form concurrently, seeming to disprove any theories that the channels formed as part of separate surging events. Changing the turbulence coefficient controlled how much material went into which channel. As there are no depositional lobes or deposits to analyze, the final volume at the base of each channel is unknown, so this cannot be used to constrain the turbulence coefficient.

For the DAN3D analysis, the same parameters as Oldedalen 1 were used and returned a good fit. It was assumed that due to the close proximity of the two events and the similarities in surficial and bedrock material (Figure 23) that there was little difference in parameters between the two sites. As Oldedalen 1 was more sensitive to changes in model parameters, it was used to approximate the parameters, with a simulation in Oldedalen 2 then being run to double check the validity of this assumption.

GeoClaw shows a marked difference in the sizes of each channel as the turbulence coefficient is increased. The material modelled in GeoClaw again has increased mobility, and a greater lateral extent to all parts of the slide. Both GeoClaw and DAN3D model the debris flow as being extremely fast moving, reaching speeds in excess of 20 m/s at times in DAN3D, and reaching Oldevatnet Lake within the first 60 seconds of the simulation (giving an average velocity of over 6 m/s).

6.3.5 Ringebu

The Ringebu event is a very small debris avalanche, where erosion was not as important as at the other events studied. The initial volume of the release area makes up almost 50% of estimated final landslide volume. However, there is still large uncertainty with this data. No detailed information on the deposits is available, and LiDAR data was not available for after the debris avalanche event to provide more detailed information on the release volume.

DAN3D underestimates the final runout, and models the landslide as slowing down and spreading out too much when extending onto the field at the base of the slope. Higher friction coefficients produced unrealistic "jumpy" and discontinuous paths in DAN3D. DAN3D does a good job of modelling the width of the main path, however overestimates the width and impact of the minor (southern) path. It is barely visible in most aerial images of the site, and is likely only a few meters wide, in contrast to the tens of meters modelled in DAN3D. It is possible more material passed through the trees here without removing them, but this is unknown.

GeoClaw greatly overestimates the width and lateral extent of the event, removing any separation in the two paths, showing them as one (early time steps show some initial separation, before closing). This merging of the two paths could also be seen in the DAN3D simulations in Figure 48. Deposit thicknesses less than 10 cm are included in the plot here, accounting for the greater lateral spread of the modelled deposits. The maximum thickness of the deposits in GeoClaw is 40 cm, less than half of that in DAN3D. Again, this is consistent with results from the other cases, and indicates the material having a much higher mobility, and lower resting angle.

6.3.6 Summary of DAN3D Results

Table 17 presents the calibrated model parameters for each of the studied landslide events, as well as comments from the simulation relating to the model accuracy. The calibrated values are within the ranges of values discovered by previous studies to be good for simulations of alpine debris flows and debris avalanches (Section 6.2.8). Values within these ranges can be used as a starting point for future modelling of debris flow and debris avalanche events, hopefully reducing the time needed to calibrate them.

Table 17: Parameters used to obtain the best fit model results for each simulation in DAN3D.

Site	μ	ξ (m/s²)	Velocity (m/s)	Runout (m)	Diff. Runout (%)	Comments
Nesbyen	0.07–0.09	600–800	13	630	-4.5	Maximum model runout achieved in wrong area, so actual difference between observed and modelled runouts is greater
Oldedalen 1	0.18–0.2	350–450	14	790	0	Lower portion of the debris avalanche path width is underestimated
Oldedalen 2	0.18–0.2	350–450	24	458	0	Slight overestimate of channel widths. Model shows lateral spreading of deposits along the road bed, which was not observed
Ringebu	0.08–0.12	350–400	9	168	-4	Maximum observed runout not achieved, and the southern channel size is overestimated. The model creates depositional lobes that are more laterally extensive than the observed

6.3.7 Comparison of DAN3D and GeoClaw

Previous studies (McKinnon, 2010; Cepeda, 2009; Hürlimann et al., 2008) found similar results when using the Voellmy rheology; the friction coefficient is the main control on landslide runout distance, while the turbulence coefficient affects the flow speed. The final runout of the landslides modelled in this thesis could be changed both by changing the friction coefficient, or the erosion rate and initial release volume of the event. This shows the importance of accurate remote sensing and field investigation data when characterizing the source area, as it greatly reduces the number of assumptions the user must make and the final uncertainty in the results.

DAN3D and the Voellmy rheology have been found to be most accurate on medium to large landslides (volumes greater than 1000 m^3) (Cepeda, 2009). This could explain the consistent underestimate of the runout lengths that was observed in DAN3D, as most of the events studied as part of this thesis were relatively small. The simulations run in GeoClaw reached further runout lengths and had less thick deposits than their DAN3D counterparts, indicating a greater material mobility in GeoClaw.

While both programs were using the Voellmy rheological model with identical input parameters, simulations were different in each program. Both programs require the same sets of input parameters and setup files. Preparing topography files for DAN3D is slightly more complicated as the program recognizes few input file types; however, many of the same steps

were required to prepare files for GeoClaw. Generally, if the topography files are ready for use in DAN3D, setting them up for use in GeoClaw is simple and easy.

As GeoClaw is open source, a greater amount of customizability is available to the user. On the other hand, DAN3D has a much cleaner and easier to understand interface, and the learning curve for it is less steep. GeoClaw runs slightly faster than DAN3D, but does not include erosion, which is typically very important when modelling debris flows and avalanches, as they are often characterised by their great erosive force compared to other landslide types. It should be noted that DAN3D does not take into account lateral erosion (undercutting of debris flow channels), but only takes into account only basal erosion when modelling landslide erosion.

Outputs from DAN3D are more visual, and require less "work" and knowledge of coding to obtain information from. While GeoClaw offers the user more customization options with the results, a certain level of knowledge with coding in either Matlab or Python is required to get the most from the output data.

Currently, DAN3D is the better program for modelling small to medium sized debris flows and avalanches, as it is both easier to use and gives more accurate results.

6.3.8 Results in a global context

The results obtained from landslide back-analysis in DAN3D in this thesis are a good fit with other studies completed on global landslide events. A 2005 study of several debris flows in Yosemite Valley in the USA (Bertolo & Wieczorek, 2005) using DAN and FlO2D found that the two parameter Voellmy model best predicted the debris flow results with friction coefficients of 0.1 – 0.12, and turbulence coefficients of 500 m/s^2 – 600 m/s^2. These values are similar to those presented in this thesis as providing the best model results.

Quan Luna et al., (2013) conducted a study investigating the calibration of input parameters for the Voellmy model (turbulence and friction coefficients) from a number of previously studied debris flows and debris avalanches. The distributions of friction and turbulence coefficients obtained from the resulting database of back-analysed landslide events are presented in Figures 50 and 51.

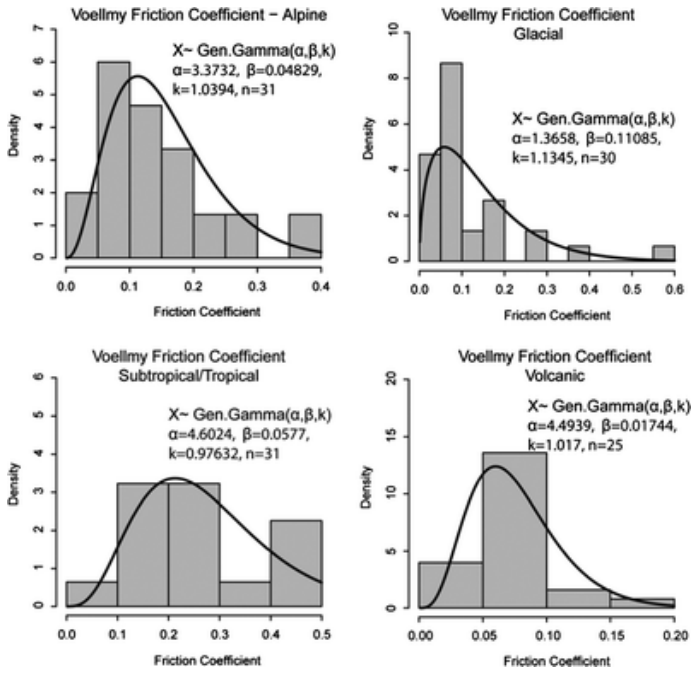

Figure 50: Probability distribution functions showing the variation in Voellmy model friction coefficients for debris flows and avalanches occurring in different environments. From Quan Luna, et al., 2013.

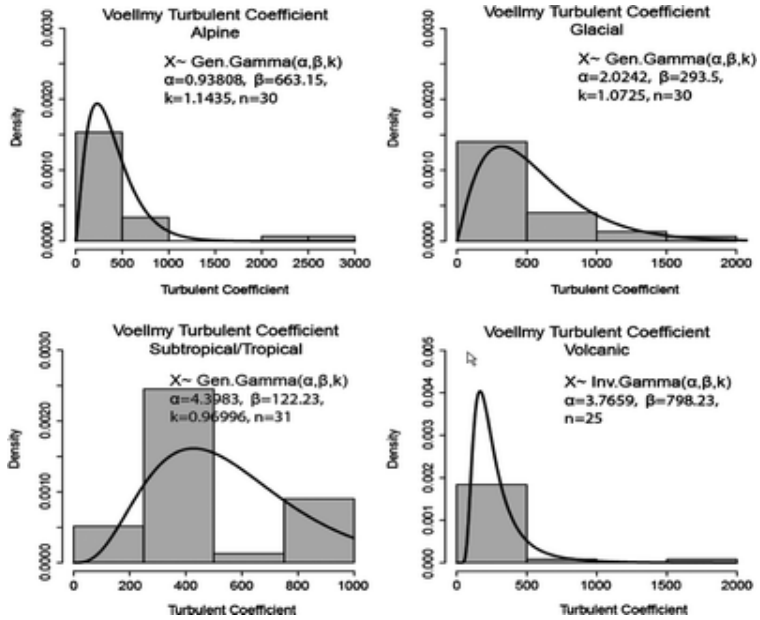

Figure 51: Probability distribution functions showing the variation in Voellmy model turbulence coefficients for debris flows and avalanches occurring in different environments. From Quan Luna, et al., 2013.

The range of friction and turbulence coefficients found in this thesis to produce the best model results for the studied debris flow and debris avalanche events fit well the distribution for "Alpine" events in figures 50 and 51 (Table 17).

6.4 Assumptions and sources of error

6.4.1 Grain size analysis

As the sieving and Coulter analyses measure different properties of the grain sizes, combining the two sets of data will introduce an error into the results. Particle diameters obtained from sieving are likely to represent the intermediate particle axis, resulting in an underestimate when compared to particle spherical volume, obtained from the Coulter analysis.

All of the material sampled in this thesis is glacial till, and as such there is are large degree of uncertainty associated with soil sample collection in the field. Till deposits are incredibly varied, and sampling at one location may return mostly sand and small gravel clasts, while a sample taken 60 cm away might include large cobbles and boulders. Additionally, some of the largest clasts included in the soil samples could not be weighed using the equipment available to the author (they weighed more than the maximum measurable by the scales used). The weight of these clasts was calculated by measuring the clast dimensions, and then calculating the weight based on an assumed density of 2.7 g/cm^3. Because of this, the error in the grain size distribution curves is greatest for the large clasts. However, of greatest interest (from a geotechnical viewpoint) in these curves is the fine grained fraction, as this has the greatest impact on material behaviour, especially when exposed to water. The constructed grain size distributions are most accurate for the silt, clay, and fine grained sand particles (those particle size ranges covered by the Coulter analysis), so any inaccuracies and error in the larger clasts are insignificant, especially when compared to the inherent variability within till material.

6.4.2 Runout Simulations

The accuracy of the runout simulations is dependent on the input topography data, and selection of back-analysis parameters and material properties by the user. All of the path topography files were created from 1m DEMs, which was the highest level of accuracy available. The Nesbyen site is assumed to have less error than the others in this thesis, as the release volume was calculated by subtracting before and after LiDAR data for the event. For the other events, the release volume topography file was prepared by the author based on information from field observations and aerial photos, with varying accuracy.

None of the landslide deposits could be seen or observed in the field, either due to the land being reworked after the event by the landowners (Ringebu and Nesbyen) or due to the presence of Oldevatnet Lake (Oldedalen 1 and 2). Model accuracy in the deposition area was therefore difficult to determine, and was based primarily on aerial imagery and photographs taken shortly after the events occurred.

7 Further work and improvements

While DAN3D is currently the better program for modelling debris flows and avalanches, the open source nature of GeoClaw and associated support software mean there are lots of opportunities for further research and development. If GeoClaw can be further developed to include an erosion term in the calculations, its usefulness and modelling accuracy will greatly improve. Additionally, work could be conducted focusing on developing tools within Matlab and Python to better visualize the results obtained from GeoClaw.

GeoClaw is currently most often used for modelling subaqueous landslides and associated tsunamis (Clawpack Development Team, 2017), so using it to model subaerial granular flows is a novel approach. Previous work at the Norwegian Geotechnical Institute (NGI) had resulted in a version of the GeoClaw software package specialized for modelling quick-clay landslides using the Bingham rheology (BingClaw, (Kim & Løvholt, 2017)), so the potential exists within the program framework for it to be optimized for granular flows.

To test the usefulness of the GeoClaw introductory user guide that was formulated as a part of this thesis, it should be used by someone new to landslide modelling in GeoClaw, but preferably with at least some knowledge of landslide runout modelling (in DAN3D, RAMMS, or similar). Modelling a landslide event that has already been studied in DAN3D or RAMMs first is easiest, as the topography files are already prepared and can quickly be added for use in GeoClaw.

To improve the accuracy of the model results, more detailed field survey should be conducted focusing on:

- Better defining the initial release area of each event (especially if LiDAR data from after the event had occurred is not available). This would help better estimate the initial release volume of the event, reducing the number of unknowns and assumptions made when modelling.

- Detailed field observations along channel margins such as mud splash marks and other damage to trees can be used to validate modelled flow depth and velocity. If possible, the radius of curvature around channel bends and any differences in levee height could also be measured and used to estimate the flow velocity.

- Detailed surveying of the deposition zone to better the shape and size of the depositional lobe. Alternatively, if the deposition zone has been modified since the event, talk to the landowners or contractors who modified it.

8 Conclusions

Of the landslide events studied in this thesis, two were classified as debris flows (Nesbyen and Oldedalen 2), and two as debris avalanches (Oldedalen 1 and Ringebu). All the events were triggered by precipitation events and the subsequent saturation and increase in pore pressure in soils present in the release area. The presence of a forest track is likely significant in the initiation of the Nesbyen debris flow. Likewise, the presence of snow higher up the mountain of Oldedalen and the late date at which the events occurred (November) may be significant when considering water supply to the hillside.

When modelling the events in DAN3D with the Voellmy rheology, the default numerical parameters associated with the program were found to be good estimates, and consistently produced models most similar to the observed events. When performing the back-analysis, adjusting the friction coefficient was found to have the greatest control on final landslide runout, while the turbulence coefficient controlled the downslope velocity of the material. Landslide paths deposit geometries modelled in DAN3D fit well those observed in the field; however, the runout length was an underestimate of the observed value.

DAN3D produced more accurate landslide back-analyses than GeoClaw, and is currently the better program software to use when characterising granular flow events. GeoClaw has great potential, but more work is required to better adapt the program for work with granular slides. It is hoped that the introductory manual on how to setup landslide back-analyses in GeoClaw included with this thesis will help future users in attempts to better optimize the software.

References

Aaheim, A. et al., 2009. *Konsekvenser av klimaendringer, tilpasning og sårbarhet i Norge,* Oslo, Norway: CICERO Senter for klimaforskning.

Aaheim, A., Romstad, B. & Sælen, H., 2010. Assessment of risks for adaptation to climate change: the case of land-slides. *Mitigation and Adaptation Strategies for Global Change, 15,* pp. 763-778.

Aleotti, P. & Chowdhury, R., 1999. Landslide Hazard Assessment: summary review and new perspectives. *Bulleting of Engineering Geology and the Environment,* August, pp. 21-44.

Ameratunga, J., Sivakugan, N. & Das, B., 2016. *Correlations of soil and rock properties in geotechnical engineering.* s.l.:Springer.

Anfinnsen, S., 2017. *Characterization of shallow landslides, based on field observations and remote sensing,* Oslo: Universitetet i Oslo.

Bargel, T. H. & Lund, M. R., 2016. *Historiske jordskred og flomskred i Arnegårdslia, Nes kommune, Buskerud,* Oslo: Norges vassdrags- og energidirektorat (NVE).

Barnes, H. A., Hutton, J. F. & Walters F.R.S, K., 1989. *An Introduction to Rheology*. Amsterdam: Elsevier Science Publishers.

Beckman Coulter, 2011. *Ls 13 320 Laser Diffraction Particle Size Analyzer: Instruction for use.* Brea, California: Beckman Coulter Inc..

Bell, F., 2002. The geotechnical properties of some till deposits occurring along the coastal areas of eastern England. *Engineering Geology 63,* pp. 49 - 68.

Berger, M., George, D., LeVeque, R. & Mandli, K., 2011. The GeoClaw software for depth-averaged flows with adaptive refinement. *Advances in Water Resources,* Volume 34, pp. 1195-1206.

Bertolo, P. & Wieczorek, G., 2005. Calibration of numerical models for small debris flows in Yosemite Valley, California, USA. *Natural Hazards and Earth System Sciences,* Volume 5, pp. 993-1001.

Cepeda, J. M., 2009. *Characterisation and Risk Management of Rainfall-Induced Landslides: a thesis presented for the degree of Philosophiae Doctor (Ph.D.) at the University of Oslo,* Oslo: Universitetet i Oslo.

Cepeda, J., Quan Luna, B. & Nadim, F., 2013. *Assessment of landslide run-out by Monte Carlo simulations. Proceedings from the 18th International Conference on Soil Mechanics and Geotechnical Engineering.* Paris, s.n.

Clawpack Development Team, 2017. *Clawpack Version 3.4.1.* s.l.:http://www.clawpack.org.

Corominas, J., 1996. The angle of reach as a mobility index for small and large landslides. *Canadian Geotechnical Journal 33*, pp. 260 - 271.

Costa, J., 1984. Physical Geomorphology of Debris Flows. In: *Developments and Applications of Geomorphology.* s.l.:Springer, pp. 268-312.

Crosta, G., Imposimato, S. & Roddeman, D., 2002. Numerical modelling of large landslides runout and stability. *Natural Hazards and Earth System Sciences,* pp. 523-538.

Dahl, M.-P.et al., 2013. Numerical runout simulation of debris avalanches in the Faroe Islands, North Atlantic Ocean. Volume 10.

Dahl, M.-P. J., 2011. *Risk management tools for flow-type landslides in the Faroe Islands, North Atlantic Ocean,* s.l.: Prinfo Paritas Digital Service.

Davies, T., 1986. Large Debris Flows: A Macro-Viscous Phenomenon. *Acta Mechanica 63,* pp. 161 - 178.

De Blasio, F. V., 2011. *Introduction to the Physics of Landslides. Lecture notes on the dynamics of mass wasting.*. s.l.:Springer Science + Business Media B.V..

Delmas, M., Calvet, M. & Gunnell, Y., 2009. Variability of Quarternary glacial erosion rates - A global perspective with a special reference to the Eastern Pyrenees. *Quarternary Science Reviews,* March, pp. 484-494.

Det Kongelige Olje- og Energidepartement, 2012. *Hvordan leve med farene - om flom og skred,* Oslo: Det Kongelige Olje- og Energidepartement.

ESRI, 2011. *ArcGIS Desktop: release 10,* Redlands, CA: Environmental Systems Research Institute.

Fell, R., Ho, K., Lacasse, S. & Leroi, E., 2005. A framework for landslide risk assessment and management. In: O. Hungr, et al. eds. *Proceedings of the Internation Conference on Landslide Risk Management.* Vancouver, Canada: s.n., pp. 3-25.

Fleming, R. W., Varnes, D. J. & Schuster, R. L., 1979. Landslide Hazards and Their Reduction. *Journal of the American Planning Association,* pp. 428-439.

FLO-2D Software Inc., 2018. *FLO-2D Products.* [Online]
Available at: https://www.flo-2d.com/flo-2d-products/
[Accessed 05 May 2018].

Fossen, H., Pedersen, R.-B., Bergh, S. & Andresen, A., 2008. Creation of a mountian chain. In: *The Making of a Land - Geology of Norway.* Trondheim: Norsk Geologisk Forening, pp. 178-232.

Fredin, O. et al., 2013. Glacial landforms and Quarternary landscape development in Norway. In: *Quarternary Geology of Norway.* Trondheim: Norges geologiske undersøkelse, pp. 5-27.

Glade, T., 2004. Linking debris-flow hazard assessments with geomorphology. *Geomorphology 66,* December, pp. 189 - 213.

Hanssen-Bauer, I. et al., 2015. *Cimate in Norway 2100,* s.l.: Miljødirektoratet.

Highland, L., Bobrowsky, P. T. & USGS, 2008. *The landslide handbook: a guide to understanding landslides,* Reston, Va.: U.S. Geological Survey.

Holtz, R. D., Kovacs, W. D. & Sheahan, T. C., 2010. *An Introduction to Geotechnical Engineering.* 2nd ed. s.l.:Pearson Higher Education.

Hungr, O., 1995. A model for the runout analysis of rapid flow slides, debrisflows and avalanches. *Canadian Geotechnical Journal,* Volume 32, pp. 610-623.

Hungr, O., 2005. Classification and terminology. In: *Debris-flow Hazards and Related Phenomena.* Chichester, UK: Praxis Publishing Ltd., pp. 9-23.

Hungr, O., Evans, S. G., Bovis, M. J. & Hutchinson, J. N., 2001. A review of the classification of landslides of the flow type. *Environment & Engineering Geoscience, Vol. VII. No. 3,* August, pp. 221-238.

Hungr, O., Leroueil, S. & Picarelli, L., 2013. The Varnes classification of landslide types, an update. *Landslides, 11,* pp. 167-194.

Hungr, O., McDougall, S. & Bovis, M., 2005. Entrainment of material by debris flows. In: *Debris-flow Hazards and Related Phenomena.* Chichester, UK: Praxis Publishing Ltd., pp. 135-158.

Hürlimann, M., Rickenmann, D., Medina, V. & Bateman, A., 2008. Evaluation of approaches to calculate debris-flow parameters for hazard assessment. *Engineering Geology,* pp. 152-163.

ICG, 2010. *Pre-processing of GIS data for DAN3D analysis,* Oslo: International Center for Geohazards.

Iverson, R. M., 2005. Debris-flow mechanics. In: *Debris-flow Hazards and Related Phenomena.* Chichester, UK: Praxis Publishing Ltd., pp. 105-134.

Jaedicke, C. et al., 2008. Spatial and temporal variations of Norwegian geohazards in a changing climate, the GeoExtreme Project.. *Nat. Hazards and Earth Syst. Sci, 8,* pp. 893-904.

Jakob, M. & Hungr, O., 2005. *Debris flow hazards and related phenomena.* Chichester, UK: Praxis Publishing.

Kartverket, 2017. *Høydedata.* [Online]
Available at: hoydedata.no
[Accessed 01 10 2017].

Kartverket, 2018a. *Norgeskart.* [Online]
Available at: http://norgeskart.no/#!?project=seeiendom
[Accessed 25 February 2018].

Kartverket, 2018b. *Norge i bilder.* [Online]
Available at: http://norgeibilder.no
[Accessed 25 February 2018].

Kim, J. & Løvholt, F., 2017. *Note 31: Viscoplastic and Granular Landslide Model - taking into account terrain deflections,* Trondheim, Norway: SINTEF Building and Infrastructure.

McDougall, S., 2006. *A new continuum model for the analysis of extremely rapid landslides across complex 3D terrain,* Vancouver: University of British Columbia.

McDougall, S. & Hungr, O., 2009. Two numerical models for landslide dynamic analysis. *Computers & Geoscience*, pp. 978-992.

McDougall, S., McKinnon, M. & Hungr, O., 2012. Developments in landslide runout prediction. In: *Landslides: Types, Mechanisms and Modeling.* s.l.:Cambridge University Press, pp. 187-195.

McKinnon, M., 2010. *Landslide Runout: Statistical Analysis of Physical Characteristics and Model Parameters,* Vancouver, Canada: The University of British Columbia.

Meyer, N. et al., 2012. Hydrometeorological threshold conditions for debris flow initiation in Norway. *Natural Hazards and Earth System Sciences*, 11 October, pp. 3059-3073.

Miljødirektoratet, 2017. *Norway's Climate.* [Online]
Available at: http://www.environment.no/Topics/Climate/

NGI, 2013a. *Nesbyen, Arnegårdslie. Vurdering av akutt fare for flomskred,* Oslo: NGI.

NGI, 2013b. *Befaringsrapport,* Oslo: NGI.

NGU, 2018a. *Berggrun.* [Online]
Available at: http://geo.ngu.no/kart/berggrunn_mobil/
[Accessed 21 March 2018].

NGU, 2018b. *Løsmassekart.* [Online]
Available at: http://geo.ngu.no/kart/losmasse_mobil/
[Accessed 21 March 2018].

Nordgulen, Ø. & Andresen, A., 2008. The Precambrian. In: *The Making of a Land - Geology of Norway.* Trondheim: Norsk Geologisk Forening, pp. 62-120.

Norem, H. & Sandersen, F., 2012. *Flom- og sørpeskred (Debris flows and slush avalanches),* s.l.: Vegdirektoratet Trafikksikkerhet, miljø- og teknologiavdelingen .

NVE, 2018. *NVE Atlas - Skredhendelser.* [Online]
Available at: https://atlas.nve.no/Html5Viewer/index.html?viewer=nveatlas#
[Accessed 3 April 2018].

O. Hungr Geotechnical Engineering Inc., 2010. *DAN3D: Dynamic Analysis of Landslides in Three Dimensions,* Vancouver, Canada: s.n.

Olsen, L., Sveian, H., Ottesen, D. & Rise, L., 2013. Quarternary glacial, interglacial and interstadial deposits of Norway and adjacent onshore and offshore areas. In: *Quarternary Geology of Norway.* Trondheim: Norges geologiske undersøkelse, pp. 79-112.

Pellegrino, A., di Santolo, A. & Schippa, L., 2015. An integrated procedure to evaluate rheological parameters to model debris flows. *Engineering Geology,* pp. 88-98.

Quan Luna, B. et al., 2013. Analysis and uncertainty quantification of dynamic run-out model parameters for landslides. In: *Landslide science and practice.* s.l.:Springer, Berlin, Heidelberg., pp. 315-318.

Rickenmann, D., 1999. Empirical relationships for debris flows. *Natural Hazards 19,* pp. 47 - 77.

Rossby, T., 1996. The North Atlantic Current and Surrounding Waters: At the Crossroads. *Review of Geophysics,* pp. 463-481.

Sassa, K. & hui Wang, G., 2005. Mechanism of landslide-triggered debris flows: liquefaction phenomena due to the undrained loading of torrent deposits. In: *Debris-flow Hazards and Related Phenomena.* Chichester, UK: Praxis Publishing Ltd., pp. 81-104.

Schanche, S., 2014. *Sikkerhet mot skred i bratt terreng.* Oslo: Norges vassdrags- og energidirektorat.

SFI, 2018. *Klima 2050 - what we do.* [Online]
Available at: http://www.klima2050.no/what-we-do/

Sharpe, C., 1938. *Landslides and Related Phenomena.* New York: Columbia University Press.

Sidel, C. & Ochai, H., 2006. *Landslides: Processes, predictions, and land use.* Washington, DC: AGU Books.

Slagstad, T., Davidsen, B. & Daly, J., 2011. Age and composition of crystalline basement rocks on the Norwegian continental margin: offshore extension and continuity of the Caledonian-Appalachian orogenic belt. *Journal of the Geological Society,* 168(5), pp. 1167 - 1185.

Slettan, O. & Smits, J., 2013. *Full Storm: naturkatastrofer og ekstremvær i Norge.* Oslo: Gyldendal.

SLF, 2010. *RAMMS: rapid mass movements.* [Online]
Available at: http://ramms.slf.ch/ramms/
[Accessed 05 May 2018].

Sorteberg, A. & Kvamstø, N. G., 2008. Hvor mye wil nedbøren øke i et varmere klima. *Klima*, pp. 36-38.

Statens vegvesen, 2014. *Laboratorieundersøkelser - Håndbok R210.* Oslo, Norway: Vegdirektoratet.

Stini, J., 1910. *Die Muren: versuch einer monographie mit besonderer berücksichtigung der verhältnisse in den Tiroler Alpen,* Innsbruck: Verlag der Wagner'schen universitäts-buchhandlung.

The World Bank, 2010. *Natural Hazards, UnNatural Disasters: The Economics of Effective Prevention,* Washington: World Bank Publications.

van Westen, C., van Asch, T. & Soeters, R., 2006. Landslide hazard and risk zonation - why is it still so difficult. *Bulleting of Engineering Geology and the Environment*, May, pp. 167-184.

Varnes, D., 1974. *Slope movement types and processes*, s.l.: TRB special report.

Vorren, T. O. & Mangerud, J., 2008. Glaciations come and go. In: *The Making of a Land - Geology of Norway*. Trondheim: Norsk Geologisk Forening, pp. 480-534.

Wentworth, C., 1922. A scale of grade and class terms for clastic sediments. *The journal of geology, 30(5)*, pp. 377 - 392.

Appendix A - GeoClaw Installation and Use Guide

Introduction – Getting started

GeoClaw is a subset of the Clawpack (*Conservation laws package*) software package, specialized for solving geophysical flow problems. This document is a guide containing instructions and useful tips for setting up granular flow-like landslide runout simulations using the Coulomb – Voellmy frictional rheology included within GeoClaw.

It is assumed that the reader of this guide has access to the NGI Linux server, and has file read/write permissions at least in their home folder.

GeoClaw can be installed from the NGI Linux server, following instructions detailed written by Finn Løvholt and Jiwan Kim (Kim & Løvholt, 2017). Alternately, the packages can be installed by copying the folder containing the files from the directory of someone with them correctly installed, to your home directory. To do this, you will need administrator privileges, and should contact the system administrator and IT.

Checking the installation:

It is suggested to save all files and associated sub-folders in the same folder (e.g. "clawpack-5.3.1" in this study). This folder also contains a README.txt file detailing how to install the python tools required to run clawpack. To test the installation, examples (located in Bingclaw, Coulomb_Voellmy, or geoclaw folders) can be run by opening terminal to the desired folder and using the command `make .plots`.

Creating a new simulation

The easiest way to create a folder for a new landslide simulation (and ensure that it contains all the required subfolders and source codes properly linked) is to create a copy of one of the examples, and then rename the copy to the new simulation. The user can then edit the parameters and input files as required, and has the original example to go back to if any errors occur.

Editing setrun.py

All parameters and data needed to run the simulation can be quickly changed by editing the file called setrun.py. A setrun.py file exists in each simulation folder, an example of the file path is:

clawpack-5.3.1/geoclaw/examples/storm-surge/ike/setrun.py

When running GeoClaw, setrun.py can be used to change the timestep, input topography files, define rheological parameters, and specify output style.

Initial parameters and rheology

The first lines of setrun.py import the required computational packages, initialize the coulomb and voellmy friction models, as well as define the turbulence coefficient (xi) and friction coefficient (calculated from fric_angle). Note that the "friction angle" mentioned here is not the static friction angle of the material, but the dynamic basal friction, and is related to the Voellmy friction coefficient by the equation:

$$\mu = \tan\left(\frac{fric.angle * \pi}{180}\right)$$

where μ is the friction coefficient.

Simulation grid size

The boundaries of the simulation area must be manually entered to correspond to the extent of the topography files being used (LATER SECTION), and depend on their coordinate system. If using files directly from ArcGIS (with UTM coordinates), the file extent can be found by right-clicking on the file in ArcMap, and selecting "properties" → "extent". This data can then be entered into GeoClaw as shown in Figure A1.

```
# Lower and upper edge of computational domain:
clawdata.lower[0] = 503899.28039994   # X coordinate of the grid left boundary
clawdata.upper[0] = 504701.28039994   # X coordinate of the grid right boundary
clawdata.lower[1] = 6716717.1779989   # Y coordinate of the grid bottom boundary
clawdata.upper[1] = 6717185.1779989   # Y coordinate of the grid upper boundary

# Number of grid cells: Coarsest grid
clawdata.num_cells[0] = 802 # number of cells in the X direction
clawdata.num_cells[1] = 468 # number of cells in the Y direction
```

Figure A 1: example input of topography file cell sizes and extents.

The number of grid cells is determined by subtracting the coordinate of the right boundary by that of the left (for the x direction) and the top by the bottom (for the y direction). If the topography files used for the simulation are NOT 1m scale, then the number of grid cells in each direction must be edited to match up to the topography file specifications. Divide the number of cells in each direction by the scale of the topography file. For the example picture above (IMAGE REF) the topography file was 1m. If the topography had been 10m scale, the number of grid cells would be 80 in the x direction, and 47 in the y.

Alternatively, the bottom left corner of the topography files can be assigned the coordinate (0, 0), and values being entered into GeoClaw so that the coordinates correspond to the topography grid size.

Initial time, output times, and time-step

By default, the start time for a simulation is set to zero (initial time). If the simulation is stopped and the user wishes to restart it, they can change the initial time to the new start-time, and define the file containing the data from the earlier simulation.

Three predefined output styles can be chosen from, by entering either 1, 2 or 3 into the line "clawdata,output_style =" (1 is the default value). Style 1 provides output at time-steps specified by the user. The default setting is once every minute, for every minute that the simulation runs. The total time the simulation runs for can be controlled by setting the number of output times. Style 2 allows the user to input an array, or list of times they desire output files for. Style 3 loops the output for every *ith* output time-step over a specified amount of time.

The time-step between each calculation run by the model can be selected by modifying the variable "clawdata.dt_initial". Similarly, the maximum allowed time can be set by modifying the variable "clawdata.dt_max" (as mentioned above the total simulation time can also be controlled by the number of outputs. If output files are set to be created for 10 minutes, the simulation will stop after 10 minutes).

Topography files and physical parameters

Path and source topography data, and physical parameters are set in the section "def setgeo(rundata):", the last section of setrun.py.

In the physical parameters, the most important thing to note is that sea level is set to 0.0. If for some reason the topography files used during the simulation have a different elevation scale, this value will need to be changed.

Topography files

GeoClaw can read topography files in .asc format, created directly from GIS software such as ArcMap. There are two places in the code to load topography files, the first must be the "path" file (topography file of the area before the landslide occurred). The second file is a "source" topography file, containing only the source area. Information on how to properly prepare these files can be found in an International Center for Geohazards (ICG) report (ICG, 2010) on preparing topography files for use in DAN3D analysis, included in the appendix of a PhD paper by Mads-Peter Dahl (Dahl, 2011).

Once the files are prepared correctly, the file paths can be added to setrun.py in the lines shown in Figure A2 below (fname = …).

```
# == settopo.data values ==                # Path file
topofiles = rundata.topo_data.topofiles
# for topography, append lines of the form
#    [topotype, minlevel, maxlevel, t1, t2, fname]
fname = '../Topo_data/Nesbyen/nes_path_claw.asc'
topofiles.append([3, 1, 3, 0., 1.e10, fname])

# == setdtopo.data values ==
dtopo_data = rundata.dtopo_data
# for moving topography, append lines of the form :   (<= 1 allowed for now!)
#   [topotype, minlevel,maxlevel,fname]

# == setqinit.data values ==                # Source file
rundata.qinit_data.qinit_type =  1
rundata.qinit_data.qinitfiles = []
qinitfiles = rundata.qinit_data.qinitfiles
fname = '../Topo_data/Nesbyen/nes_source_claw.asc'
qinitfiles.append([3,3,fname])
```

Figure A 2: Adding path and source topography file locations to the code.

Setting plots

GeoClaw returns a plot of the landside at each output time-step, and the plot settings can be adjusted by editing the setplot.py file, located in the same directory as setrun.py. The colour scales of the plots need to be changed to correspond to the elevation range and expected thickness of the landslide being simulated.

- Scroll down the code until finding the section “Figure for pcolor plot”.
- Chart axes, labels, and title can also be changed here. Contour lines can also be enabled or disabled here.
- Continue scrolling down to “Landslide”
    - Change “plotitem.pcolor_cmin” to the lower limit of landslide thickness desired to be shown, in meters (0 or 0.1 suggested)
    - Change “plotitem.pcolor_cmax” to the maximum thickness of the landslide.
- Continue scrolling to “Land”
    - Change “plotitem.pcolor_cmin” to the approximate elevation (in meters) of the bottom of the landslide slope, or valley bottom.
    - Change “plotitem.pcolor_cmax” to the approximate elevation (in meters) of the landslide release area.

- **NOTE:** “Figure for pcolor plot” appears three times in the setplot.py code, and the ranges changed above should be changed each time.

Save and close setplot.py

Running simulations and outputs

To run a simulation, open terminal to the directory containing setrun.py, and enter the command “make .plots”. If all topography files and boundary conditions were set correctly, the simulation should begin to run.

When the simulation is complete, two folders will have been created in the file directory containing setrun.py, "_outputs" and "_plots". The plots folder contains a number of .png files (frame00nfig.png) where *n* is the output time. By default, the plot will show the title "Landslide at *n* minutes".

The "_outputs" folder contains a number of .data and text files relating the simulation. The most relevant files are "fort.q00n", where *n* again is the output minute. These files can be opened as text files using notepad or notepad++, and contain data on the grid files used to run the simulation at the top (number of x grid spaces, number of y grid spaces, coordinates of the lower left corner, and spacing between x and y grid spaces; this spacing should match the resolution of the DEM used to create the topography files). The file then contains 4 columns:

- First column is the thickness of the landslide, in meters
- Second column is the landslide velocity in the x direction, in m/s
- Third column is the landslide velocity in the y direction, in m/s
- Fourth column is the elevation above sea level of each grid node (in meters)

Each row of data corresponds to a grid node. The first row is the lower left corner, the second is one space to the right, and so on. Figure A3 shows a sample output file. As the topography grid for this simulation was 802 x 468, the output file has 375,336 rows.

```
  1                grid_number
  1                AMR_level
802                mx
468                my
  0.50389928E+06   xlow
  0.67167172E+07   ylow
  0.10000000E+01   dx
  0.10000000E+01   dy

  0.0000000000000000E+00   0.0000000000000000E+00   0.0000000000000000E+00   0.3941275000010921E+03
  0.0000000000000000E+00   0.0000000000000000E+00   0.0000000000000000E+00   0.4643884250518162E+03
  0.0000000000000000E+00   0.0000000000000000E+00   0.0000000000000000E+00   0.4639474501215141E+03
  0.0000000000000000E+00   0.0000000000000000E+00   0.0000000000000000E+00   0.4634675251901448E+03
  0.0000000000000000E+00   0.0000000000000000E+00   0.0000000000000000E+00   0.4629856002453327E+03
  0.0000000000000000E+00   0.0000000000000000E+00   0.0000000000000000E+00   0.4625381752707509E+03
  0.0000000000000000E+00   0.0000000000000000E+00   0.0000000000000000E+00   0.4621299003061390E+03
  0.0000000000000000E+00   0.0000000000000000E+00   0.0000000000000000E+00   0.4617329003575282E+03
  0.0000000000000000E+00   0.0000000000000000E+00   0.0000000000000000E+00   0.4613289004193878E+03
  0.0000000000000000E+00   0.0000000000000000E+00   0.0000000000000000E+00   0.4609168504732447E+03
```

Figure A 3: Example of data output from GeoClaw.

References

Kim, J. & Løvholt, F., 2017. *Note 31: Viscoplastic and Granular Landslide Model - taking into account terrain deflections,* Trondheim, Norway: SINTEF Building and Infrastructure.

ICG, 2010. *Pre-processing of GIS data for DAN3D analysis,* Oslo: International Center for Geohazards.

Dahl, M.-P. J., 2011. *Risk management tools for flow-type landslides in the Faroe Islands, North Atlantic Ocean,* s.l.: Prinfo Paritas Digital Service.

Appendix B

This appendix contains an overview of the simulation files created in DAN3D, and links detailing the file locations on the NGI P:\ drive. The folders contain summary output text files from each simulation, as well as .jpg files showing the model at the final time-step. Some simulations include additional output files (maximum deposit thickness, erosion thickness, maximum velocity, etc.) that can be viewed in ArcGIS. The text below is an example of one of the summary output files (in this case for the Nesbyen event). To obtain specific files, contact the author (gcarey@shaw.ca).

```
C:\Users\GCa\Documents\Thesis\Dan3D\Nesbyen\Nesbyen_Test.dn3
Project:        Nesbyen Numerical control
Job:    Nes
Input by:       Graeme
Number of Materials:    1
Number of Particles:    2000
Erosion Rate (m^-1):    0.003
Smoothing Length Constant:      4
Velocity Smoothing Coefficient: 0
Stiffness Coefficient:  200
Time Step (s):  0.1
Elevation File Name:    C:\Users\GCa\Documents\Thesis\GIS\Nesbyen\Path\Nes_PATH.grd
Depth File Name:        C:\Users\GCa\Documents\Thesis\GIS\Nesbyen\Source\Nes_SOURCE.grd
Erosion File Name:      None

Material 1
Unit Weight (kN/m^3):   20
Voellmy Rheology
Shear Strength (kPa):   0
Friction Angle (deg.):  4.57392
Friction Coefficient:   0.08
Pore-pressure Coefficient:      0
Viscosity (kPa.s):      0
Turbulence Coefficient (m/s^2): 500
Power Law Exponent:     0
Internal Friction Angle (deg.): 35

End Time (s):   600
Final COM X-Position (m):       504554
Final COM Y-Position (m):       6.71703e+006
Maximum Slide Velocity (m/s):   12.3584
Travel Angle (deg.):    6.65946
Start Volume (m^3):     458.372
Final Volume (m^3):     2916.74

Output files saved in:  C:\Users\GCa\Documents\Thesis\Dan3D\Nesbyen\Nes Test\
Output time interval (s):       30
```

Site							
Nesbyen - numerical parameters							
File name	Time-step (s)	No. of particles	Smoothing Length Constant	μ	ξ (m/s^2)	Max. Velocity (m/s)	File location
RT1	0.05	2000	4	0.12	550	12.0	P:\2015\01\20150145\Gca\Dan3d\Nes\Numerical parameters
RT2	0.1	2000	4	0.12	550	12.2	P:\2015\01\20150145\Gca\Dan3d\Nes\Numerical parameters
RT3	0.15	2000	4	0.12	550	12.2	P:\2015\01\20150145\Gca\Dan3d\Nes\Numerical parameters
RT4	0.2	2000	4	0.12	550	11.9	P:\2015\01\20150145\Gca\Dan3d\Nes\Numerical parameters
RT5	0.3	2000	4	0.12	550	12.0	P:\2015\01\20150145\Gca\Dan3d\Nes\Numerical parameters
RT6	0.5	2000	4	0.12	550	13.1	P:\2015\01\20150145\Gca\Dan3d\Nes\Numerical parameters
RP1	0.1	1000	4	0.12	550	12.2	P:\2015\01\20150145\Gca\Dan3d\Nes\Numerical parameters
RP2	0.1	2000	4	0.12	550	12.2	P:\2015\01\20150145\Gca\Dan3d\Nes\Numerical parameters
RP3	0.1	3000	4	0.12	550	12.8	P:\2015\01\20150145\Gca\Dan3d\Nes\Numerical parameters
RP4	0.1	4000	4	0.12	550	12.2	P:\2015\01\20150145\Gca\Dan3d\Nes\Numerical parameters
SL1	0.1	2000	1	0.12	550	43.4	P:\2015\01\20150145\Gca\Dan3d\Nes\Numerical parameters
SL2	0.1	2000	2	0.12	550	13.0	P:\2015\01\20150145\Gca\Dan3d\Nes\Numerical parameters
SL3	0.1	2000	3	0.12	550	13.0	P:\2015\01\20150145\Gca\Dan3d\Nes\Numerical parameters
SL4	0.1	2000	4	0.12	550	12.2	P:\2015\01\20150145\Gca\Dan3d\Nes\Numerical parameters
SL5	0.1	2000	5	0.12	550	12.0	P:\2015\01\20150145\Gca\Dan3d\Nes\Numerical parameters
SL6	0.1	2000	6	0.12	550	12.0	P:\2015\01\20150145\Gca\Dan3d\Nes\Numerical parameters
SL7	0.1	2000	7	0.12	550	11.9	P:\2015\01\20150145\Gca\Dan3d\Nes\Numerical parameters

Site	Time-step (s)	No. of particles
Nesbyen	0.1	2000

File name	μ	ξ (m/s^2)	Erosion rate (m^{-1})	Max. Velocity (m/s)	Final volume (m^3)	File location
Run1	0.1	100	0.004	7.1	2582	P:\2015\01\20150145\Gca\Dan3d\Nes
Run2	0.1	250	0.004	9.6	3626	P:\2015\01\20150145\Gca\Dan3d\Nes
Run3	0.1	400	0.004	11.1	4174	P:\2015\01\20150145\Gca\Dan3d\Nes
Run4	0.1	550	0.004	12.1	4442	P:\2015\01\20150145\Gca\Dan3d\Nes

Run5	0.1	700	0.004	13.0	4533	P:\2015\01\20150145\Gca\Dan3d\Nes	
Run6	0.1	850	0.004	13.6	4735	P:\2015\01\20150145\Gca\Dan3d\Nes	
Run7	0.1	1000	0.004	14.1	4890	P:\2015\01\20150145\Gca\Dan3d\Nes	
Run8	0.15	100	0.004	6.5	1944	P:\2015\01\20150145\Gca\Dan3d\Nes	
Run9	0.15	250	0.004	9.0	2876	P:\2015\01\20150145\Gca\Dan3d\Nes	
Run10	0.15	400	0.004	10.5	3263	P:\2015\01\20150145\Gca\Dan3d\Nes	
Run11	0.15	550	0.004	11.5	3546	P:\2015\01\20150145\Gca\Dan3d\Nes	
Run12	0.15	700	0.004	12.2	3727	P:\2015\01\20150145\Gca\Dan3d\Nes	
Run13	0.15	850	0.004	13.1	3946	P:\2015\01\20150145\Gca\Dan3d\Nes	
Run14	0.15	1000	0.004	13.2	4026	P:\2015\01\20150145\Gca\Dan3d\Nes	
Run15	0.2	100	0.004	6.2	1143	P:\2015\01\20150145\Gca\Dan3d\Nes	
Run16	0.2	250	0.004	8.5	1903	P:\2015\01\20150145\Gca\Dan3d\Nes	
Run17	0.2	400	0.004	9.9	2262	P:\2015\01\20150145\Gca\Dan3d\Nes	
Run18	0.2	550	0.004	10.8	2555	P:\2015\01\20150145\Gca\Dan3d\Nes	
Run19	0.2	700	0.004	11.3	2698	P:\2015\01\20150145\Gca\Dan3d\Nes	
Run20	0.2	850	0.004	11.8	2850	P:\2015\01\20150145\Gca\Dan3d\Nes	
Run21	0.2	1000	0.004	12.4	2883	P:\2015\01\20150145\Gca\Dan3d\Nes	
Run22	0.3	100	0.004	5.6	672	P:\2015\01\20150145\Gca\Dan3d\Nes	
Run23	0.3	250	0.004	7.4	712	P:\2015\01\20150145\Gca\Dan3d\Nes	
Run24	0.3	400	0.004	8.6	751	P:\2015\01\20150145\Gca\Dan3d\Nes	
Run25	0.3	550	0.004	9.4	821	P:\2015\01\20150145\Gca\Dan3d\Nes	
Run26	0.3	700	0.004	9.9	906	P:\2015\01\20150145\Gca\Dan3d\Nes	
Run27	0.3	850	0.004	10.1	996	P:\2015\01\20150145\Gca\Dan3d\Nes	
Run28	0.3	1000	0.004	10.6	1081	P:\2015\01\20150145\Gca\Dan3d\Nes	
Test1	0.087	550	0.003	12.4	2866	P:\2015\01\20150145\Gca\Dan3d\Nes	
Test2	0.08	700	0.003	13.5	3023	P:\2015\01\20150145\Gca\Dan3d\Nes	
Nes test	0.08	500	0.003	12.4	2916	Nes Test	Folder containing detailed output files from simulation that can be opened in ArcGIS or similar

Site	**Time-step (s)**	**No. of particles**
Oldedalen 1	0.1	2000

File name	μ	ξ (m/s^2)	Erosion rate (m^{-1})	Max. Velocity (m/s)	Final volume (m^3)	File location	
Run1	0.15	100	0.003	8.6	12430	P:\2015\01\20150145\Gca\Dan3d\Old 1	
Run2	0.15	250	0.003	11.9	14280	P:\2015\01\20150145\Gca\Dan3d\Old 1	
Run3	0.15	400	0.003	13.8	15260	P:\2015\01\20150145\Gca\Dan3d\Old 1	
Run4	0.15	550	0.003	14.9	15623	P:\2015\01\20150145\Gca\Dan3d\Old 1	
Run5	0.15	700	0.003	15.5	16384	P:\2015\01\20150145\Gca\Dan3d\Old 1	
Run6	0.15	850	0.003	16.4	15775	P:\2015\01\20150145\Gca\Dan3d\Old 1	
Run7	0.15	1000	0.003	17.1	15336	P:\2015\01\20150145\Gca\Dan3d\Old 1	
Run8	0.2	100	0.003	8.3	11289	P:\2015\01\20150145\Gca\Dan3d\Old 1	
Run9	0.2	250	0.003	11.6	13243	P:\2015\01\20150145\Gca\Dan3d\Old 1	
Run10	0.2	400	0.003	13.6	14319	P:\2015\01\20150145\Gca\Dan3d\Old 1	
Run11	0.2	550	0.003	14.8	15075	P:\2015\01\20150145\Gca\Dan3d\Old 1	
Run12	0.2	700	0.003	15.5	15206	P:\2015\01\20150145\Gca\Dan3d\Old 1	
Run13	0.2	850	0.003	16.8	15326	P:\2015\01\20150145\Gca\Dan3d\Old 1	
Run14	0.2	1000	0.003	17.0	15666	P:\2015\01\20150145\Gca\Dan3d\Old 1	
Run15	0.3	100	0.003	6.5	4847	P:\2015\01\20150145\Gca\Dan3d\Old 1	
Run16	0.3	250	0.003	10.6	8745	P:\2015\01\20150145\Gca\Dan3d\Old 1	
Run17	0.3	400	0.003	12.4	10467	P:\2015\01\20150145\Gca\Dan3d\Old 1	
Run18	0.3	550	0.003	13.9	11380	P:\2015\01\20150145\Gca\Dan3d\Old 1	
Run19	0.3	700	0.003	14.7	11657	P:\2015\01\20150145\Gca\Dan3d\Old 1	
Run20	0.3	850	0.003	15.5	10700	P:\2015\01\20150145\Gca\Dan3d\Old 1	
Run21	0.3	1000	0.003	16.1	10409	P:\2015\01\20150145\Gca\Dan3d\Old 1	
Test1	0.185	400	0.003	13.6	15650	Old1 Test	Folder containing detailed output files from simulation that can be opened in ArcGIS or similar

Site	Time-step (s)	No. of particles
Oldedalen 2	0.1	2000

File name	μ	ξ (m/s^2)	Erosion rate (m^{-1})	Max. Velocity (m/s)	Final volume (m^3)	File location

Run1	0.15	100	0.004	14.2	3847	P:\2015\01\20150145\Gca\Dan3d\Old 2
Run2	0.15	250	0.004	17.2	3971	P:\2015\01\20150145\Gca\Dan3d\Old 2
Run3	0.15	400	0.004	20.8	4016	P:\2015\01\20150145\Gca\Dan3d\Old 2
Run4	0.15	550	0.004	20.4	4057	P:\2015\01\20150145\Gca\Dan3d\Old 2
Run5	0.15	700	0.004	20.3	4162	P:\2015\01\20150145\Gca\Dan3d\Old 2
Run6	0.15	850	0.004	26.8	4063	P:\2015\01\20150145\Gca\Dan3d\Old 2
Run7	0.15	1000	0.004	22.0	4129	P:\2015\01\20150145\Gca\Dan3d\Old 2
Run8	0.2	100	0.004	32.1	3611	P:\2015\01\20150145\Gca\Dan3d\Old 2
Run9	0.2	250	0.004	28.6	3863	P:\2015\01\20150145\Gca\Dan3d\Old 2
Run10	0.2	400	0.004	21.1	3981	P:\2015\01\20150145\Gca\Dan3d\Old 2
Run11	0.2	550	0.004	26.6	4048	P:\2015\01\20150145\Gca\Dan3d\Old 2
Run12	0.2	700	0.004	27.2	4006	P:\2015\01\20150145\Gca\Dan3d\Old 2
Run13	0.2	850	0.004	32.0	4104	P:\2015\01\20150145\Gca\Dan3d\Old 2
Run14	0.2	1000	0.004	40.9	4019	P:\2015\01\20150145\Gca\Dan3d\Old 2
Run15	0.3	100	0.004	22.6	2514	P:\2015\01\20150145\Gca\Dan3d\Old 2
Run16	0.3	250	0.004	30.5	3196	P:\2015\01\20150145\Gca\Dan3d\Old 2
Run17	0.3	400	0.004	32.6	3455	P:\2015\01\20150145\Gca\Dan3d\Old 2
Run18	0.3	550	0.004	43.2	3699	P:\2015\01\20150145\Gca\Dan3d\Old 2
Run19	0.3	700	0.004	29.0	3809	P:\2015\01\20150145\Gca\Dan3d\Old 2
Run20	0.3	850	0.004	31.8	3849	P:\2015\01\20150145\Gca\Dan3d\Old 2
Run21	0.3	1000	0.004	30.6	3883	P:\2015\01\20150145\Gca\Dan3d\Old 2
Test1	0.185	400	0.003	23.9	2500	Old2 Test — Folder containing detailed output files from simulation that can be opened in ArcGIS or similar

Site	**Time-step (s)**	**No. of particles**
Ringebu	0.1	2000

File name	**μ**	**ξ (m/s²)**	**Erosion rate (m⁻¹)**	**Max. Velocity (m/s)**	**Final volume (m³)**	**File location**
Run1	0.15	100	0.006	5.3	406	P:\2015\01\20150145\Gca\Dan3d\Rbu
Run2	0.15	250	0.006	7.0	409	P:\2015\01\20150145\Gca\Dan3d\Rbu
Run3	0.15	400	0.006	8.4	408	P:\2015\01\20150145\Gca\Dan3d\Rbu

Run4	0.15	550	0.006	8.6	408	P:\2015\01\20150145\Gca\Dan3d\Rbu
Run5	0.15	700	0.006	9.5	410	P:\2015\01\20150145\Gca\Dan3d\Rbu
Run6	0.15	850	0.006	9.9	411	P:\2015\01\20150145\Gca\Dan3d\Rbu
Run7	0.15	1000	0.006	10.1	413	P:\2015\01\20150145\Gca\Dan3d\Rbu
Run8	0.2	100	0.006	4.9	398	P:\2015\01\20150145\Gca\Dan3d\Rbu
Run9	0.2	250	0.006	6.4	403	P:\2015\01\20150145\Gca\Dan3d\Rbu
Run10	0.2	400	0.006	7.3	403	P:\2015\01\20150145\Gca\Dan3d\Rbu
Run11	0.2	550	0.006	8.2	404	P:\2015\01\20150145\Gca\Dan3d\Rbu
Run12	0.2	700	0.006	8.2	404	P:\2015\01\20150145\Gca\Dan3d\Rbu
Run13	0.2	850	0.006	8.5	405	P:\2015\01\20150145\Gca\Dan3d\Rbu
Run14	0.2	1000	0.006	9.0	406	P:\2015\01\20150145\Gca\Dan3d\Rbu
Run15	0.3	100	0.006	4.1	330	P:\2015\01\20150145\Gca\Dan3d\Rbu
Run16	0.3	250	0.006	5.0	356	P:\2015\01\20150145\Gca\Dan3d\Rbu
Run17	0.3	400	0.006	5.7	369	P:\2015\01\20150145\Gca\Dan3d\Rbu
Run18	0.3	550	0.006	6.3	377	P:\2015\01\20150145\Gca\Dan3d\Rbu
Run19	0.3	700	0.006	6.5	382	P:\2015\01\20150145\Gca\Dan3d\Rbu
Run20	0.3	850	0.006	7.0	383	P:\2015\01\20150145\Gca\Dan3d\Rbu
Run21	0.3	1000	0.006	7.4	386	P:\2015\01\20150145\Gca\Dan3d\Rbu
Source1	0.1	400	0.005	9.24	357	Rbu Test — Folder containing detailed output files from simulation that can be opened in ArcGIS or similar

Site	**Time-step (s)**	**No. of particles**
All (GeoClaw comparison simulations)	0.1	2000

File name	**μ**	**ξ (m/s²)**	**Max. Velocity (m/s)**	**File location**	
nes_comp1	0.15	150	7.5	P:\2015\01\20150145\Gca\Dan3d\Nes	Folder containing detailed output files from simulation that can be opened in ArcGIS or similar
nes_comp2	0.15	450	11.0	P:\2015\01\20150145\Gca\Dan3d\Nes	
nes_comp3	0.15	750	12.7	P:\2015\01\20150145\Gca\Dan3d\Nes	Folder containing detailed output files from simulation that can be opened in ArcGIS or similar
nes_comp4	0.1	450	11.8	P:\2015\01\20150145\Gca\Dan3d\Nes	
nes_comp5	0.2	450	10.3	P:\2015\01\20150145\Gca\Dan3d\Nes	

old1_comp1	0.15	150	8.1	P:\2015\01\20150145\Gca\Dan3d\Old 1	Folder containing detailed output files from simulation that can be opened in ArcGIS or similar
old1_comp2	0.15	450	12.1	P:\2015\01\20150145\Gca\Dan3d\Old 1	
old1_comp3	0.15	750	14.8	P:\2015\01\20150145\Gca\Dan3d\Old 1	Folder containing detailed output files from simulation that can be opened in ArcGIS or similar
old1_comp4	0.1	450	12.8	P:\2015\01\20150145\Gca\Dan3d\Old 1	
old1_comp5	0.2	450	11.7	P:\2015\01\20150145\Gca\Dan3d\Old 1	
old2_comp1	0.15	150	16.4	P:\2015\01\20150145\Gca\Dan3d\Old 2	Folder containing detailed output files from simulation that can be opened in ArcGIS or similar
old2_comp2	0.15	450	20.2	P:\2015\01\20150145\Gca\Dan3d\Old 2	
old2_comp3	0.15	750	22.2	P:\2015\01\20150145\Gca\Dan3d\Old 2	Folder containing detailed output files from simulation that can be opened in ArcGIS or similar
old2_comp4	0.1	450	24.5	P:\2015\01\20150145\Gca\Dan3d\Old 2	
old2_comp5	0.2	450	17.8	P:\2015\01\20150145\Gca\Dan3d\Old 2	
rbu_comp1	0.15	150	6.0	P:\2015\01\20150145\Gca\Dan3d\Rbu	Folder containing detailed output files from simulation that can be opened in ArcGIS or similar
rbu_comp2	0.15	450	8.6	P:\2015\01\20150145\Gca\Dan3d\Rbu	
rbu_comp3	0.15	750	9.8	P:\2015\01\20150145\Gca\Dan3d\Rbu	Folder containing detailed output files from simulation that can be opened in ArcGIS or similar
rbu_comp4	0.1	450	9.6	P:\2015\01\20150145\Gca\Dan3d\Rbu	
rbu_comp5	0.2	450	7.8	P:\2015\01\20150145\Gca\Dan3d\Rbu	